Chemical and Biological Oceanographic Conditions on the Scotian Shelf and in the Eastern Gulf of Maine during 2024

Benoit Casault, Catherine L. Johnson, Emmanuel Devred,
Stephanie Clay, and Lindsay Beazley

Fisheries and Oceans Canada
Maritimes Region
Bedford Institute of Oceanography
P.O. Box 1006
Dartmouth, Nova Scotia
B2Y 4A2

2025

Canadian Technical Report of
Fisheries and Aquatic Sciences 3744

Fisheries and Oceans Canada | Pêches et Océans Canada

Canada

Canadian Technical Report of Fisheries and Aquatic Sciences

Technical reports contain scientific and technical information that contributes to existing knowledge but which is not normally appropriate for primary literature. Technical reports are directed primarily toward a worldwide audience and have an international distribution. No restriction is placed on subject matter and the series reflects the broad interests and policies of Fisheries and Oceans Canada, namely, fisheries and aquatic sciences.

Technical reports may be cited as full publications. The correct citation appears above the abstract of each report. Each report is abstracted in the data base *Aquatic Sciences and Fisheries Abstracts*.

Technical reports are produced regionally but are numbered nationally. Requests for individual reports will be filled by the issuing establishment listed on the front cover and title page.

Numbers 1-456 in this series were issued as Technical Reports of the Fisheries Research Board of Canada. Numbers 457-714 were issued as Department of the Environment, Fisheries and Marine Service, Research and Development Directorate Technical Reports. Numbers 715-924 were issued as Department of Fisheries and Environment, Fisheries and Marine Service Technical Reports. The current series name was changed with report number 925.

Rapport technique canadien des sciences halieutiques et aquatiques

Les rapports techniques contiennent des renseignements scientifiques et techniques qui constituent une contribution aux connaissances actuelles, mais qui ne sont pas normalement appropriés pour la publication dans un journal scientifique. Les rapports techniques sont destinés essentiellement à un public international et ils sont distribués à cet échelon. II n'y a aucune restriction quant au sujet; de fait, la série reflète la vaste gamme des intérêts et des politiques de Pêches et Océans Canada, c'est-à-dire les sciences halieutiques et aquatiques.

Les rapports techniques peuvent être cités comme des publications à part entière. Le titre exact figure au-dessus du résumé de chaque rapport. Les rapports techniques sont résumés dans la base de données *Résumés des sciences aquatiques et halieutiques.*

Les rapports techniques sont produits à l'échelon régional, mais numérotés à l'échelon national. Les demandes de rapports seront satisfaites par l'établissement auteur dont le nom figure sur la couverture et la page du titre.

Les numéros 1 à 456 de cette série ont été publiés à titre de Rapports techniques de l'Office des recherches sur les pêcheries du Canada. Les numéros 457 à 714 sont parus à titre de Rapports techniques de la Direction générale de la recherche et du développement, Service des pêches et de la mer, ministère de l'Environnement. Les numéros 715 à 924 ont été publiés à titre de Rapports techniques du Service des pêches et de la mer, ministère des Pêches et de l'Environnement. Le nom actuel de la série a été établi lors de la parution du numéro 925.

Canadian Technical Report of
Fisheries and Aquatic Sciences 3744

2025

Chemical and Biological Oceanographic Conditions on the Scotian Shelf and in the Eastern Gulf of Maine during 2024

by

Benoit Casault, Catherine L. Johnson, Emmanuel Devred, Stephanie Clay, and Lindsay Beazley

Fisheries and Oceans Canada
Maritimes Region
Bedford Institute of Oceanography
P.O. Box 1006
Dartmouth, Nova Scotia
B2Y 4A2

Cat. No. Fs97-6/3744E-PDF ISBN 978-0-660-97572-6 ISSN 1488-5379

https://doi.org/10.60825/p6ad-1k52

Correct citation for this publication:

Casault, B., Johnson, C.L., Devred, E., Clay, S., and Beazley, L. 2025. Chemical and Biological Oceanographic Conditions on the Scotian Shelf and in the Eastern Gulf of Maine during 2024. Can. Tech. Rep. Fish. Aquat. Sci. 3744: vi + 58 p. https://doi.org/10.60825/p6ad-1k52

TABLE OF CONTENTS

ABSTRACT

Casault, B., Johnson, C.L., Devred, E., Clay, S., and Beazley, L. 2025. Chemical and Biological Oceanographic Conditions on the Scotian Shelf and in the Eastern Gulf of Maine during 2024. Can. Tech. Rep. Fish. Aquat. Sci. 3744: vi + 58 p. https://doi.org/10.60825/p6ad-1k52

Nutrient and plankton conditions were assessed in the context of physical conditions observed in the Maritimes Region in 2024. Nutrient depletion was widespread across the region, with Prince 5 (P5) station recording its tenth consecutive year of below-normal surface and subsurface nitrate inventories, while Cabot Strait section recorded record-low inventories for surface nitrate, silicate, and phosphate. Lower nutrient conditions likely influenced phytoplankton productivity, as chlorophyll-*a* measured *in situ* or derived from satellite remote sensing was mainly near or below normal across the region. The spring phytoplankton bloom was earlier than normal in the eastern area, near normal in the central area, and later than normal in the western area of the region. The intensity of the spring bloom was mainly normal to slightly below normal regionwide (except for Lurcher Shoal). The onset of the fall phytoplankton bloom was delayed across most areas, with the Eastern Scotian Shelf indicating a record-late onset. The intensity of the fall bloom was variable but mainly within near-normal ranges. *Calanus finmarchicus* abundance was near normal for the core sections, but negative and positive anomalies were recorded at the Halifax-2 (HL2) and P5 stations, respectively. *Pseudocalanus* spp. abundance reached record-high levels for the Halifax section, but was otherwise near normal. Mesozooplankton biomass was above normal at P5 but mainly below normal elsewhere, with record-low biomass observed at HL2. Arctic *Calanus* species and warm-water offshore copepods mainly remained at or below normal abundances, while warm-water shelf copepods showed near-normal abundances except for negative anomalies observed for the Halifax section and at P5.

RÉSUMÉ

Casault, B., Johnson, C.L., Devred, E., Clay, S., and Beazley, L. 2025. Chemical and Biological Oceanographic Conditions on the Scotian Shelf and in the Eastern Gulf of Maine during 2024. Can. Tech. Rep. Fish. Aquat. Sci. 3744: vi + 58 p. https://doi.org/10.60825/p6ad-1k52

Les conditions liées aux sels nutritifs et au plancton sont évaluées dans le contexte des conditions physiques observées dans la région des Maritimes en 2024. L'appauvrissement en éléments nutritifs était prédominant dans toute la région, avec la station Prince 5 (P5) enregistrant des inventaires de nitrate en surface et en profondeur inférieurs à la normale pour une dixième année consécutive, tandis que des valeurs minimales record étaient observées sur la section du détroit de Cabot pour le nitrate, le silicate et le phosphate en surface. L'appauvrissement en éléments nutritifs a probablement influencé la productivité du phytoplancton alors que la chlorophylle-*a* mesurée *in situ* ou dérivée des mesures par télédétection satellitaire était principalement proche ou inférieure à la normale dans toute la région. La floraison printanière du phytoplancton était précoce par rapport à la normale dans la zone est, normale dans la zone centrale, et tardive dans la zone ouest. L'intensité était généralement normale à légèrement inférieure à la normale (sauf pour le haut-fond Lurcher). La floraison automnale était tardive dans la plupart des zones, dont l'est du plateau néo-écossais où un délai record a été observé. L'intensité de la floraison automnale était variable mais près des niveaux normaux. L'abondance de *Calanus finmarchicus* était près de la normale pour les sections principales, mais des anomalies négatives et positives ont été enregistrées aux stations Halifax-2 (HL2) et P5, respectivement. L'abondance de *Pseudocalanus* spp. était près de la normale sauf pour la section d'Halifax où une valeur maximale record a été observée. La biomasse du mésozooplancton était supérieure à la normale à P5, mais principalement inférieure à la normale ailleurs, dont une valeur minimale record observée à HL2. L'abondance des espèces de *Calanus* arctiques et des copépodes d'eau chaude extracôtiers est restée principalement proche ou inférieure à la normale, tandis que les copépodes d'eau chaude côtiers ont montré des abondances proches de la normale, à l'exception d'anomalies négatives observées pour la section d'Halifax et à la station P5.

1. INTRODUCTION

The Atlantic Zone Monitoring Program (AZMP) was implemented in 1998 to enhance Fisheries and Oceans Canada's (DFO's) capacity to describe, understand, and forecast the state of the marine ecosystem (Therriault et al. 1998). The AZMP derives its information on the marine environment and ecosystem from data collected at a network of sampling locations (high-frequency sampling stations, cross-shelf sections, and ecosystem trawl surveys) in four DFO regions (Québec, Gulf, Maritimes, and Newfoundland and Labrador), sampled at a frequency of twice-monthly to once-annually. The sampling design provides fundamental information on the variability in physical, chemical, and biological properties of the Northwest Atlantic continental shelf and slope on seasonal and inter-annual scales. Ecosystem trawl surveys and cross-shelf sections provide information on broad-scale environmental variability (Harrison et al. 2005) but their seasonal coverage is limited. High-frequency sampling stations complement the broad-scale sampling by providing detailed information on seasonal changes in ocean properties. *In situ* sampling is also complemented by remote sensing of ocean colour measurements, providing additional information on the distribution of phytoplankton in the surface layer on a broad spatio-temporal scale.

The Scotian Shelf (SS) is located in a transition zone influenced by subpolar waters, mainly flowing into the region from the Gulf of St. Lawrence (GSL) and the Newfoundland Shelf and slope, and by warmer offshore waters of Gulf Stream origin. The deep-water properties of the SS exhibit significant shifts in temperature and nutrients in response to sustained periods of weak and strong large-scale meteorological forcing represented by the winter North Atlantic Oscillation index (Petrie 2007). These shifts result in changes in the relative contribution of the cold, low-nutrient Labrador slope water and the warmer, nutrient-rich Atlantic slope water to the source of the deep slope water to the shelf. Temperature and salinity on the SS are also influenced by heat transfer between the atmosphere and ocean, local mixing, precipitation, and, to some extent, runoff from land. Physical changes in the pelagic environment influence both plankton community composition and annual biological production cycles, with implications for energy transfer to higher trophic levels.

The objective of this report is to describe the nutrient, oxygen, and plankton conditions across the SS and in the eastern Gulf of Maine (GoM) in 2024 in the context of variability in shelf conditions observed since the beginning of AZMP surveys. It complements assessments of the Maritimes Region's physical environment (Layton et al. 2025) and of the state of the Canadian Northwest Atlantic shelf system as a whole (Galbraith et al. 2025). A set of simple metrics is used to represent important processes related to plankton production cycles and composition. These include surface and subsurface nutrient inventories, which represent the availability of nutrients required for phytoplankton production. Phytoplankton metrics, including biomass and spring and fall bloom dynamics, are represented by *in situ* chlorophyll-*a* inventories in the upper water column and near-surface chlorophyll-*a* concentrations measured by satellite remote sensing. Zooplankton metrics include biomass and copepod and non-copepod abundance, representing the overall quantity of zooplankton present, and abundances of taxa or groups that represent dominant species (*Calanus finmarchicus*, *Pseudocalanus* spp.) or biogeographic associations (Arctic copepods, warm-water offshore copepods, and warm-water shelf copepods). Copepod relative abundance patterns are used to assess community variability at the high-frequency sampling stations.

2. METHODS

Sample collection and processing conform to established standard protocols to the best extent possible (Mitchell et al. 2002). Non-standard measurements or derived variables are described below.

2.1 Surveys and Sampling

AZMP sampling in the Maritimes Region consists of high-frequency sampling at two fixed stations (Halifax-2 and Prince 5), seasonal sampling during dedicated oceanographic cross-shelf surveys conducted in spring and fall, and through participation in the ecosystem trawl surveys conducted in winter and summer. In 2024, sampling was conducted on the spring and fall cross-shelf surveys and on the winter and summer ecosystem trawl surveys (collectively referred to as 'broad-scale' surveys herein), and on day trips to the two high-frequency sampling stations (Table 1, Figures 1-3). A total of 517 hydrographic station occupations were completed, with 218 plankton net samples collected (Table 1).

2.1.1 High-frequency Sampling Stations

The standard sampling suite for the Halifax-2 (HL2) and Prince 5 (P5) high-frequency sampling stations (Figure 1) includes the following:

- Conductivity, temperature, depth (CTD) profiles with dissolved oxygen, pH (HL2), fluorescence, photosynthetically active radiation (PAR), and turbidity measurements.
- Niskin water bottle samples at standard depths (see Gear Deployment) for nutrients, salinity, and oxygen (for CTD data validation), chlorophyll-*a* analyses, and microscopic phytoplankton enumeration. Accessory phytoplankton pigments are also measured near the surface but are not reported in this document.
- Vertical ring net tows (202-µm mesh net) for zooplankton biomass (wet and dry weights), species and/or group abundance, and community composition.
- Secchi depth measurement for light attenuation when possible.

The HL2 and P5 stations were occupied 20 and 14 times, respectively, in 2024 (Table 1). However, at HL2, water samples were not collected on one occupation, and zooplankton samples were not collected on three occupations, due to inclement conditions. At P5, the CTD failed during the March 28 occupation, but bottle samples were collected.

2.1.2 Cross-shelf Sections

During the regular spring and fall seasonal surveys, samples are collected on the four core sections (Cabot Strait [CSL]; Louisbourg [LL]; Halifax [HL]; Browns Bank [BBL]; Figure 1) and at several ancillary sections/stations (black markers in Figure 2). The standard sampling suite for the cross-shelf section stations is the same as for the high-frequency sampling stations listed above, except integrated samples for phytoplankton enumeration and Secchi depth measurements are only collected at station HL2 when occupied as part of the HL section. Also, observations from the ancillary sections are not reported in this document due to inconsistent sampling over time.

In addition to the standard suite of analyses performed on water samples, parameters including particulate organic carbon, phytoplankton pigment composition, partial pressure of carbon dioxide (pCO_2), total alkalinity (TA), total inorganic carbon (TIC), and methane are measured at various depths. These parameters are not reported in this document; however, some of them (e.g., pCO_2, TA, pH, dissolved inorganic carbon, and calcite and aragonite saturation state) are included in a separate technical report (Galbraith et al. 2025).

In 2024, the spring survey took place from April 11th to May 1st, and the fall survey took place from October 4th to October 22nd (Table 1 and Figure 2). A description of activities conducted during the 2024 spring and fall surveys is presented in Beazley et al. (2024) and Beazley et al. (2025), respectively.

2.1.3 Ecosystem Trawl Surveys

Ecosystem trawl surveys in the Maritimes Region are led by DFO Science's Population Ecology Science Division with AZMP staff participation. The sampling suite for the ecosystem trawl survey stations includes the measurements listed above for the high-frequency sampling stations, but the standard set of water bottle sampling depths is reduced to four or five depths, and vertical ring net tows (202-µm mesh) are only collected at a subset of stations (Table 1 and Figure 3).

In 2024, the winter survey on the western SS, Georges Bank (GB), and in the Bay of Fundy (BoF) took place from March 2nd to April 2nd, and the summer survey on the SS and in the eastern GoM took place from June 25th to August 6th (Table 1 and Figure 3).

2.2 Gear Deployment

2.2.1 Conductivity, Temperature, Depth, and Water Sampling

Standard depths for water samples include:

- High-frequency sampling stations:
    1. HL2: 1 m, 5 m, 10 m, 20 m, 30 m, 40 m, 50 m, 75 m, 100 m, 140 m
    2. P5: 1 m, 10 m, 25 m, 50 m, 95 m
- Cross-shelf sections: near-surface, 10 m, 20 m, 30 m, 40 m, 50 m, 60 m, 80 m, 100 m, 250 m, 500 m, 1000 m, 1500 m, 2000 m, to near-bottom (defined as ca. 5 m from bottom; depths sampled are limited by bottom depth)
- Ecosystem trawl surveys: 5 m, 25 m, 50 m, 100 m (in water near or deeper than 200 m), and near-bottom (defined as ca. 1-2 m from bottom) when possible.

2.2.2 Net Tows

Ring nets of a standard 202-µm mesh are towed vertically from near-bottom to surface at a speed of approximately 1 $m \cdot s^{-1}$. In deep offshore waters, the maximum tow depth is 1000 m. Samples are preserved in a 4% solution of buffered formaldehyde and analyzed according to the protocol outlined in Mitchell et al. (2002).

2.3 Derived Metrics

2.3.1 Vertically Integrated Variables

Integrated chlorophyll-*a* and nutrient inventories are calculated over various depth intervals (i.e., 0–100 m for chlorophyll-*a* concentration, and 0–50 m and 50–150 m for nutrients) using trapezoidal numerical integration. When the maximum depth at a given station is shallower than the lower depth limits noted above, the inventories are calculated by setting the lower integration limit to the maximum depth at that station (e.g., 95 m for P5). Data at the surface (0 m) is taken as the closest near-surface sampled value. Data at the lower depth is taken as:

1. the interpolated value when sampling occurs below the lower integration limit; or
2. the closest deep-water sampled value when sampling is shallower than the lower integration limit.

2.3.2 Phytoplankton Taxonomic Groups

Phytoplankton abundance and taxonomic composition at the high-frequency sampling stations are normally estimated from pooled aliquots of water collected in the upper 100 m (140 m for HL2) of the water column using the Utermöhl technique (Utermöhl 1931) as described in Mitchell et al. (2002). However, analysis of phytoplankton abundance and taxonomy was not performed in 2024 due to the unavailability of a trained phytoplankton taxonomist.

2.4 Remote Sensing of Ocean Color

Data products from the Ocean Color Climate Change Initiative (OC-CCI; accessed on September 24, 2025) of the European Space Agency (ESA) were used to assemble time series of near-surface chlorophyll-*a* concentrations for different sub-regions of the Maritimes Region (HL2, Cabot Strait [CS], Eastern Scotian Shelf [ESS], Central Scotian Shelf [CSS], Western Scotian Shelf [WSS], Lurcher Shoal [LS], Georges Bank [GB]; Figure 4). In previous reports, ocean color data from the Moderate Resolution Imaging Spectroradiometer (MODIS; accessed on September 24, 2025) sensor were used but a decline in the data quality from the sensor was observed in recent years (see MODIS Data Degradation Notice - Earthdata Forum; accessed on September 24, 2025), hence the change to a more reliable data source. The OC-CCI product, for which the time series extends from September 1997 to present, offers improved spatial and temporal coverage due to the merging of data from multiple satellite optical sensors. Daily 4 km-resolution remote sensing reflectance (Rrs) data were downloaded from ESA's Ocean Color website (accessed on September 24, 2025). Chlorophyll-*a* concentrations were derived from Rrs data using the POLY4 band-ratio algorithm (Clay et al. 2019), which is based on the O'Reilly et al. (1998) algorithm. For the HL2, ESS, CSS, WSS, LS, and GB sub-regions, coefficients of the POLY4 algorithm were tuned using the regional database of *in situ* chlorophyll-*a* concentrations derived from high-performance liquid chromatography (HPLC). For the CS sub-region, coefficients of the POLY4 algorithm were tuned using the database of chlorophyll-*a* derived from Turner fluorometer measurements, as HPLC data are not available for that region. The resulting daily chlorophyll-*a* data were downloaded through the R Shiny app *PhytoFit* (accessed on September 24, 2025; Clay et al. 2021) for the purpose of visualizing the annual cycle, calculating weekly, monthly, seasonal, and annual means and anomalies, and for estimating the descriptive parameters of the spring and fall phytoplankton blooms. Four metrics were computed to describe the timing and intensity characteristics of the spring and fall blooms:

day of year of the maximum chlorophyll-*a* concentration during spring, day of year of the fall bloom initiation, and the spring and fall weighted average chlorophyll-*a* concentrations with weights proportional to the percentage of valid pixels (i.e., a proxy for cloud coverage) for a given sub-region.

2.5 Annual Anomaly Scorecards

Scorecards of key indices, based on normalized, seasonally-adjusted annual anomalies, represent changes in physical, chemical, and biological observations in a compact format. Annual estimates of phytoplankton abundance, water column inventories of nutrients and chlorophyll-*a,* zooplankton biomass, and the mean abundance of key zooplankton species or groups, at the high-frequency sampling stations and/or as an overall average along each of the four standard sections, are based on general linear models of the form:

$$Density = \alpha + \beta_{YEAR} + \delta_{MONTH} + \varepsilon$$

for the high-frequency sampling stations, and

$$Density = \alpha + \beta_{YEAR} + \delta_{STATION} + \gamma_{SEASON} + \varepsilon$$

for the sections.

Density is in units of concentration, abundance, or biomass per unit area or volume (e.g., individuals·m^{-2}, mg$_{chl\text{-}a}$·m^{-3}, etc.), α is the intercept and ε is the error. For the high-frequency sampling stations, β and δ are categorical effects for year and month, respectively. For the sections, β, δ *and* γ take into account the effect of year, station and season, respectively.

In addition to annual estimates, seasonal estimates of zooplankton indices (i.e., zooplankton biomass and *Calanus finmarchicus* abundance) for the individual sections were also calculated using a general linear model. In this case, a reduced model including the year and station effects was fitted to the seasonal data subsets.

Density in terms of surface chlorophyll-*a* concentration and *in situ* chlorophyll-*a* inventory was log-transformed [$log_{10}(n)$] to normalize the skewed distribution of the observations. For zooplankton and phytoplankton abundance, one is added to the log-transformed *Density* term [$log_{10}(n+1)$] to include observations for which the value equals zero. Integrated inventories of nutrients and zooplankton biomass were not log-transformed. An estimate of the least-squares means based on Type III Sums of Squares (Lenth et al. 2024) is used as the measure of the overall year effect.

For the ecosystem trawl surveys, seasonal mean indices were calculated as the arithmetic mean of the zooplankton biomass or the log-transformed *C. finmarchicus* abundance data collected within each season/year and each Northwest Atlantic Fisheries Organization (NAFO) area. The reporting of the zooplankton indices based on the NAFO areas for the ecosystem trawl surveys conforms with similar reporting for the physical indices (e.g., Galbraith et al. 2025) and with most fisheries stock assessment reports.

Annual anomalies are calculated as the deviation of an individual year from the mean of the annual estimates over the period 1999–2020. For the bottom oxygen data analysis, a pseudo-climatology is constructed by averaging the data over the period 2014-2024 due to data quality issues before 2014. The annual anomalies are expressed either in absolute units or as normalized quantities (i.e., by dividing by the standard deviation [sd] of the annual estimates over the same period). For the purpose of data interpretation, normalized anomalies are

considered near normal when within ±0.5 sd, slightly above/below normal when between ±0.5 sd and ±1 sd, and above/below normal otherwise (i.e., larger/smaller than ±1 sd).

A standard set of indices representing anomalies of nutrient availability, phytoplankton biomass, and the abundance of dominant zooplankton species and groups (*C. finmarchicus*, *Pseudocalanus* spp., total copepods, and total non-copepods) is produced in each of the AZMP regions, including the Maritimes Region. To visualize Northwest Atlantic shelf-scale patterns of variability, a zonal scorecard including observations from all AZMP regions is presented in a separate technical report (Galbraith et al. 2025).

3. OBSERVATIONS

3.1 Nutrients and Oxygen

The primary dissolved inorganic nutrients (i.e., nitrate, silicate, and phosphate) measured by the AZMP strongly co-vary in space and time (Petrie et al. 1999). For this reason, and because the availability of nitrogen is most often associated with phytoplankton growth limitation in coastal waters of the Maritimes Region (DFO 2000), this report focuses mainly on variability patterns for nitrate, with information on silicate and phosphate concentrations presented to help interpret phytoplankton taxonomic group succession at HL2 and P5 when phytoplankton abundance and taxonomic classification data are available.

3.1.1 High-frequency Sampling Stations

At HL2, the highest surface nitrate concentrations are typically observed in the winter when the water column is well mixed and primary production is low (Figure 5). Surface nitrate declines with the onset of the spring phytoplankton bloom, and the lowest surface nitrate concentrations are observed in spring through early fall. Deep-water nitrate concentrations are lowest from late fall until early spring, and increase from May to August, perhaps reflecting sinking and decomposition of the spring phytoplankton bloom (Petrie and Yeats 2000).

In 2024, the surface nitrate inventory over the 0-50 m layer at HL2 was near normal during the winter (January through early-April) and late-fall (mid-October through December; Figure 6). Otherwise, the surface nitrate inventory was mainly below normal, except for early-August (Figure 6) when the nitracline was temporarily observed higher in the water column (Figure 5). Overall, the surface nitrate annual inventory at HL2 was slightly lower than normal in 2024, in contrast with the previous five years when it was mainly near normal (Figure 7).

The subsurface nitrate inventory over the 50-150 m layer at HL2 was near normal from January to mid-April but remained slightly below or below normal for the rest of the year (Figure 6). Deep-water nitrate concentrations were especially lower than normal during the period of May to October, when they typically reach their highest levels (Figure 5). Overall, the annual subsurface nitrate inventory at HL2 was below normal in 2024 for a second consecutive year (Figure 7). The annual inventory of surface silicate was slightly below normal in 2024, while the subsurface inventory reached a record-low value, similar to 2018 (Figure 7). Both the surface and subsurface phosphate inventories were below normal in 2024, continuing the general pattern of below-normal conditions recorded during the previous ten years (Figure 7).

The nitrate dynamics at P5 differ considerably from those at HL2 due to the high nutrient input from the outflow of the nearby Saint John River, combined with the strong tidal mixing which contributes to a lower nitrate accumulation in the deep water while maintaining a higher overall surface inventory. The highest nitrate concentrations are typically observed in the winter and

late fall (Figure 5), when the water column is well mixed from surface to bottom and phytoplankton growth is minimal due to light limitation. Nitrate concentrations start to decline in the upper water column when the spring phytoplankton bloom starts in April or May, and the lowest surface nitrate concentrations and corresponding inventory are typically observed from May to September (Figures 5 and 6).

At P5 in 2024, the surface nitrate inventory was mainly near or slightly below normal throughout the year, except in May when it was below normal, reflecting earlier-than-normal and more intense nitrate depletion in the upper water column (Figures 5 and 6). The subsurface nitrate inventory was mainly near or slightly below normal throughout the year, except in late May and June when it was below normal (Figure 6). Overall, both the annual surface and subsurface nitrate inventories at P5 were slightly below normal in 2024, continuing the pattern of below-normal annual inventories observed during the previous nine years (Figure 7). In parallel with the nitrate conditions, the annual surface and subsurface inventories for phosphate at P5 were below and slightly below normal, respectively, continuing the general pattern of near- to below-normal annual inventories observed during the previous eleven years (Figure 7). On the other hand, weak positive anomalies for surface and subsurface silicate inventories were recorded in 2024 for a second consecutive year (Figure 7).

3.1.2 Broad-scale Surveys

During the spring survey, low nitrate concentrations were observed in the upper 50 m at all stations of all sections and were likely indicative of depleted surface nitrate conditions that typically follow the spring phytoplankton bloom (Figure 8a). Surface nitrate anomalies during spring were mainly negative across the region except at stations HL3, HL4, and BBL4, where weakly-positive or positive anomalies were observed (Figure 8a). For the 50-150 m subsurface layer, nitrate concentrations gradually increased with depth but the anomalies remained mainly negative except in central CSL (CSL4 and CSL5), and at the offshore stations of LL (LL9), HL (HL7), and BBL (BBL6 and BBL7) where weakly-positive or positive anomalies were observed (Figure 8a).

During the fall survey, low nitrate concentrations were also observed in the upper 50 m at all stations of all sections, suggesting that replenishment of the surface layer had not yet occurred (Figure 8b). Surface nitrate anomalies were variable within each section, with LL indicating positive anomalies at all but two of the eight stations sampled (Figure 8b). Similar to the spring survey, nitrate concentrations gradually increased with depth in the 50-150 m subsurface layer; however, the anomalies were variable within each section, with HL and BBL predominantly exhibiting negative anomalies (Figure 8b).

The highest nitrate concentrations during spring and fall were observed in the deep (i.e., >150 m) water of each core section, particularly in central CSL, and at the offshore stations of LL, HL, and BBL (Figures 8a and 8b). Nitrate concentrations below 50 m were notably consistently below normal during both spring and fall in 2024 in Emerald Basin (station HL3), at the shelf-break of the HL section (HL6), and at most shelf stations of BBL (Figures 8a and 8b).

Overall, the annual inventory of both surface and subsurface nitrate, silicate, and phosphate was mainly slightly below or below normal for all sections in 2024 (Figure 7). Record-low surface inventories were observed for CSL for all three nutrients (Figure 7). Surface and subsurface phosphate inventories have remained mainly near or below normal since 2015-16 for all sections (Figure 7).

Nitrate concentration profiles collected during the 2024 summer ecosystem trawl survey were used to estimate bottom nitrate fields using Barnes interpolation (Kelley et al. 2025) with

parameters tuned for the SS following Layton et al. (2025). The results indicated predominantly lower-than-normal bottom nitrate levels over most of the SS and the eastern GoM (Figure 9). However, higher-than-normal bottom nitrate concentrations were observed on St. Anns Bank and Banquereau Bank in area 4V, on Middle Bank, Sable Island Bank, and around Emerald Bank in area 4W, and at the shelf-break near Baccaro Bank and in the northern part of Lurcher Shoal in area 4X (Figure 9; refer to Figure 1 for location of major banks and basins).

The same approach was used to estimate bottom oxygen saturation fields during the 2024 summer ecosystem trawl survey. The highest saturation levels are typically observed over most of the shallow areas of the SS and in the BoF (Figure 10). In 2024, saturation levels near or below 60% (i.e., a threshold for moderately oxygenated water) were mainly observed in deeper water (i.e., at the shelf break along the Laurentian Channel in area 4V, in Emerald Basin in area 4W, in LaHave Basin in area 4X east, and in Georges, Crowell, and Jordan Basin in area 4X west) (Figure 10; refer to Figure 1 for location of major banks and basins). Due to quality issues with oxygen data collected before 2014, anomalies of bottom oxygen saturation were calculated using a shortened pseudo-climatology covering the years 2014-2024. The results indicated predominantly near- or lower-than-normal bottom oxygen saturation levels in the BoF and in shallow areas, including St Anns, Misaine and Banquereau Bank in area 4V, parts of Middle and Western Bank in area 4W, and Baccaro Bank, Lurcher Shoal and eastern GoM in area 4X (Figure 10). On the other hand, near- or above-normal bottom oxygen saturation levels were observed in the western Cabot Strait, Sable Island area, most of the central and western SS, and in the Northeast Channel and the nearby Georges and Crowell Basin (Figure 10).

3.2 Phytoplankton

Although phytoplankton temporal and spatial variability is high in coastal and shelf waters, a recurrent annual pattern is observed across the SS, including a pronounced spring diatom-dominated phytoplankton bloom and a smaller secondary fall bloom (e.g., Halifax-2, Figure 11). Blooms develop as phytoplankton growth outpaces losses due to grazing, sinking and other processes (Behrenfeld and Boss 2014). Spring bloom initiation is thought to be regulated by the light environment and temperature, starting with the onset of water column stratification in late winter and early spring (Sverdrup 1953). Bloom magnitude is thought to be regulated largely by nutrient supply, while bloom duration is regulated by both nutrient supply and, to a lesser extent, by loss processes such as aggregation-sinking, grazing by zooplankton (Johnson et al. 2012), and lysis (Mojica et al. 2016). Phytoplankton biomass is assessed in terms of two complementary indices: i) the integrated chlorophyll-*a* inventory derived from *in situ* measurements, and ii) the surface chlorophyll-*a* concentration derived from remote sensing observations. The abundance of the main phytoplankton functional groups (i.e., diatoms, dinoflagellates, ciliates, and flagellates) is not available for 2024; however, their annual anomalies are presented for prior years for consistency with previous reporting.

3.2.1 High-frequency Observations

The *in situ* chlorophyll-*a* concentration profiles at HL2 in 2024 indicated an initial relatively weak chlorophyll-*a* peak extending from the surface to ca. 60 m in mid-March (Figure 11). A second peak, representative of the spring phytoplankton bloom, was observed in early to mid-April and was characterized by a normal timing, a shorter-than-normal duration, and a higher-than-normal intensity (Figure 11). Similarly, observations of surface chlorophyll-*a* concentrations from remote sensing indicated a near-normal timing of the peak of the spring bloom, with, however, a normal intensity as expressed by the surface chlorophyll-*a* concentration averaged over the spring season (Figure 12 panel C). Following the spring phytoplankton bloom, the *in situ* chlorophyll-*a*

inventory remained near normal throughout the rest of the year, with no evidence of fall bloom conditions (Figure 11). A well-defined subsurface (ca. 20-40 m) chlorophyll-*a* maximum layer persisted from mid-June to late-September(Figure 11).

Surface chlorophyll-*a* measured by remote sensing remained near normal throughout the year (Figure 12 panel B) and suggested the occurrence of fall bloom conditions characterized by a slightly delayed onset and slightly lower-than-normal intensity (Figure 12 panel C). PAR-based euphotic depth estimates at HL2 were near or shallower than normal throughout the year in 2024, while Secchi-based estimates were fewer and more variable (Figure A1). Shallower euphotic depth estimates in April and August coincided with the peak of the spring bloom and the subsurface summer chlorophyll-*a* maximum, respectively (Figure 11). Overall, at HL2 in 2024, the annual estimate of the *in situ* chlorophyll-*a* inventory was normal, and the mean annual surface chlorophyll-*a* measured by remote sensing was near normal with a weak negative anomaly (Figure 13).

The chlorophyll-*a* dynamics at P5 differ considerably from those at HL2. The spring phytoplankton bloom typically occurs in June, followed by a secondary late-summer bloom occurring in late August to mid-September (Figure 11). The relatively high nitrate content in the surface layer (0-50 m) during summer (Figure 6) also sustains elevated chlorophyll-*a* inventories throughout this period. In 2024, the *in situ* chlorophyll-*a* concentration profiles at P5 indicated that the spring phytoplankton bloom peaked slightly earlier than normal and had a shorter-than-normal duration (Figure 11). The intensity of the spring bloom was above normal as indicated by the substantially large inventory and the higher-than-normal chlorophyll-*a* concentrations extending from the surface to the bottom of the water column in May (Figure 11). A second summer bloom of weaker magnitude also peaked slightly earlier than normal in late-July (Figure 11). Apart from the peak of the spring bloom, the *in situ* chlorophyll-*a* inventory at P5 in 2024 remained within near to slightly above or slightly below normal conditions for the rest of the year (Figure 11), such that its annual estimate for 2024 was slightly above normal for a second consecutive year (Figure 13). Surface chlorophyll-*a* concentrations measured by remote sensing and their derived spring and fall bloom metrics are not presented here as a new chlorophyll-*a* algorithm is being implemented for the processing of P5 data to account for the influence of the Case 2 water properties (e.g., high content of suspended matter) characteristic of the outer BoF. Both the PAR-based and Secchi-based estimates of the euphotic depth at P5 were mainly near or slightly shallower than normal in 2024 (Figure A1) and seemingly unaffected by the chlorophyll-*a* peaks observed in May and July (Figure 11).

3.2.2 Broad-scale Observations

The annual integrated *in situ* chlorophyll-*a* inventory in 2024 was below normal for CSL and LL, and near or slightly above normal for HL and BBL (Figure 14). The same pattern was observed for the spring anomalies (Figure B1), suggesting that the spring anomalies were the main drivers of the annual anomalies in 2024 and were possibly linked to the timing of *in situ* sampling relative to the timing of the spring bloom. The time series of the *in situ* chlorophyll-*a* inventory annual anomalies indicate considerable short-term variability (ca. one to three years) within each section, as well as important spatial variability within specific years (Figure 14).

Annual averages of surface chlorophyll-*a* concentrations measured by satellite remote sensing ranged from normal for CS, CSS, WSS, and LS, to slightly below normal for ESS and GB in 2024 (Figure 14). Except for GB, the annual surface chlorophyll-*a* concentrations in 2024 were in sharp contrast with the previous two years, when record-high values were observed in three of the sub-regions (Figure 14).

Contradictory patterns between the *in situ* integrated chlorophyll-*a* inventory and the surface chlorophyll-*a* concentrations from remote sensing are not unusual (e.g., years 2005 and 2006; Figure 14). These two indices are complementary and present inherent differences in the vertical extent of the signal they capture (i.e., surface vs. water column integrated), the temporal resolution of the observations (i.e., daily vs. semi-annual), and the spatial extent they represent (i.e., averaging over sub-regions vs. section means).

Observations of surface chlorophyll-*a* concentrations from satellite remote sensing indicated an earlier-than-normal timing of the peak of the spring bloom for CS and ESS, and near-normal to later-than-normal timing for CSS, WSS, LS, and GB (Figure 15, Figures 16a and 16b). On the other hand, except for LS, fall bloom initiation was later than normal across the region (Figure 15). The observed anomalies of the timing of the spring bloom translate to peak timing occurring around April 1 for CS, ESS, and CSS, and April 14 for WSS (Figures 16a and 16b). This supports in part the above statement linking the anomalies of the *in situ* chlorophyll-*a* inventory on the core sections to the timing of sampling relative to the timing of the spring bloom, where positive anomalies for HL (sampled on April 11-12) and BBL (sampled on April 18-19) resulted from sampling near the peak of the spring bloom, whereas negative anomalies on LL (sampled on April 27-29) and CSL (sampled on April 29-30) resulted from sampling after the spring bloom.

The spring and fall bloom intensity is expressed as the weighted-average surface chlorophyll-*a* concentration in each season. The intensity of the spring bloom in 2024 was mainly near or slightly below normal, except for LS where it was slightly above normal (Figure 15). On the other hand, the intensity of the fall bloom was mainly near normal across the region, except for CS where it was slightly below normal (Figure 15). Anomalies of the fall bloom intensity followed a longitudinal gradient with slightly negative values in the eastern area (CS and ESS), near-neutral values in the central and western shelf (CSS and WSS), and weakly positive values in the westernmost part of the region (LS and GB) (Figure 15). The weekly time series of surface chlorophyll-*a* concentrations indicate that concentrations in 2024 were relatively close to their climatological means for all sub-regions, except during the spring bloom for CS, during July and August for CSS, and during January for WSS and LS, when above-normal concentrations were observed (Figures 16a and 16b).

3.3 Zooplankton

Zooplankton are a diverse group of small animals that feed primarily on phytoplankton and hence, are a critical link between primary producers and larger organisms. AZMP sampling focuses on the mesozooplankton, those zooplankton in the size range ca. 0.2 to 20 mm in length. Copepods are the most abundant zooplankton organisms in the Northwest Atlantic, while the less abundant non-copepods consist mostly of larval stages of benthic invertebrates, carnivorous groups that feed on other zooplankton, and small-particle feeders. *Calanus finmarchicus* is a large, energy-rich, and broadly distributed copepod species throughout the region and represents an important prey for planktivorous consumers such as herring, mackerel, North Atlantic right whales, and other pelagic species. *Pseudocalanus* spp. are smaller and less energy-rich than *Calanus* spp., but they are also important prey for small fish due to their high abundance and wide spatial distribution. Zooplankton is primarily assessed here in terms of the abundance of copepods, non-copepods, *C. finmarchicus* and *Pseudocalanus* spp., and the biomass of the mesozooplankton of size class 0.2 to 10 mm.

3.3.1 High-frequency Sampling Stations

At HL2, the total abundance of zooplankton is, on average, lowest in January and February, and increases to maximum values in April, similar to the spring phytoplankton bloom peak timing, before declining to low levels again in the fall (Figure 17). In 2024, the total zooplankton abundance was mainly near or below normal throughout the year, except in late August when it was above normal (Figure 17). The zooplankton community at HL2 was dominated by copepods, similar to climatological conditions. Copepods represented approximately 85 to 90% or more of the total zooplankton abundance throughout most of the year, except in April when their contribution dropped to about 65% of the total abundance (Figure 17). Overall, at HL2, the annual mean abundances of copepods and non-copepods in 2024 were below normal and normal, respectively (Figure 18).

At P5, the total abundance of zooplankton is typically lowest from January through May and increases to maximum values between July and October, lagging the increase in phytoplankton by about a month (Figure 11), before declining to low levels again in the late fall (Figure 17). In 2024, zooplankton abundance was near or slightly above normal during winter, spring and late fall, and well below normal during summer and early fall (Figure 17). The relative abundance of cirripede nauplii (Others) and *Fritillaria borealis* (Cnidaria+Appendicularia) was above normal during spring, and that of euphausiid eggs (Euphausiidae+Decapoda) during summer (Figure 17). Overall, at P5, the annual mean abundances of copepods and non-copepods in 2024 were slightly below normal and normal, respectively, despite the very low total zooplankton abundances in summer and early fall (Figure 18).

Because copepods typically dominate the local zooplankton community at both stations, their seasonal abundance pattern closely follows that of total zooplankton abundance (Figure 17, Figure 19a, and Figure 19b). Therefore, the total copepod abundance at HL2 in 2024 was mainly near or below normal throughout the year, except in late August when it was above normal (Figure 19a). Among the eleven most abundant copepod taxa at HL2, only *Microcalanus* sp. and *Paracalanus* sp. had slightly-above or above-normal abundances in 2024 (Figure 20). A record-low abundance anomaly was recorded for *Metridia lucens* in 2024 (Figure 20) as its relative abundance remained below normal throughout the year (Figure 19a). Higher-than-normal relative abundances of *Microcalanus* sp. were observed during winter, early spring, and fall, and of *Pseudocalanus* spp. during May through July (Figure 19a). On the other hand, *Centropages* spp. were relatively less abundant than normal during late summer and fall (Figure 19a).

At P5, the total copepod abundance in 2024 was near normal during winter, spring, and late fall, and below normal during summer and early fall (Figure 19b). Annual average abundance of the nine most abundant taxa of the top nine copepod taxa was above normal for *C. finmarchicus* and *Microcalanus* sp., and normal to below normal for all other taxa (Figure 20). A record-low anomaly was recorded for *Centropages* spp. in 2024 as it was nearly absent throughout the year, with the exception of the fall (Figure 19b). A record-low anomaly was also recorded for *Temora longicornis* in 2024 due to the low relative abundance observed during summer when it is typically relatively more abundant (Figure 20). Above-normal relative abundances of *C. finmarchicus* were observed during spring and late summer, and of *Microcalanus* sp. throughout the year (Figure 19b). On the other hand, below-normal relative abundances were observed for *Acartia* spp., and for *Paracalanus* sp. during fall (Figure 19b).

The abundance of *C. finmarchicus* at HL2 in 2024 was near or slightly below normal throughout the year, except in April and December when it was slightly above normal (Figure 21). The first generation of *C. finmarchicus*, characterized by a higher abundance of early stages in spring, peaked slightly ahead of normal time in early April, and a second generation, albeit less

abundant, developed later in late July and August (Figure 21). The abundance of *C. finmarchicus* in January was low but normal, with stages CIV, CV, and CVI accounting for over 95% of the abundance at that time (Figure 21). The *C. finmarchicus* population during fall was dominated by stage CV with an above-normal proportion of CIV in November and December (Figure 21). Overall at HL2, the abundance of *C. finmarchicus* was slightly below normal in 2024, reverting to the pattern mainly observed over the 2011-2022 period (Figure 18 and Figure 20).

At P5, the abundance of *C. finmarchicus* was near or slightly above/below normal throughout the year in 2024, except in May and September when it was above normal (Figure 21). The first generation of *C. finmarchicus* peaked within the normal time interval in mid-May as indicated by the high relative abundance of early stages CI and CII. The development of a second generation in late July was considerably earlier and less intense compared to the peak typically observed in October (Figure 21). Overall at P5, the abundance of *C. finmarchicus* was above normal in 2024, which, along with 2019, contrasts with the sequence of mainly near- or below-normal abundances since 2012 (Figure 18 and Figure 20).

Zooplankton biomass typically peaks around April-May at HL2 and between July and October at P5 (Figure 22). There is a strong similarity in the annual variability pattern of dry and wet biomass at both the HL2 and P5 stations (Figure 22). The dry biomass estimates are a close representation of the mesozooplankton size class (i.e., 0.2 mm to 10 mm) while the wet biomass estimates can represent both mesozooplankton and macrozooplankton (i.e., larger than 10 mm), including gelatinous plankton. Wet biomass is not reported for samples containing large amounts of algae or jelly plankton. In 2024, the mesozooplankton dry biomass at HL2 was near or lower than normal throughout the year (Figure 22). The spring peak of zooplankton biomass was observed at the normal time in April (Figure 22). At P5, the mesozooplankton dry biomass was well above normal in June, August, and September, but otherwise mainly near or slightly below normal (Figure 22). The large biomass observed at P5 in September coincides with the above-normal abundance of *C. finmarchicus* CV at that time (Figure 21). Overall, the annual mean mesozooplankton dry biomass in 2024 was below normal at HL2 and above normal at P5 (Figure 18). For HL2, the 2024 biomass is the second lowest of the time series, similar to 1999 (Figure 18).

3.3.2 Broad-scale Surveys

The abundance of *C. finmarchicus* (Figure 23) and mesozooplankton dry biomass (Figure 24) during the winter ecosystem trawl survey in area 5Ze were respectively above normal and normal in 2024. Those averages were based on a total of eleven samples collected on Georges Bank (Figure 23 and Figure 24), which reflects the reduced spatial coverage of the newly implemented winter survey design in the Georges Bank area. The abundance *C. finmarchicus* during the 2024 summer ecosystem trawl survey was slightly below normal in area 4V and 4X, and normal in area 4W (Figure 23). The mesozooplankton biomass during summer was below or slightly below normal in all three areas (Figure 24). This continues a pattern observed since 2021, especially for area 4W (Figure 24).

The abundance of *C. finmarchicus* on the core sections during the 2024 spring survey was above or slightly above normal for all sections (Figure 25). Abundances were particularly high at the outer stations of BBL (BBL4 and BBL7) and the mid-shelf stations of HL (HL3 and HL4). During the fall survey, abundances were fairly uniform within each section; they were normal for LL, HL, and BBL, and slightly below-normal for CSL (Figure 25). Overall, the estimated annual abundance of *C. finmarchicus* was near normal or slightly above normal for all four sections (Figure 18). The mesozooplankton dry biomass was near or slightly below normal for all

sections during the spring 2024 survey, and slightly below or below normal during the fall survey (Figure 26). Record-low biomass levels were reached during fall for CSL and HL (Figure 26). Overall, the annual estimates of mesozooplankton biomass for 2024 varied from near normal to below normal for the core sections (Figure 18). For the central (HL) and easternmost (LL and CSL) sections, mesozooplankton biomass anomalies have remained mainly negative since 2015 while BBL has shown more variability during that period (Figure 18).

The annual abundance of *Pseudocalanus* spp. in 2024 reached a record-high anomaly for the HL section but was otherwise near normal for the other core sections (Figure 18). For HL, the abundance of *Pseudocalanus* spp. was near or above normal during both the spring and fall surveys (not shown). Total copepod abundance was slightly above normal for HL in 2024 but otherwise normal for the other core sections (Figure 18).

The non-copepod abundance anomalies for the core sections were variable in 2024 and followed a longitudinal gradient, going from above-normal abundance for CSL to normal abundance for BBL (Figure 18). For CSL, non-copepod abundance was in sharp contrast with 2023 when a record-low anomaly was reached (Figure 18). With the exception of polychaetes, ostracods, bivalves, and echinoderms, the abundance of all other major non-copepod groups was either near normal, slightly above, or above normal in 2024 (Figure 27). Ostracods have shown mainly lower-than-normal abundances since 2017, while other non-copepod groups have shown considerable inter-annual variability during recent years such that trends in their abundances are not apparent (Figure 27).

3.3.3 Indicator Species

The abundance of Arctic *Calanus* species (*C. hyperboreus* and *C. glacialis*) was near or below normal across the region in 2024, which is consistent with the general pattern observed since 2012 (Figure 28). Similarly, the abundance of warm-water offshore species (*Clausocalanus* spp., *Mecynocera clausi*, and *Pleuromamma borealis*) was below or slightly below normal across the region in 2024 (Figure 28). For CSL, this is consistent with the general pattern of near- or below-normal abundances observed in the last eight years. The abundance of warm-water shelf copepod species (the summer-fall copepods *Paracalanus* sp. and *Centropages typicus*) was slightly below normal for HL and P5, and near normal elsewhere in 2024 (Figure 28). Considerable spatial and temporal variability in the abundance of warm-water offshore and shelf species has been observed across the region during the last 6-8 years (Figure 28).

4. DISCUSSION

In the Maritimes Region, the Scotian Shelf (SS) pelagic environment is characterized by a strong annual temperature and stratification cycle, and spatial variability in the form of longitudinal and cross-shelf gradients. While the temperature annual cycle and its perturbations are mostly driven by meteorological forcing, spatial gradients are driven by the varying contributions of the dominant source water originating from the Gulf of St. Lawrence (GSL), the Labrador Current (LC), and the Gulf Stream (GS). Conditions at the tail of the Grand Banks (TGB), particularly sea surface height anomalies, are relevant in this context as they may help predict impending downstream shelf conditions with up to a year of lead time and with positive anomalies translating into reduced contribution of the LC to the shelf (Gonçalves Neto et al. 2021). Furthermore, Brickman et al. (2018) suggest that the interaction between the LC and the GS at the TGB leads to the creation of anomalous warm/salty (or cold/fresh) eddies that travel east-to-west along the shelf break, having direct impacts on the spatial variability of temperature and salinity. In addition, the complex bathymetry of the SS, with its shallow banks, deep basins,

and trenches, contributes to local circulation patterns (Hannah et al. 2001), which, combined with the temporal and spatial hydrographic patterns, have direct and indirect influences on the distribution and dynamics of plankton and nutrients in the region.

Ocean temperatures on the SS and in the eastern Gulf of Maine (GoM) have exhibited strong inter-decadal variability since the 1950s, with recent years (2010 and onward) being generally warmer than the long-term average. In 2024, although surface conditions continued to be warmer than normal across the region, bottom temperatures were near or cooler than normal in some areas (Figures 54 and 55 in Layton et al. 2025). The composite anomaly (i.e., the sum of normalized anomalies) for bottom temperature indices for 2024 was indeed the lowest since 2010 (Figure 55 in Layton et al. 2025). A similar cooling of bottom waters was also observed in 2024 in the GoM and was attributed to an influx of LC water entering the gulf through the Northeast Channel (Record et al., 2024). The mean annual stratification on the SS remained above normal in 2024; it reached its fourth-highest value of the 75-year time series and was consistent with the general increasing trend resulting from the combined warming and freshening of surface waters (Figures 41 and 42 in Layton et al. 2025). The contrasting pattern between surface (continued warming) and bottom (cooling) conditions likely reflects the influence of air-sea heat exchange on surface waters and changes in source water contribution in the region resulting from changes in shelf circulation, including positive shelfbreak transport anomalies (Figure 47 and Figure 48 in Layton et al. 2025), usually associated with negative deep temperature anomalies. These changes, combined with increased stratification, may be linked to changes observed in the nutrients and lower trophic level conditions presented in this report.

The nutrient environment on the SS is influenced by water inputs from upstream, including the outflow from the GSL through Cabot Strait, intrusions of slope water, and GS meanders (Pepin et al. 2013). The main advective source of nitrate and silicate for the SS is the GSL outflow during winter, while the contribution of on-shelf transport during summer can be almost as strong in some areas (Petrie and Yeats 2000). Surface nutrients display strong seasonality linked to phytoplankton production, with surface nutrient depletion typically associated with high production during spring and summer, followed by surface nutrient replenishment during late fall and winter when phytoplankton production is low and vertical mixing is high. On the other hand, deep nutrients, especially nitrate, provide a better representation of the nutrient pool available for new primary production. In addition to changes in shelf circulation, deep nitrate concentrations are also dependent on changes in the export of surface particulate nitrogen and its remineralization at depth, and on the vertical transport toward the surface via mixing and/or upwelling. Nutrient-poor subsurface conditions on the SS have been reported over the period 2010-2020 despite evidence of a GS-dominated water source (Lehmann et al. 2023). The general pattern of below-normal deep nutrient levels observed on LL, CSL, and BBL between ca. 2015 and 2020 (Figure 7) is consistent with the corresponding decreasing trend observed at the scale of the ESS, CSS, and WSS, respectively (Figure 4 in Lehmann et al. 2023).

Subsurface and bottom nitrate levels were predominantly below normal across the region in 2024. The strongest negative anomalies of the subsurface nitrate inventory were observed for HL2, due in part to low replenishment of the bottom layer during summer (Figure 5), and for the HL section, where strong negative anomalies were observed in both spring and fall in Emerald Basin (Figure 8a and 8b). Deep basins on the central SS are directly connected to the slope water, for which the properties are determined by the interactions between the LC and the GS (Zwanenburg et al. 2006). The below-normal subsurface nitrate levels observed in 2024 could be associated with an increased influence of lower-nutrient LC waters along the Scotian Slope, as reported in recent years (Hebert et al. 2024; Cyr et al. 2024). Increased contribution of LC water source to the shelf could also be responsible for the predominantly cooler-than-normal

bottom temperatures observed during summer in area 4W in 2024 (Figure 37 in Layton et al. 2025), which reached its coldest temperatures since 2008 (Figure 38 in Layton et al. 2025). Nevertheless, additional analyses are needed for a better understanding of the processes linking subsurface nutrient availability to changes in shelf circulation. Despite indications of increased nitrate and silicate levels in 2021 and 2022, the relatively low subsurface nutrient availability that has been observed since 2016, coupled with the increase in stratification observed on the SS, could drive lower primary productivity, with potential impacts on the community composition and productivity of the shelf ecosystem.

In ocean regions where annual-scale environmental variability is a dominant frequency, plankton life history, behaviour, and physiology provide adaptations that focus reproductive effort at favorable times of the year and minimize exposure to risk at unfavorable times of the year. However, unpredictable perturbations in the range of environmental seasonality and in seasonal timing can disrupt these adaptations (Greenan et al. 2008, Mackas et al. 2012). Large-scale shifts in water mass boundaries also influence local plankton community composition (e.g., Keister et al. 2011). The main recurring feature of the phytoplankton dynamics on the SS and in the GoM is the spring bloom, which generally develops under favorable conditions of increased insolation, warming water temperatures, and water column stratification and stability. However, Ross et al. (2017) observed spring blooms on the SS when stratification was at its lowest, water temperature at its coldest, and when the surface mixed layer was still much deeper than the euphotic depth, in apparent contradiction with Sverdrup's (1953) critical-depth hypothesis. Similar observations of phytoplankton spring bloom initiation in the absence of vertical stratification have also been reported in the GoM (Townsend et al. 1992) and on the Newfoundland and Labrador shelf (Cyr et al. 2023).

The higher-than-normal stratification on the SS in 2024, combined with the overall lower-than-normal nitrate levels across the region, was perhaps responsible for the return to normal chlorophyll-*a* conditions, following two consecutive years where satellite observations revealed record-high annual surface chlorophyll-a concentrations in some areas (Figure 14). In terms of chlorophyll dynamics, the timing of the spring phytoplankton bloom in 2024 followed to some extent the general pattern of westward progression (Song et al. 2010), with peak chlorophyll-*a* concentrations observed in late-March/early-April in the eastern and central parts of the region, to mid- to late-April in the western part of the region (Figure 16a and 16b). For the CS sub-region in particular, the timing of the spring bloom was considerably ahead of normal time by ca. 15 days in 2024 (occurring on March 31), and its intensity (as represented by the mean spring chlorophyll-*a* concentration) was normal (Figure 15). The earlier bloom conditions might have been driven in part by warmer-than-normal conditions, as sea-surface temperatures approximately 2.5 sd above normal were observed from February through April in that area (Figure 9 panel A in Layton et al. 2025). However, this appears to contradict Friedland et al. (2024), who suggest that warm winter conditions should have limited effects on spring bloom phenology but would instead result in a decreased bloom magnitude and intensity, and hence negative effects on overall bloom productivity. While phytoplankton growth increases with temperature (Eppley 1972), temperature effects are not solely responsible for controlling the seasonal evolution of phytoplankton populations since nutrient supply, light history, and other ecosystem-linked processes (e.g., grazing) also play prominent roles (Moisan et al. 2002).

Unusual chlorophyll-*a* dynamics were also observed from *in situ* measurements at the high-frequency sampling stations in 2024. At HL2, bloom-like conditions started to develop during March without, however, reaching peak intensity until mid-April (Figure 11). Early increases in phytoplankton biomass can be linked to intermittent events of mixed layer restratification (Lacour et al. 2017) or intermittency in vertical stability (Keerthi et al. 2021), typically associated with sufficiently long periods of reduced surface wind and cooling, at timescales of days, which

is necessary for phytoplankton population growth before the vernal restratification. In this case, peak bloom conditions were triggered by the increase in stratification (and the corresponding shoaling of the mixed layer) that occurred between the end of March and the start of April (Figure 17 in Layton et al. 2025). At P5, stratification plays a lesser role in the establishment of the spring bloom due to the strong tidal mixing. Nevertheless, the exceptionally high levels of chlorophyll-*a* reached during the 2024 spring bloom at P5 are difficult to interpret as they coincided with low nitrate levels and high abundance of *C. finmarchicus*, thus combining for low nutrient uptake and increased grazing pressure. It is worth noting that *in situ* water temperature anomalies during the spring bloom period were +0.5 to +1 sd from surface to ca. 50 m at HL2, and +1 sd from surface to ca. 75 m at P5 (Figure 15 and Figure 12 in Layton et al. 2025, respectively), reinforcing the expected effect of temperature on phytoplankton growth during the period of the bloom. Chlorophyll dynamics at HL2 also indicate a relatively strong and lengthy subsurface chlorophyll-*a* maximum that occurred from mid-June to late September in 2024 (Figure 11), which benefited from an upward flux of nitrate in early August (Figure 5). Although summertime chlorophyll is a poor proxy of the phytoplankton biomass (Craig et al., 2015), the presence of chlorophyll subsurface maxima is nevertheless indicative of phytoplankton production in the subsurface layer, which can represent a significant portion of the annual primary production on the SS (Ross et al. 2017).

The period from 2011 to 2022 was characterized by a persistent change in the zooplankton assemblage on the SS, marked most notably by the decline in the abundance of *C. finmarchicus*, the biomass-dominant member of the zooplankton assemblage, and an associated decline in mesozooplankton biomass. The year 2011 marked a regime shift to lower biomass of *Calanus* spp. on the SS, which coincided with a shift to warmer temperatures (Sorochan et al. 2019). However, in 2023 and 2024, *C. finmarchicus* abundance returned to near- or above-normal levels in the region, while the mesozooplankton biomass remained below normal, except in the BoF (P5) (Figure 18). Stage-specific abundance of *C. finmarchicus* reveals above-normal levels of early-stage individuals, particularly CI and CII, in recent years (Figure B2), which explains in part the counterintuitive relationship between *C. finmarchicus* abundance and mesozooplankton biomass for most areas, with the exception of P5 where both indices are concordant.

The winter abundance level of *C. finmarchicus* is an indicator of initial conditions for production, while the late-fall abundance level is an indicator of the overwintering stock for production in the following year. At HL2, a ten-fold decrease in the abundance of *C. finmarchicus* was observed between the successive samples collected on December 6, 2023 (Figure 22 in Casault et al. 2025) and January 24, 2024 (Figure 21). This decline in abundance likely reflects a combination of advective losses and mortality due to predation (e.g., Wiebe et al. 2022).

Declining *C. finmarchicus* abundance as observed in previous years is particularly significant because copepods of the genus *Calanus* are an important food source for the endangered North Atlantic right whale (Pershing and Stamieszkin 2020), and the decline in *C. finmarchicus* abundance observed during the last decade has been linked to changes in the foraging environment and habitat use of right whales (Meyer-Gutbrod et al. 2021). During the same period, *in situ* observations as well as observations from the Continuous Plankton Recorder (Casault et al. 2024) both suggest changes in the phytoplankton community characterized by a higher abundance of smaller taxa and lower abundance of larger diatoms, with possible effects on the zooplankton assemblage. It is still unclear whether the return of *C. finmarchicus* abundance to near or above normal levels observed in 2023 and 2024 signals a return to more normal conditions for this species or, alternatively, a change in its seasonal dynamics as seen at HL2 and P5. On the one hand, at HL2 in 2024, the first generation peaked slightly earlier than normal, suggesting earlier emergence from diapause and resumption of active development,

and the late-summer and fall production was more intense with higher relative abundances of early stages. On the other hand, at P5 in 2024, a weak second generation developed in late July, nearly two and a half months ahead of normal time and coinciding with the summer phytoplankton bloom. Match/mismatch between phytoplankton and zooplankton resulting from shifts in their respective phenologies can have important consequences throughout the entire food web (e.g., Suchy et al. 2022).

Warmer temperatures are often associated with a shift to a smaller average size in the copepod community (Campbell et al. 2021). Although recent years point toward cooling of bottom water, surface conditions continue to be warmer than normal (Layton et al. 2025), which could favour a switch to smaller species as seen by near- or above-normal abundances of *O. similis*, *Pseudocalanus* spp., *Paracalanus* sp., and *Microcalanus* sp. at the high-frequency sampling stations in recent years (Figure 20). *Pseudocalanus* spp., in particular, an important food source for larval and juvenile fish, has been more abundant than normal over the last decade on the Newfoundland and Labrador shelf (Bélanger et al. in preparation[1]).

The relationships among environmental and plankton conditions are complex, and their interpretation from a deterministic perspective requires a comprehensive analysis that is beyond the scope of this report. However, observations in recent years provide increasing evidence for changes in deep-nutrient availability, coupled with a shift in both phytoplankton and zooplankton communities away from the dominance of large phytoplankton cells and large, energy-rich copepods like *C. finmarchicus* toward smaller phytoplankton and copepod species. Since "classical" food webs, dominated by diatoms and *C. finmarchicus,* are associated with more efficient transfer of energy to higher trophic level pelagic animals than are food webs dominated by small phytoplankton cells and small zooplankton taxa, this shift may indicate a change to less-productive conditions for planktivorous fish, marine mammals, and planktivorous or piscivorous seabirds in the Maritimes Region.

5. SUMMARY

- Surface nitrate inventories were mainly below normal in the region in 2024, with a record-low inventory observed for CSL. The surface nitrate inventory at P5 in 2024 remained below normal for a tenth consecutive year.
- Subsurface nitrate inventories were also mainly below normal across the region in 2024. The subsurface nitrate inventory at P5 in 2024 also remained below normal for a tenth consecutive year. With the exception of 2021 and 2022, subsurface nitrate inventories have remained mainly below normal across the region since 2016.
- The inventory of *in situ* chlorophyll-*a* over the 0–100 m layer was mainly near or slightly above normal in the central (HL and HL2) and western (BBL and P5) parts of the region in 2024. Negative anomalies were observed in the eastern (LL and CSL) part of the region, owing partly to sampling on those sections having occurred after the spring phytoplankton bloom. On the other hand, the mean annual surface chlorophyll-*a* measured by remote sensing was mainly near normal across the region in 2024.
- Remote sensing observations of surface chlorophyll-*a* indicated that the peak of spring phytoplankton bloom in 2024 was earlier than normal in the eastern (CS and ESS) part

[1] Bélanger, D., et al. Biogeochemical oceanographic conditions on the Newfoundland and Labrador Shelf during 2023 and 2024. Can. Tech. Rep. Fish. Aquat. Sci. In preparation.

of the region but otherwise near or later than normal elsewhere. The intensity of the spring phytoplankton bloom was mainly near or slightly below normal across the region, except for LS where it was slightly above normal. On the other hand, the onset of the fall phytoplankton bloom was mainly later than normal, with a record-late timing observed for ESS. The intensity of the fall phytoplankton bloom was slightly lower than normal in the east, near normal on the central SS, and slightly higher than normal in the west.

- The abundance of phytoplankton taxonomic groups was not available in 2024 due to the unavailability of a trained phytoplankton taxonomist. These observations, when available, complement the interpretation of the phytoplankton biomass and phenology indices.
- The abundance of copepods in 2024 was near normal for the core sections, but negative anomalies were recorded at HL2 and P5. The abundance of non-copepods was near normal in the central (HL and HL2) and western (BBL and P5) parts of the region and above normal in the eastern (CS and ESS) part of the region in 2024.
- The abundance of *C. finmarchicus* in 2024 was slightly below normal at HL2 but otherwise near or above normal elsewhere, with P5 indicating the strongest positive anomaly. The abundance of *Pseudocalanus* spp. was mainly near normal across the region in 2024, except for HL where a record-high positive anomaly was observed.
- The mesozooplankton biomass was mainly below normal across the region in 2024, except at P5 where it was above normal owing to large biomass levels measured during summer. The mesozooplankton biomass at HL2 in 2024 was similar to the record-low biomass level observed in 1999.
- The abundance of Arctic *Calanus* species was near or below normal across the region in 2024. Similarly, the abundance of warm-water offshore copepod species was mainly below normal across the region in 2024. The abundance of warm-water shelf copepod species was near normal, except for HL and P5 where negative anomalies were observed.

6. ACKNOWLEDGEMENTS

The authors thank the personnel at the Bedford Institute of Oceanography and St. Andrews Biological Station who contributed to sample collection, sample analysis, data analysis, data management, and data sharing. We also thank the officers and crews of the Canadian Coast Guard Ships *Capt. Jacques Cartier,* S*igma-T*, *Teleost, Viola M. Davidson,* the Passamaquoddy Recognition Group Inc. *Hartford Hybrid*, and the British RRS *Discovery,* for their assistance in the collection of oceanographic data during 2024. Reviews by Marjolaine Blais (Maurice Lamontagne Institute, Québec Region) and David Bélanger (Northwest Atlantic Fisheries Centre, Newfoundland and Labrador Region) improved the manuscript.

7. REFERENCES

Beazley, L., Cardoso, D., Gordon, C., and Gjerdrum, C. 2024. Mission Report for the Maritimes Region Atlantic Zone Monitoring Program 2024 Spring Survey (TEL2024880). Can. Tech. Rep. Hydrogr. Ocean Sci. 386: vii + 102 p.

Beazley, L., Lawson, M., Colbourne, N., Gordon, C., Upson, P., Gjerdrum, C., Warman, K., Cardoso, D. 2025. Mission Report for the Maritimes Region Atlantic Zone Monitoring Program 2024 Fall Survey (DY18402). Can. Tech. Rep. Hydrogr. Ocean Sci. 402: vii + 109 p.

Behrenfeld, M.J., and Boss, E.S. 2014. Resurrecting the Ecological Underpinnings of Ocean Plankton Blooms. Annu. Rev. Mar. Sci. 6: 167–194.

Brickman, D., Hebert, D., and Wang, Z. 2018. Mechanism for the recent ocean warming events on the Scotian Shelf of eastern Canada. Cont. Shelf Res. 156: 11–22.

Campbell, M. D. et al. 2021. Testing Bergmann's rule in marine copepods. Ecography. 44: 1283–1295.

Casault, B., Beazley, L., Johnson, C., Devred, E., and Head, E. 2024. Chemical and Biological Oceanographic Conditions on the Scotian Shelf and in the Eastern Gulf of Maine during 2022. Can. Tech. Rep. Fish. Aquat. Sci. 3589 : vi + 72 p.

Casault, B., Johnson, C.L., Devred, E., and Beazley, L. 2025. Chemical and Biological Oceanographic Conditions on the Scotian Shelf and in the Eastern Gulf of Maine during 2023. Can. Tech. Rep. Fish. Aquat. Sci. 3658: vi + 57 p.

Churilova, T., Suslin, V., Krivenko, O., Efimova, T., Moiseeva, N., Mukhanov, V., and Smirnova L. 2017. Light Absorption by Phytoplankton in the Upper Mixed Layer of the Black Sea: Seasonality and Parametrization. Frontiers in Mar. Sci. 4: 90.

Clay, S., Peña, A., DeTracey, B., and Devred, E. 2019. Evaluation of Satellite-Based Algorithms to Retrieve Chlorophyll-a Concentration in the Canadian Atlantic and Pacific Oceans. Remote Sens. 11(22): 2609.

Clay, S., Layton, C., and Devred, E. 2021. BIO-RSG/PhytoFit: First release (Version v1.0.0). Zenodo.

Craig, S.E., Thomas, H., Jones, C.T., Li, W.K., Greenan, B.J., Shadwick, E.H., and Burt, W.J., 2015. The effect of seasonality in phytoplankton community composition on CO2 uptake on the Scotian Shelf. J. Mar. Syst. 147:52–60.

Cyr, F., Lewis, K., Bélanger, D., Regular, P., Clay, S., and Devred, E. 2023. Physical controls and ecological implications of the timing of the spring phytoplankton bloom on the Newfoundland and Labrador shelf. Limn. Ocean. Letters.

Cyr, F., Coyne, J., Snook, S., Bishop, C., Galbraith, P.S., Chen, N., Han, G. 2024. Physical Oceanographic Conditions on the Newfoundland and Labrador Shelf during 2023. Can. Tech. Rep. Hydrogr. Ocean Sci. 382: iv + 54 p.

DFO. 2000. Chemical and Biological Oceanographic Conditions in 1998 and 1999 – Maritimes Region. DFO Sci. Stock Status Rep. G3-03 (2000).

Eppley, R.W. 1972. Temperature and phytoplankton growth in the sea. Fishery Bull. 70(4): 1063–1085.

Friedland, K.D., Nielsen, J.M., Record, N.R, Brady, D.C., and Morrow, C.J. 2024. The phenology of the spring phytoplankton bloom in the North Atlantic does not trend with temperature. Elem. Sci. Anth., 12: 1.

Galbraith, P.S., Lizotte, M., Blais, M., Bélanger, D., Casault, B., Coyne, J., Layton, C., AzetsuScott, K., Beazley, L., Chassé, J., Clay, S., Cyr, F., Devred, E., Fudge, A., Gabriel, C.-E., Greenan, B., Hébert, A.-J., Johnson, C.L., Maillet, G., Penney, J., Rastin, S., Ringuette, M., Shaw, J.-L., Snook, S., Starr, M. 2025. Oceanographic conditions in the Atlantic zone in 2024. Can. Tech. Rep. Hydrogr. Ocean. Sci. 400 : viii + 49 p.

Gonçalves Neto, A., Langan, J.A., and Palter, J.B. 2021. Changes in the Gulf Stream preceded rapid warming of the Northwest Atlantic Shelf. Commun. Earth Environ. 2(74).

Greenan B.J.W., Petrie B.D., Harrison W.G., Strain P.M. 2008. The onset and evolution of a spring bloom on the Scotian Shelf. Limnol. Oceanogr. 53(5): 1759-1775.

Hannah, C. G., Shore, J. A., Loder, J. W., and Naimie, C. E. (2001). Seasonal circulation on the western and central Scotian Shelf. J. Phys. Oceanogr., 31(2), 591–615.

Harrison, G., Colbourne, E., Gilbert, D., and Petrie, B. 2005. Oceanographic Observations and Data Products Derived from Large-scale Fisheries Resource Assessment and Environmental Surveys in the Atlantic Zone. AZMP/PMZA Bull. 4: 17–23.

Hebert, D., Layton, C., Brickman, D., and Galbraith, P.S. 2024. Physical Oceanographic Conditions on the Scotian Shelf and in the Gulf of Maine during 2023. Can. Tech. Rep. Hydrogr. Ocean Sci. 380: vi + 71 p.

Holmes, R.W. 1970. The Secchi Disk in Turbid Coastal Waters. Limnol. Oceanogr. 15(5): 688–694.

Johnson, C., Harrison, G., Head, E., Casault, B., Spry, J., Porter, C., and Yashayaev, I. 2012. Optical, Chemical, and Biological Oceanographic Conditions in the Maritimes Region in 2011. DFO Can. Sci. Advis. Sec. Res. Doc. 2012/071.

Keerthi, M.G., Lévy, M., and Aumont, O. 2021. Intermittency in phytoplankton bloom triggered by modulations in vertical stability. Sci. Rep. 11, 1285.

Keister, J.E., Di Lorenzo, E., Morgan, C.A., Combes, V., and Peterson, W.T. 2011. Zooplankton species composition is linked to ocean transport in the Northern California Current. Global Change Biol. 17: 2498–2511.

Kelley, D., and Richards, C. 2025. oce: Analysis of Oceanographic Data. R package version 1.8-4.

Lacour, L., Ardyna, M., Stec, K., Claustre, H., Prieur, L., Poteau, A., Ribera D'Alcala, M., and Iudicone, D. 2017. Unexpected winter phytoplankton blooms in the North Atlantic subpolar gyre. Nature Geosci. 10: 836–839.

Layton, C., Brickman, D., Greenan, B., Galbraith, P.S., and Shaw, J.-L. 2025. Physical Oceanographic Conditions on the Scotian Shelf and in the Gulf of Maine during 2024. Can. Tech. Rep. Hydrogr. Ocean Sci. 403: vi + 82 p.

Lehmann, N., Reed, D.C., Buchwald, C., Lavoie, D., Yeats, P.A., Mei, Z.-P., and Johnson, C.L. 2023. Decadal Variability in Subsurface Nutrient Availability on the Scotian Shelf Reflects Changes in the Northwest Atlantic Ocean. J. Geophys. Res.: Oceans. 128: e2023JC019928.

Lenth, R., Bolker, B., Buerkner, P., Giné-Vázquez, I., Herve, M., Jung, M., Love, J., Miguez, F., Riebl, H., and Singmann, H. 2024. emmeans: Estimated Marginal Means, aka Least-Squares Means. R package version 1.10.1.

Mackas, D.L., Greve, W., Edwards, M., Chiba, S., Tadokoro, K., Eloire, D., Mazzocchi, M.G., Batten, S., Richardson, A.J., Johnson, C., Head, E., Conversi, A., and Pelosi, T. 2012. Changing zooplankton seasonality in a changing ocean: Comparing time series of zooplankton phenology. Progr. Oceanogr. 97–100: 31–62.

Meyer-Gutbrod, E.L., Greene, C.H., Davies, K.T.A., and Johns, D.G. 2021. Ocean regime shift is driving collapse of the north Atlantic right whale population. Oceanography 34: 22–31.

Mitchell, M., Harrison, G., Pauley, K., Gagné, A., Maillet, G., and Strain, P. 2002. Atlantic zonal monitoring program sampling protocol. Can. Tech. Rep. Hydrogr. Ocean Sci. 223.

Moisan, J.R., Moisan, T.A., and Abbott, M.R. 2002. Modelling the effect of temperature on the maximum growth rates of phytoplankton populations. Ecol. Model. 153: 197–215.

Mojica, K.D.A., Huisman, J., Wilhelm, S.W., and Brussaard, C.P.D. 2016. Latitudinal variation in virus-induced mortality of phytoplankton across the North Atlantic Ocean. ISME J. 10: 500–513.

O'Reilly, J.E., Maritorena, S., Mitchell, B. G., Siegel, D. A., Carder, K. L., Garver, S. A., Kahru, M., and McClain, C. R. 1998. Ocean color chlorophyll algorithms for SeaWiFS. J. Geophys. Res. 103: 24937–24953.

Pepin, P., Maillet, G.L., Lavoie, D., and Johnson, C. 2013. Temporal trends in nutrient concentrations in the Northwest Atlantic basin. Ch. 10 (pp. 127–150) In: Aspects of climate change in the Northwest Atlantic off Canada [Loder, J.W., G. Han, P.S. Galbraith, J. Chassé and A. van der Baaren (Eds.)]. Can. Tech. Rep. Fish. Aquat. Sci. 3045: x + 190 p.

Pershing, A.J. and Stamieszkin, K. 2020. The North Atlantic Ecosystem, from Plankton to Whales. Annu. Rev. Mar. Sci. 12(1): 339–359.

Petrie, B. 2007. Does the North Atlantic oscillation affect hydrographic properties on the Canadian Atlantic continental shelf? Atmos. Ocean 45(3): 141–151.

Petrie, B., and Yeats, P. 2000. Annual and interannual variability of nutrients and their estimated fluxes in the Scotian Shelf - Gulf of Maine region. Can. J. Fish. Aquat. Sci. 57: 2536–2546.

Petrie, B., Yeats, P., and Strain, P. 1999. Nitrate, Silicate and Phosphate Atlas for the Scotian Shelf and the Gulf of Maine. Can. Tech. Rep. Hydrogr. Ocean Sci. 203.

Record, N.R., A.J. Pershing, and Rasher, D.B. 2024. Early warning of a cold wave in the Gulf of Maine. *Oceanography* 37(3):6–9.

Ross, T., Craig, S.E., Comeau, A., Davis, R., Dever, M., and Beck, M. 2017. Blooms and subsurface phytoplankton layers on the Scotian Shelf: Insights from profiling gliders. J Marine Syst. 172: 118–127.

Song, H., Ji, R., Stock, C., et Wang, Z. 2010. Phenology of phytoplankton blooms in the Nova Scotian Shelf–Gulf of Maine region: remote sensing and modeling analysis. *J. Plankton Res.,* 32(11), 1485–1499.

Sorochan, K.A., Plourde, S., Morse, R., Pepin, P., Runge, J., Thompson, C., and Johnson, C.L. 2019. North Atlantic right whale (Eubalaena glacialis) and its food: (II) interannual variations in biomass of Calanus spp. on western North Atlantic shelves. J. Plankton Res. 41(5): 687–708.

Suchy, K.D., Young, K., Galbraith, M., Perry, R.I., and Costa, M. 2022. Match/Mismatch Between Phytoplankton and Crustacean Zooplankton Phenology in the Strait of Georgia, Canada. Front. Mar. Sci. 9.

Sverdrup, H.U. 1953. On Conditions for the Vernal Blooming of Phytoplankton. J. Cons. Perm. Int. Explor. Mer. 18: 287–295.

Therriault, J.-C., Petrie, B., Pepin, P., Gagnon, J., Gregory, D., Helbig, J., Herman, A., Lefaivre, D., Mitchell, M., Pelchat, B., Runge, J., and Sameoto, D. 1998. Proposal for a Northwest Atlantic Zonal Monitoring Program. Can. Tech. Rep. Hydrogr. Ocean Sci. 194.

Townsend, D.W., Keller, M.D., Sieracki, M.E., and Ackleson, S.G. 1992. Spring phytoplankton blooms in the absence of vertical water column stratification. Nature. 360: 59–62.

Utermöhl, von H. 1931. Neue Wege in der quantitativen Erfassung des Plankton.(Mit besonderer Berücksichtigung des Ultraplanktons.). Verh. Int. Verein. Theor. Angew. Limnol. 5**:** 567–595.

Wiebe, P.H., Baumgartner, M.F., Copley, N.J., Lawson, G.L., Davis, C., Ji, R., and Greene, C.H. 2022. Does predation control the diapausing stock of Calanus finmarchicus in the Gulf of Maine?. Progr. Oceanogr., 206.

Zwanenburg, K.C.T., Bundy, A., Strain, P., Bowen, W.D., Breeze, H., Campana, S.E., Hannah, C., Head, E., and Gordon, D. 2006. Implications of ecosystem dynamics for the integrated management of the Eastern Scotian Shelf. Can. Tech. Rep. Fish. Aquat. Sci. 2652: xiii + 91 p.

8. TABLES

Table 1. Atlantic Zone Monitoring Program sampling surveys in the Maritimes Region in 2024.

Group	Location	Survey ID	Dates	# Hydro Stations	# Net Stations
Ecosystem Trawl Survey - Winter	Western Scotian Shelf/Georges Bank/Bay of Fundy	TEL2024-002	Mar 2–Apr 2	108	18
Ecosystem Trawl Survey - Summer	Scotian Shelf	CAR2024-010	Jun 25–Aug 6	239	44
Seasonal Sections - Spring	Scotian Shelf	TEL2024-880	Apr 11–May 1	79	72
Seasonal Sections - Fall	Scotian Shelf	DY18402	Oct 4–Oct 22	71	65
High-frequency Stations	Halifax-2	BCD2024-666	Jan 12–Dec 6	20(7)[1]	17(5)[1]
High-frequency Stations	Prince 5	BCD2024-669	Jan 12–Dec 12	13	14
			Total:	517	218

[1]For Halifax-2, the first number indicates the total number of occupations (including occupations during the ecosystem trawl surveys and the seasonal sections), and the number in parentheses indicates the number of dedicated occupations with station-specific survey ID. For high-frequency station Halifax-2, bottle samples were only collected on 19 of 20 occupations.

9. FIGURES

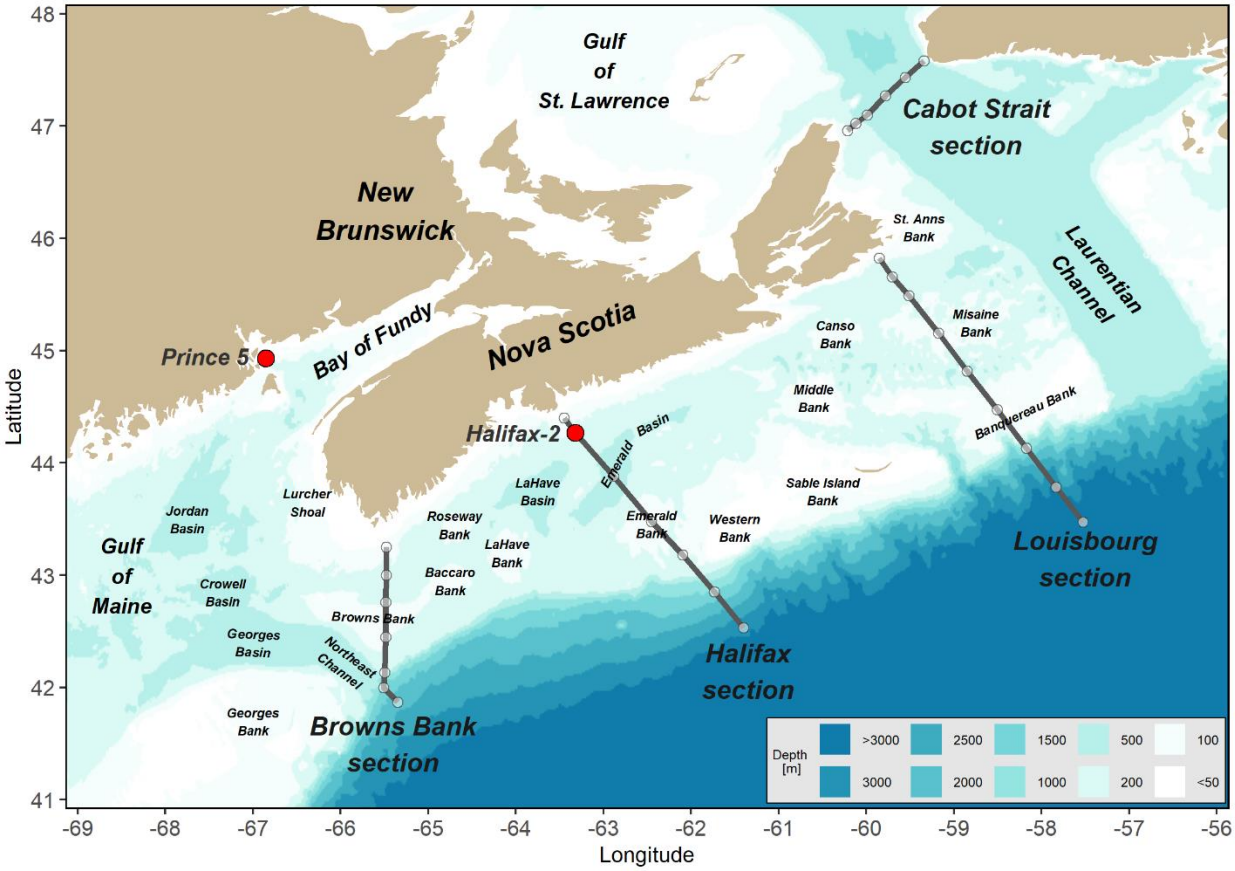

Figure 1. Map of core sections (Cabot Strait [CSL]; Louisbourg [LL]; Halifax [HL]; Browns Bank [BBL]) and high-frequency sampling stations (Halifax-2 [HL2]; Prince 5 [P5]) sampled in the DFO Maritimes Region. Gray open circles indicate the location of sampling stations on each section.

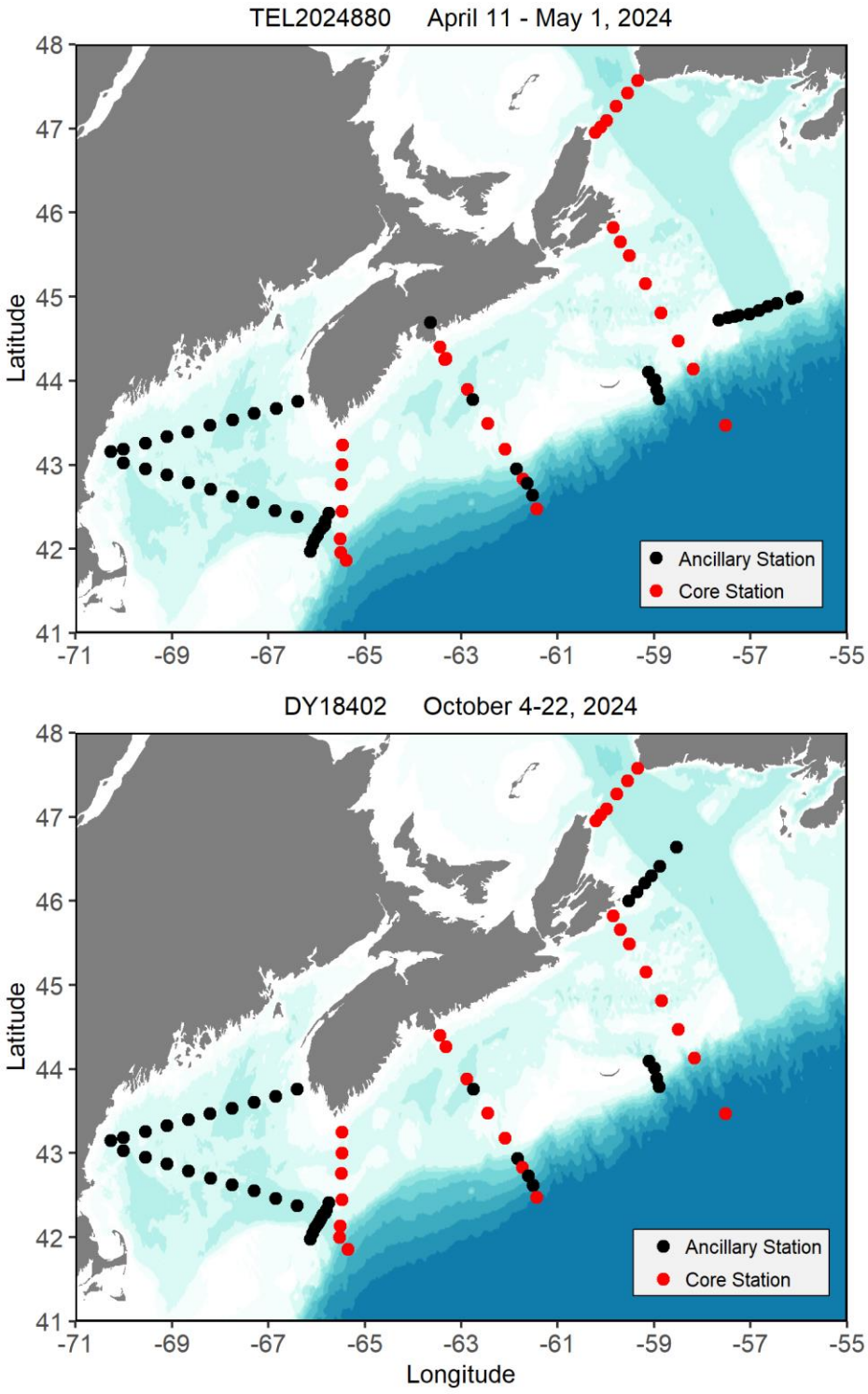

Figure 2. Stations sampled during the 2024 spring (top panel) and fall (bottom panel) surveys. Red markers indicate core stations and black markers indicate stations sampled for ancillary programs.

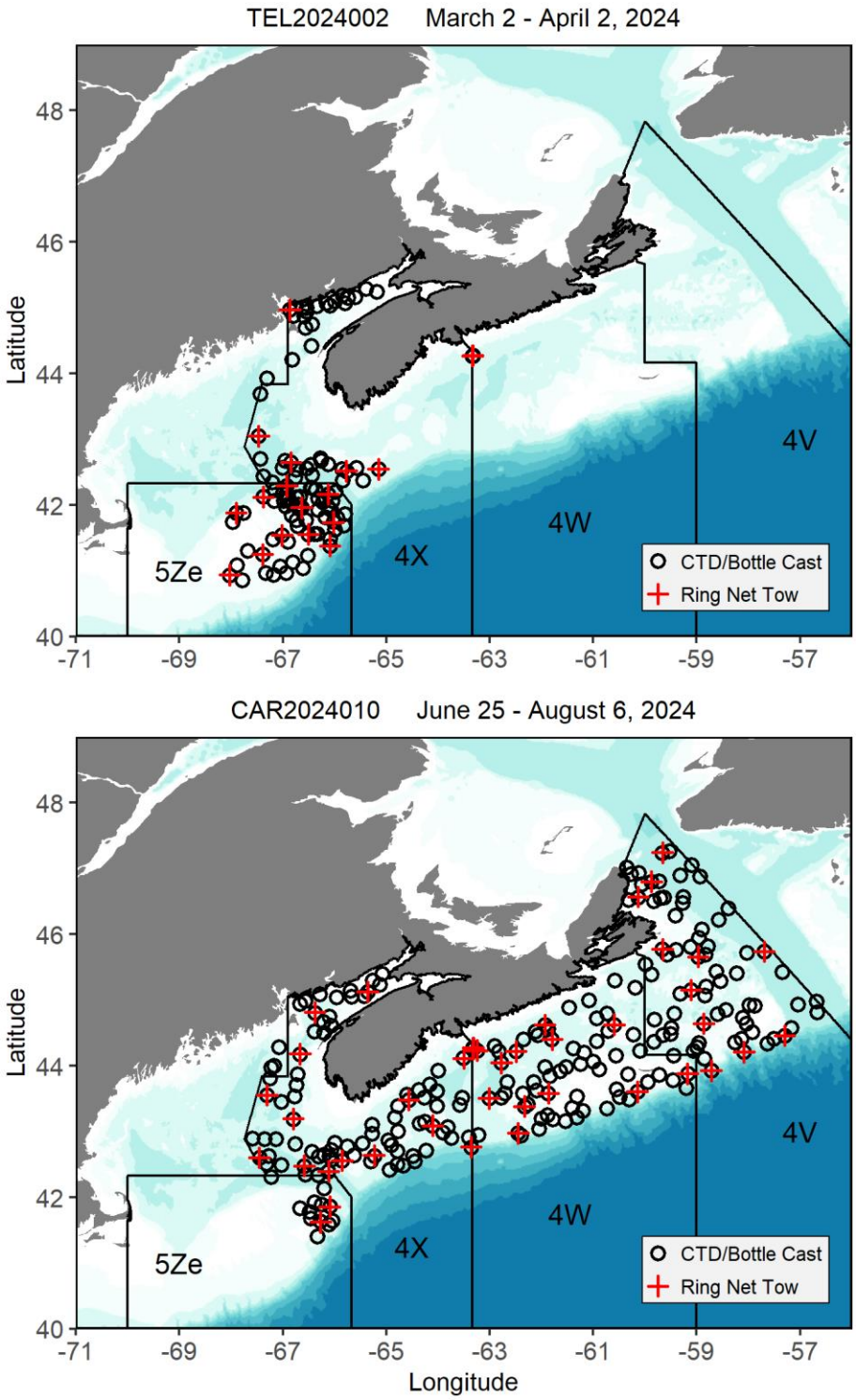

Figure 3. Stations sampled during the 2024 winter (top panel) and summer (bottom panel) ecosystem trawl surveys. Station locations are superimposed on NAFO areas.

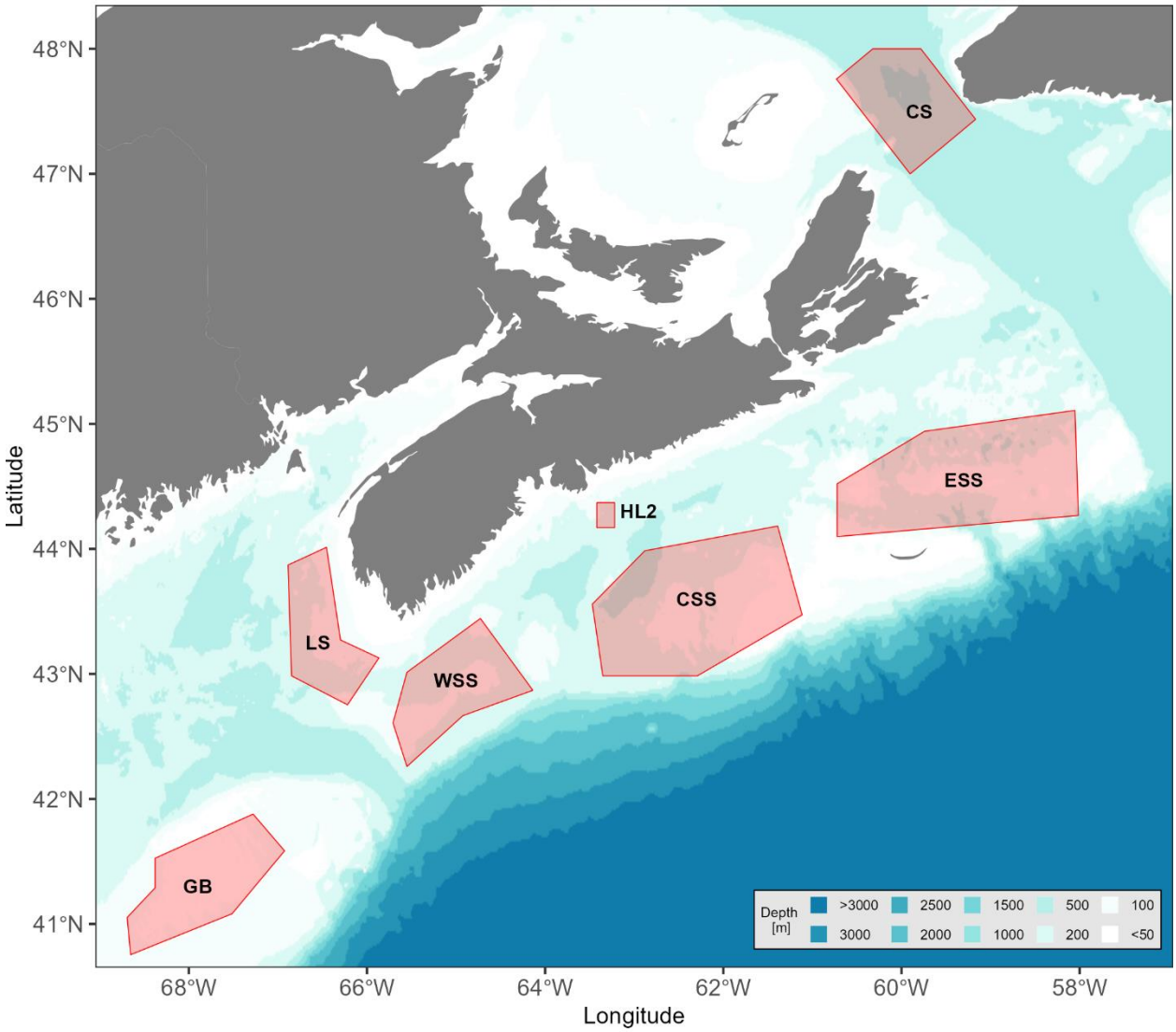

Figure 4. Sub-regions in the Maritimes Region identified for spatial/temporal analysis of satellite ocean color data. Halifax-2 [HL2]; Cabot Strait [CS]; Eastern Scotian Shelf [ESS]; Central Scotian Shelf [CSS]; Western Scotian Shelf [WSS]; Lurcher Shoal [LS]; Georges Bank [GB].

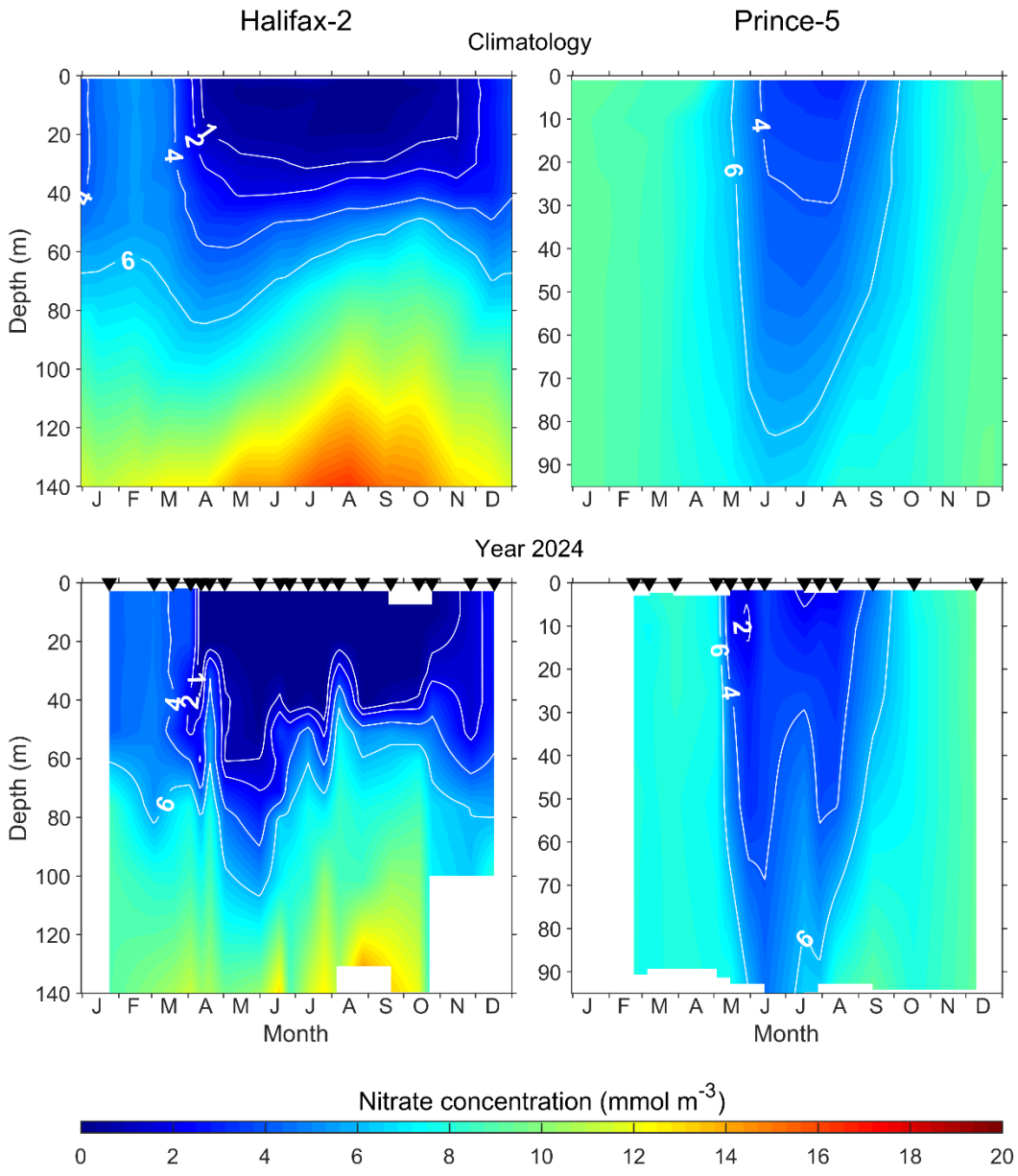

Figure 5. Nitrate concentrations at the Maritimes high-frequency sampling stations. Top panels: Climatological mean vertical structure of nitrate concentrations for the reference period 1999-2020. Bottom panels: Vertical structure of nitrate concentrations in 2024. Black triangles in the bottom panels indicate sampling dates. White areas indicate no data.

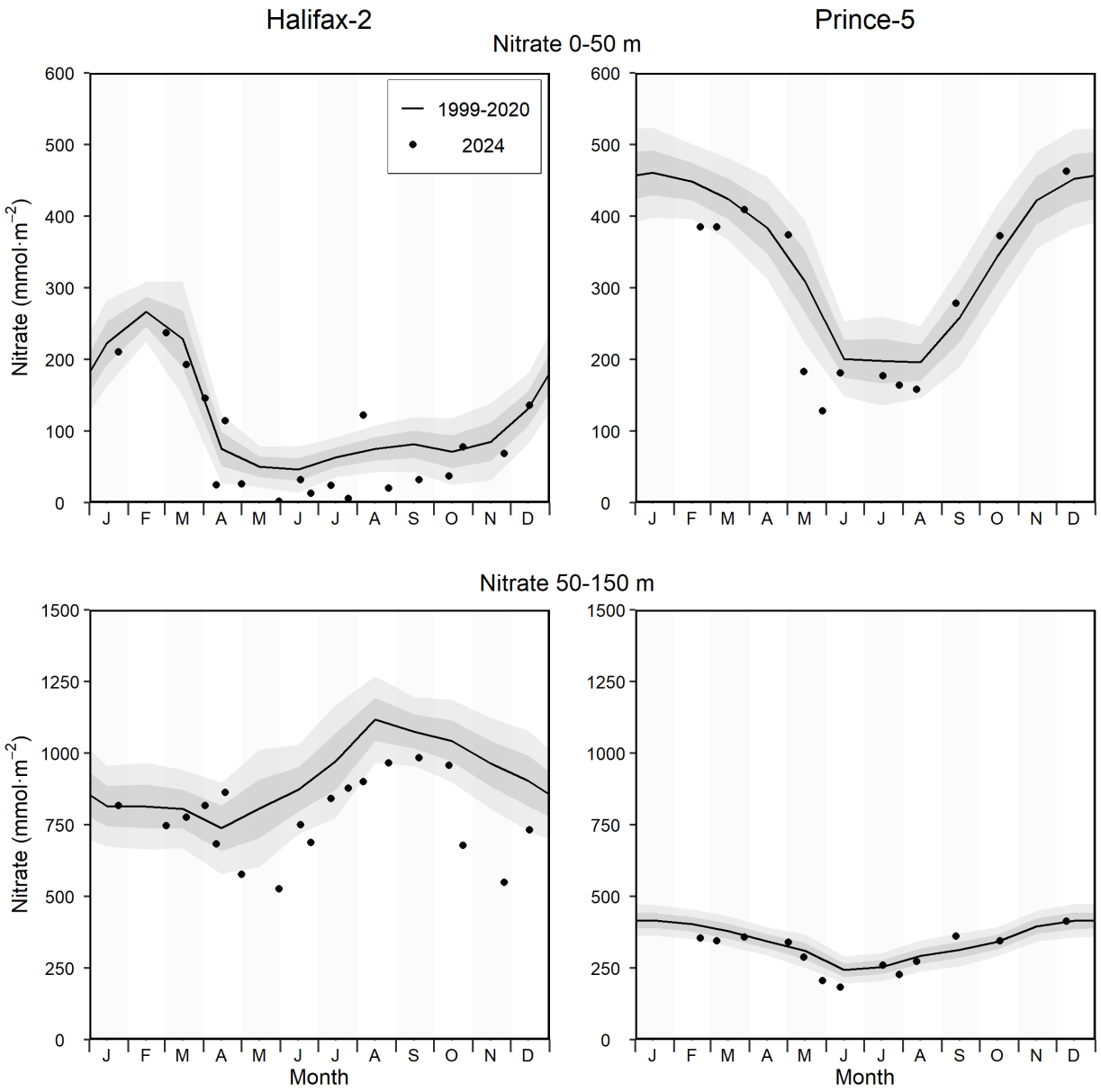

Figure 6. Nitrate inventories at the Maritimes high-frequency sampling stations. Top panels: Surface (0–50 m) nitrate inventory. Bottom panels: Subsurface (50–150 m for Halifax-2 and 50–95 m for Prince 5) nitrate inventory. The solid circles represent the 2024 data; the solid line represents the monthly climatological means for the reference period 1999-2020; the gray shaded ribbons represent the standard deviation (±0.5 and ±1 sd) of the monthly means.

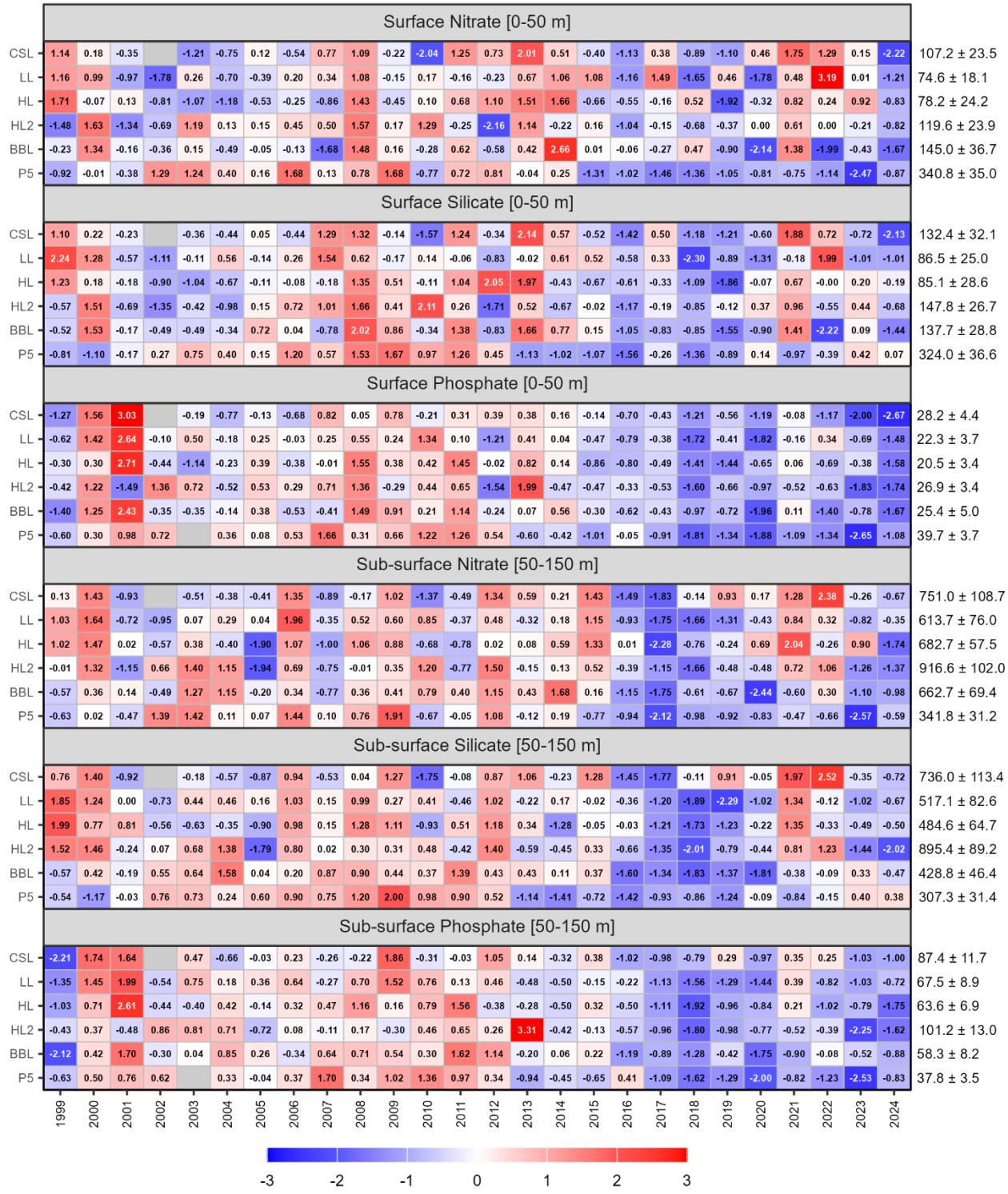

Figure 7. Annual anomaly scorecards for surface (0–50 m) and subsurface (50–150 m) nitrate, silicate, and phosphate inventories. Values in each cell are anomalies from the mean for the reference period 1999–2020, in standard deviation (sd) units (mean and sd listed at right in units of mmol·m^{-2}). Red (blue) cells indicate higher- (lower-) than-normal nutrient inventories, with shading intensity reflecting the magnitude of the anomaly. Gray cells indicate missing data. CSL: Cabot Strait section; LL: Louisbourg section; HL: Halifax section; HL2: Halifax-2; BBL: Browns Bank section; P5: Prince 5.

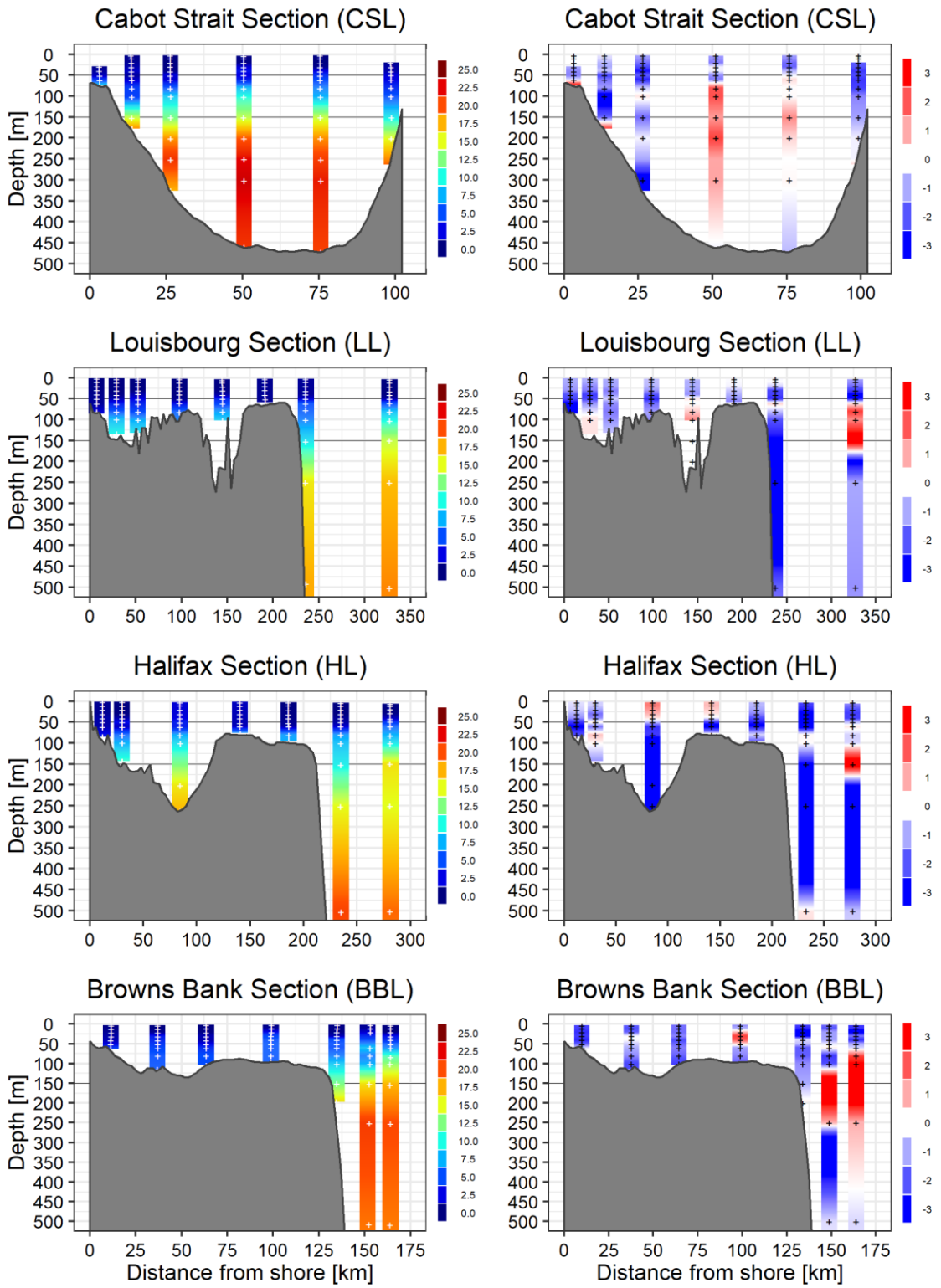

Figure 8a. Nitrate concentrations on the core sections in spring 2024. Left panels: Nitrate concentration profiles (mmol·m^{-3}) measured in spring 2024. Right panels: Nitrate concentration anomalies (mmol·m^{-3}) from the climatological means for the reference period 1999–2020. White markers on the left panels indicate the actual sampling depths. Black markers on the right panels indicate the depths at which station-specific climatological values were calculated.

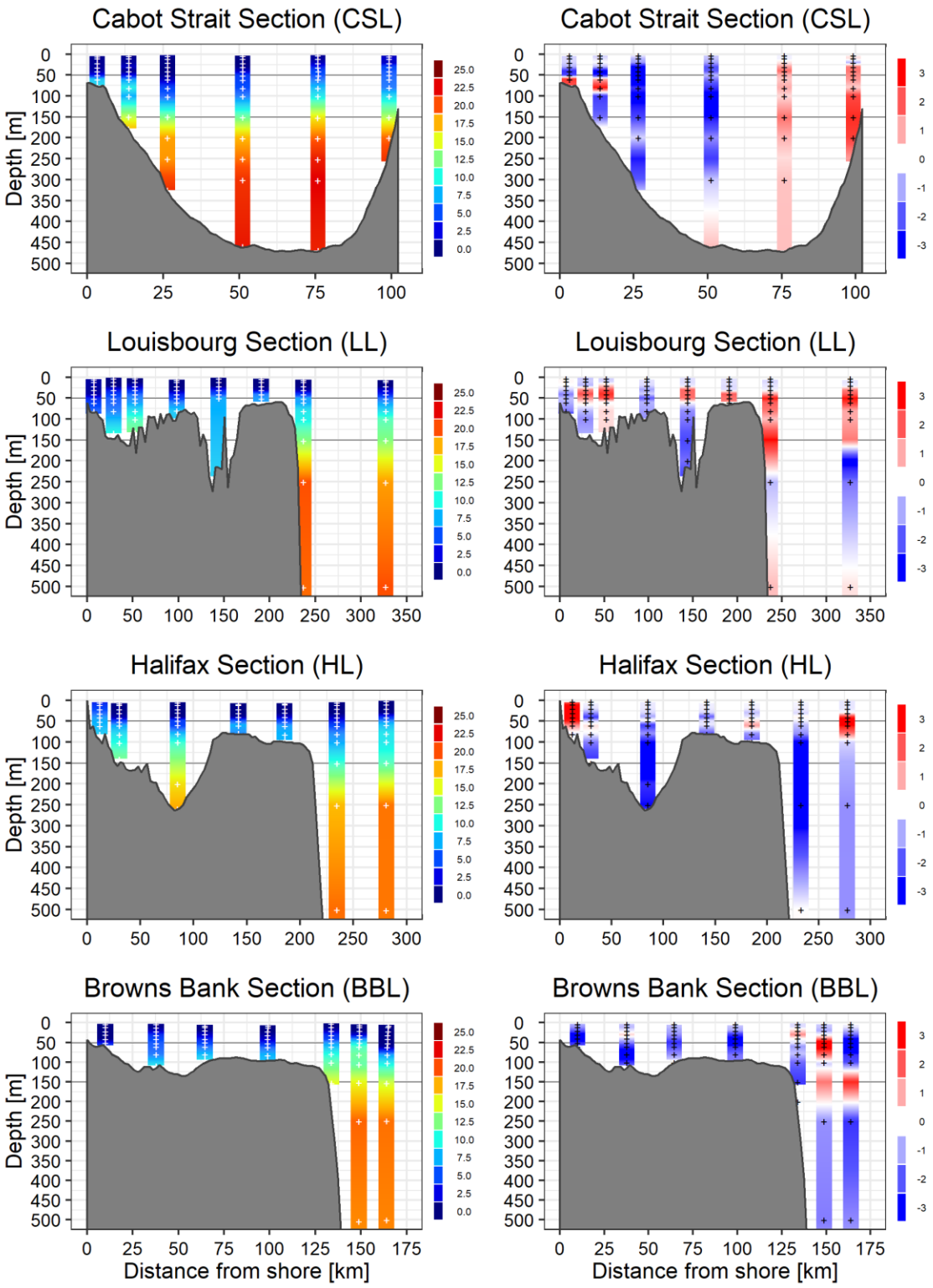

Figure 8b. Nitrate concentrations on the core sections in fall 2024. Left panels: Nitrate concentration profiles (mmol·m^{-3}) measured in fall 2024. Right panels: Nitrate concentration anomalies (mmol·m^{-3}) from the climatological means for the reference period 1999–2020. White markers on the left panels indicate the actual sampling depths. Black markers on the right panels indicate the depths at which station-specific climatological values were calculated.

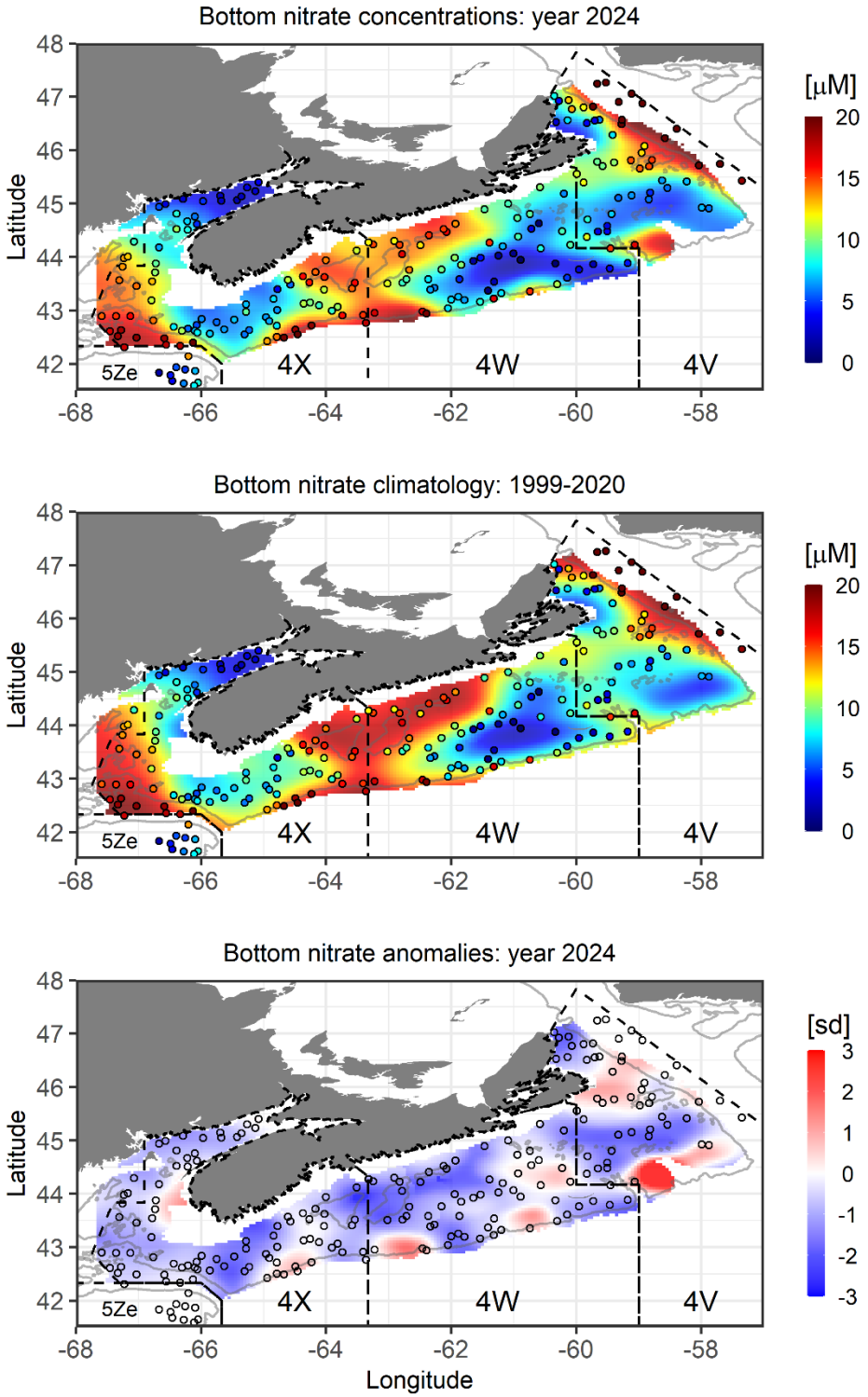

Figure 9. Bottom nitrate concentrations during the summer ecosystem trawl survey. Top panel: Nitrate concentrations during 2024. Middle panel: Climatological mean spatial structure of nitrate concentrations for the reference period 1999-2020. Bottom panel: Normalized anomalies (in units of standard deviations, sd) of bottom nitrate concentrations. Markers in the top and bottom panels represent the 2024 sampling locations. The light gray line is the 200 m isobath.

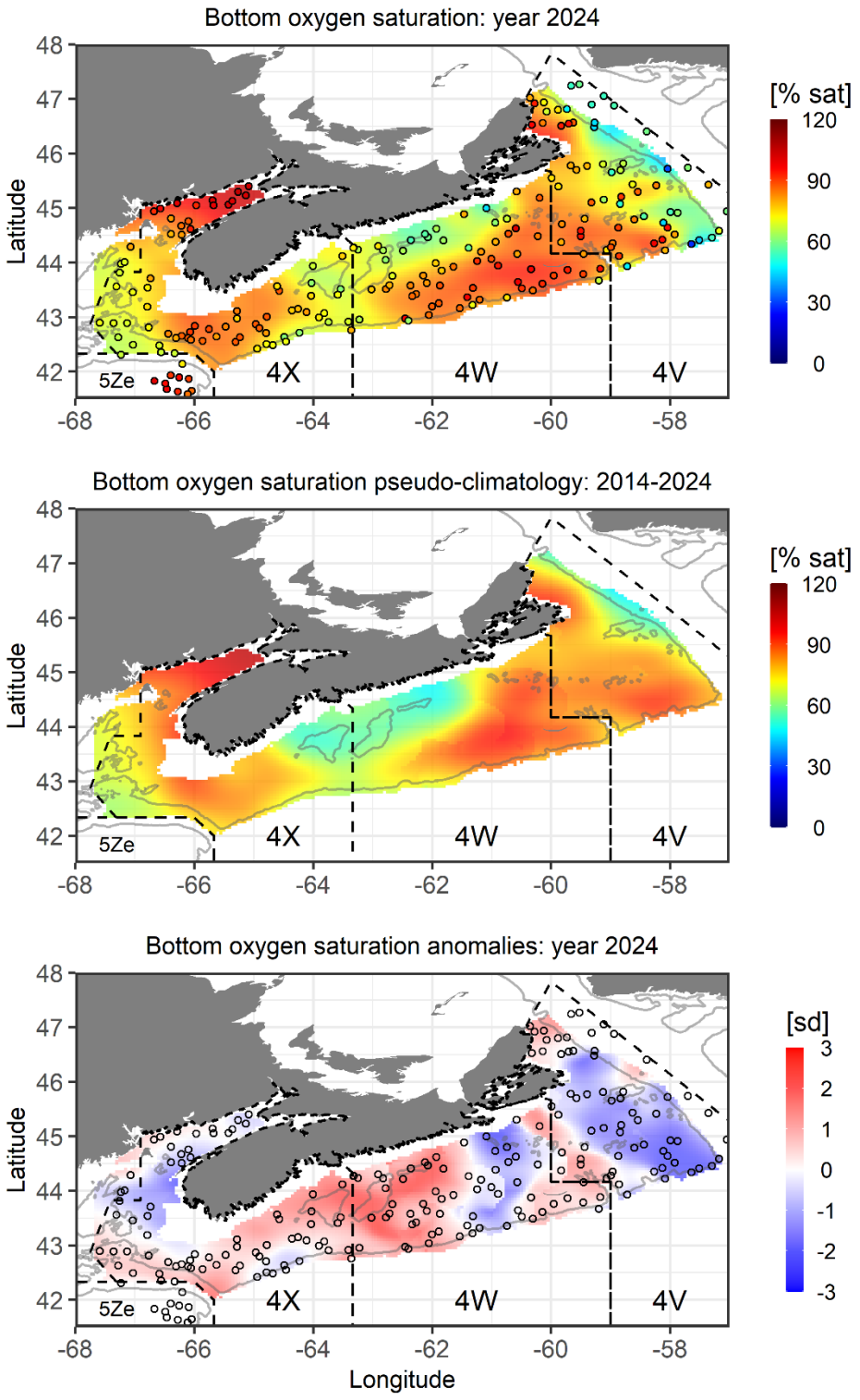

Figure 10. Bottom oxygen saturation during the summer ecosystem trawl survey. Top panel: Bottom oxygen saturation during 2024. Middle panel: Pseudo-climatological mean spatial structure of bottom oxygen saturation for the reference period 2014-2024. Bottom panel: Normalized anomalies (in units of standard deviations, sd) of bottom oxygen saturation. Markers in the top and bottom panels represent the 2024 sampling locations. The light gray line is the 200 m isobath.

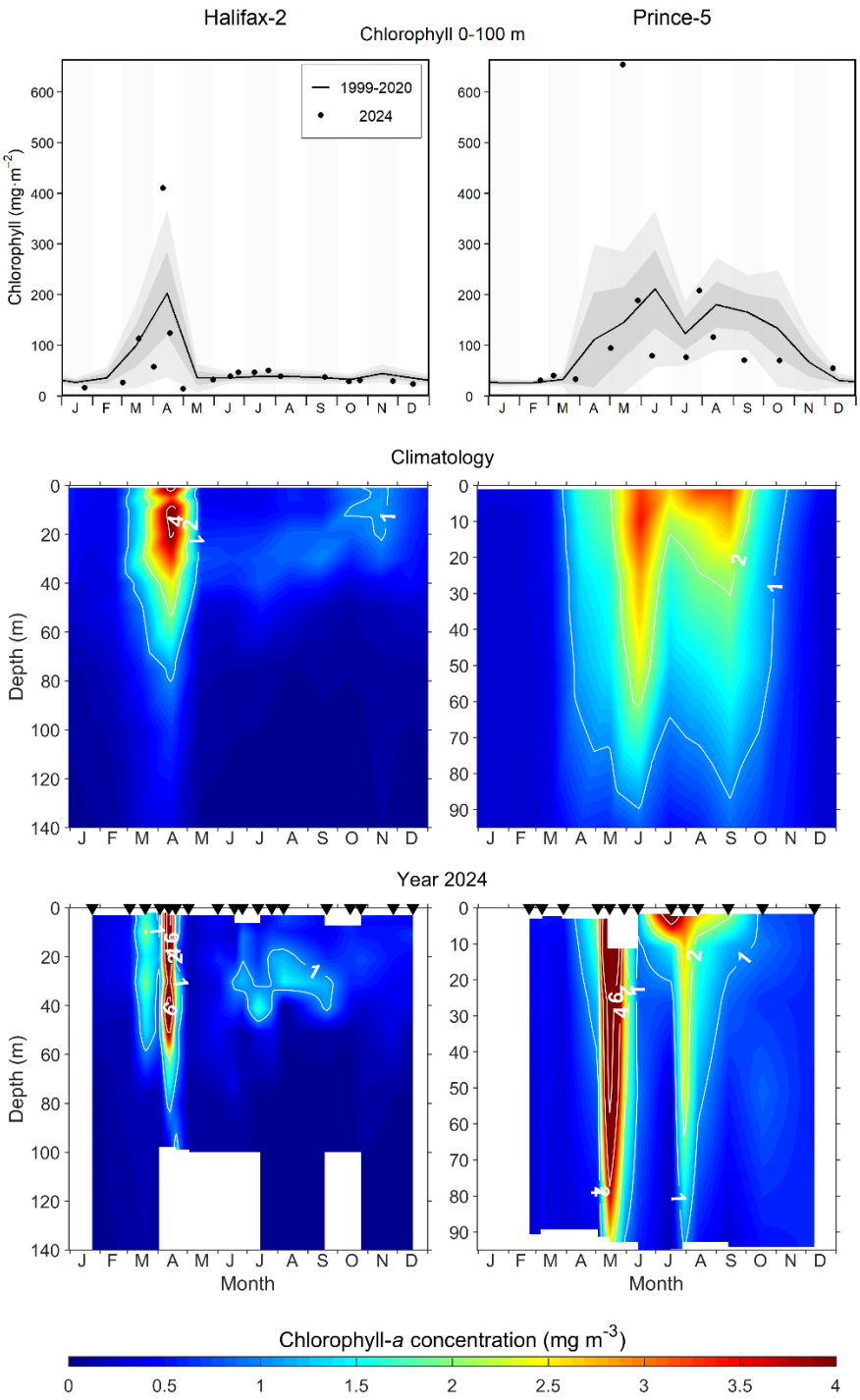

Figure 11. Chlorophyll-a inventory and concentrations at the Maritimes high-frequency sampling stations. Top panels: Chlorophyll-a inventory (0–100 m for Halifax-2 and 0–95 m for Prince 5); the solid circles represent the 2024 data; the solid line represents the monthly climatological means for the reference period 1999-2020; the gray shaded ribbons represent the standard deviation (±0.5 and ±1 sd) of the monthly means. Middle panels: Monthly climatological mean vertical structure of chlorophyll-a concentrations for the reference period 1999-2020. Bottom panels: Vertical structure of chlorophyll-a concentrations in 2024. Black triangles in the bottom panels indicate sampling dates. White areas indicate no data.

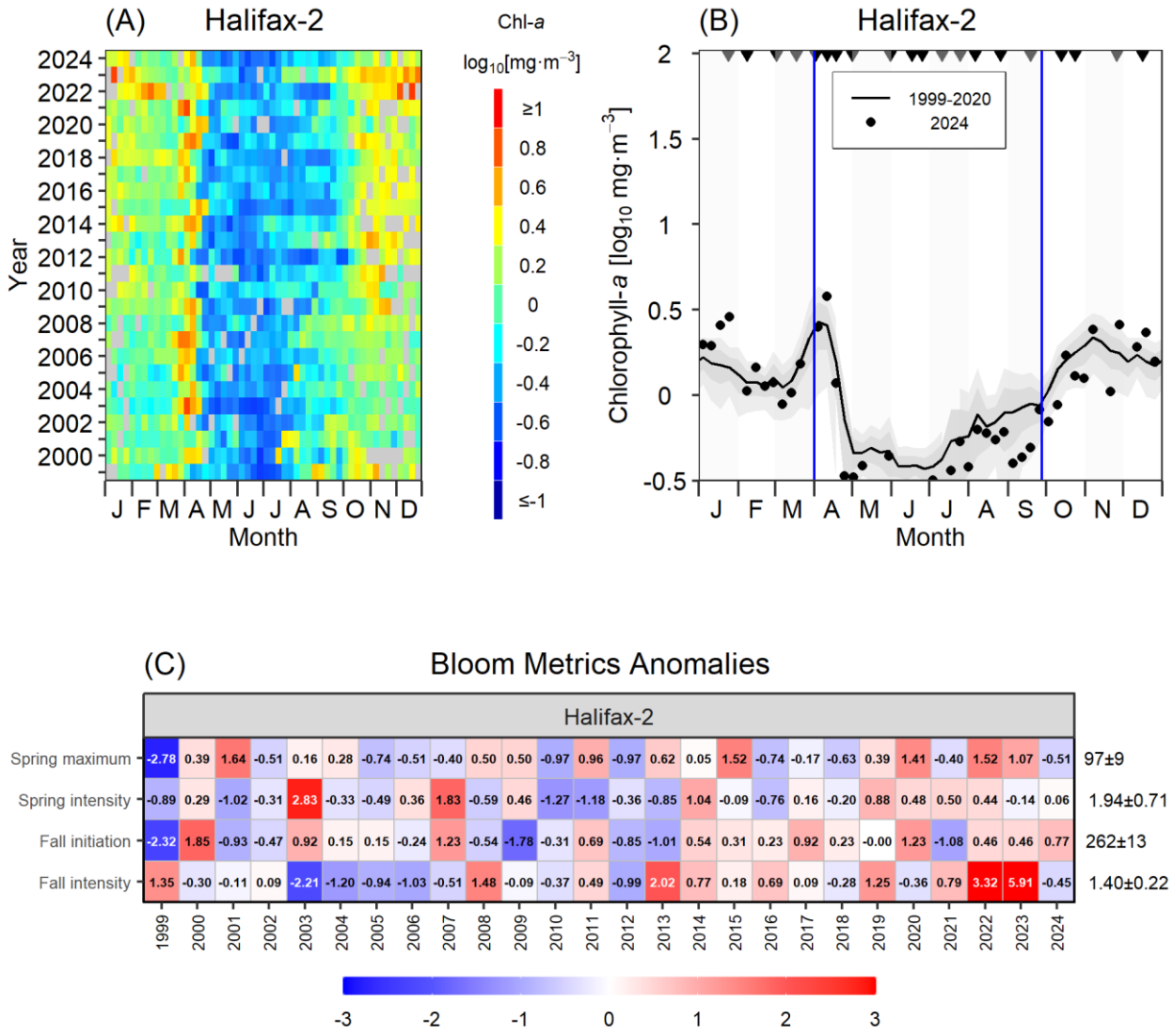

Figure 12. Surface chlorophyll-a concentrations and phytoplankton bloom metrics derived from remote sensing ocean color data for Halifax-2 sub-region. Top left panel (A): Time series of weekly mean surface chlorophyll-a concentrations; gray pixels indicate missing data. Top right panel (B): Weekly mean surface chlorophyll-a concentrations; the solid circles represent the 2024 data; the solid line represents the weekly climatological means for the reference period 1999-2020; the gray shaded ribbons represent the standard deviation (±0.5 and ±1 sd) of the weekly means; the vertical blue lines indicate the timing of the spring bloom maximum intensity (left) and the timing of the fall bloom initiation (right) in 2024;); black triangles indicate in situ chlorophyll-a sampling dates. Bottom panel (C): Annual anomaly scorecard for the spring and fall phytoplankton bloom metrics; values in each cell are anomalies from the mean for the reference period 1999–2020, in standard deviation (sd) units (mean and sd listed at right in units of Day-of-Year for spring maximum and fall initiation, $mg_{chl}·m^{-3}$ for spring and fall intensity); red (blue) cells indicate later (earlier) timing, or higher- (lower-) than-normal intensity of the bloom, with shading intensity reflecting the magnitude of the anomaly.

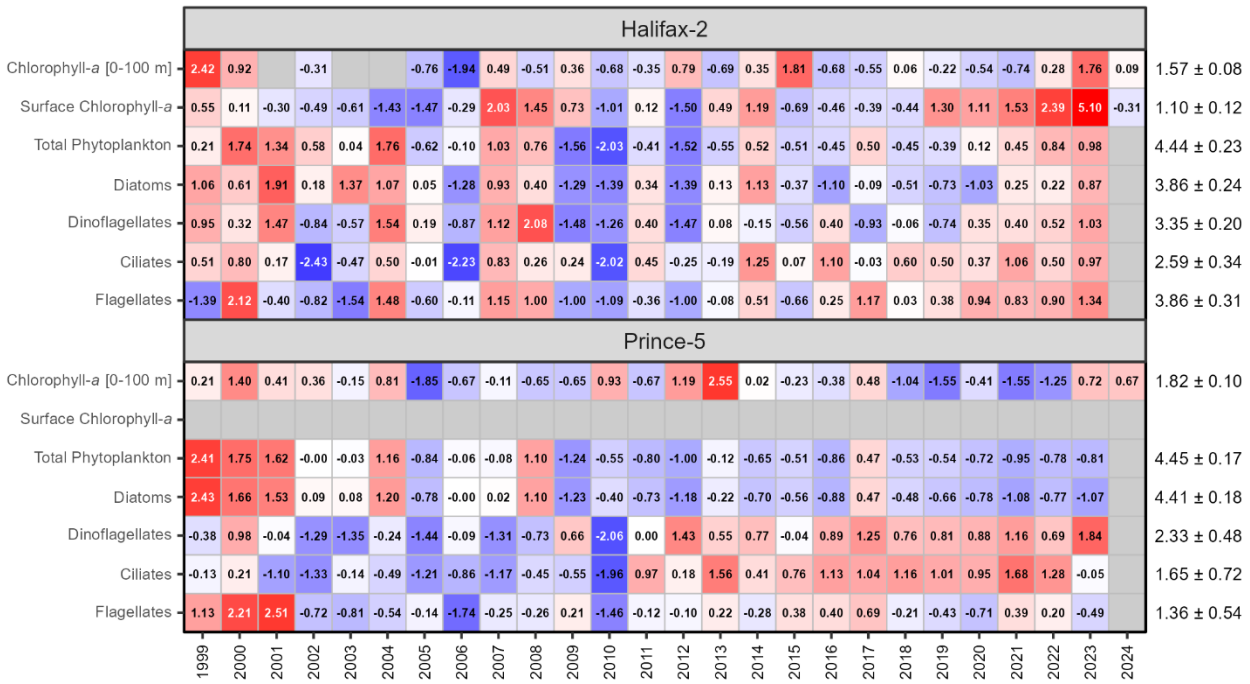

Figure 13. Annual anomaly scorecards for in situ chlorophyll-a inventory, remote sensing surface chlorophyll-a concentration, and phytoplankton abundance at the Maritimes high-frequency sampling stations. Values in each cell are anomalies from the mean for the reference period 1999–2020 in standard deviation (sd) units (mean and sd listed at right in units of $log_{10}(mg \cdot m^{-2})$ for chlorophyll-a inventory, $log_{10}(mg \cdot m^{-3})$ for chlorophyll-a concentration, and $log_{10}(cells \cdot L^{-1}+1)$ for phytoplankton abundance). Red (blue) cells indicate higher- (lower-) than-normal chlorophyll-a inventories/concentrations or phytoplankton abundances, with shading intensity reflecting the magnitude of the anomaly. Gray cells indicate missing data.

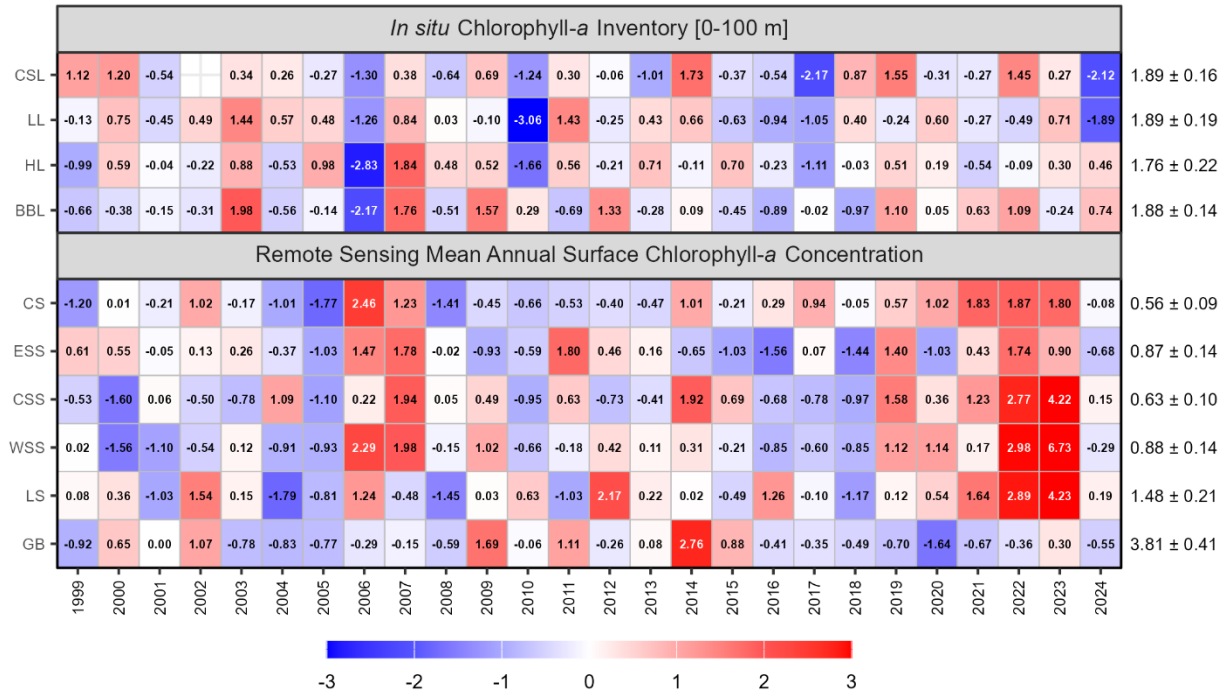

Figure 14. Annual anomaly scorecards for in situ chlorophyll-a inventory (0–100 m) on the Cabot Strait [CSL], Louisbourg [LL], Halifax [HL] and Browns Bank [BBL] sections (top panel) and for remote sensing surface chlorophyll-a concentrations on the Cabot Strait [CS], Eastern Scotian Shelf [ESS], Central Scotian Shelf [CSS], Western Scotian Shelf [WSS], Lurcher Shoal [LS], and Georges Bank [GB] sub-regions (bottom panel). Values in each cell are anomalies from the mean for the reference period 1999–2020, in standard deviation (sd) units (mean and sd listed at right in units of $log_{10}(mg \cdot m^{-2})$ for chlorophyll-a inventory and $log_{10}(mg \cdot m^{-3})$ for chlorophyll-a concentration). Red (blue) cells indicate higher- (lower-) than-normal chlorophyll-a inventories or surface chlorophyll-a concentrations, with shading intensity reflecting the magnitude of the anomaly. Gray cells indicate missing data.

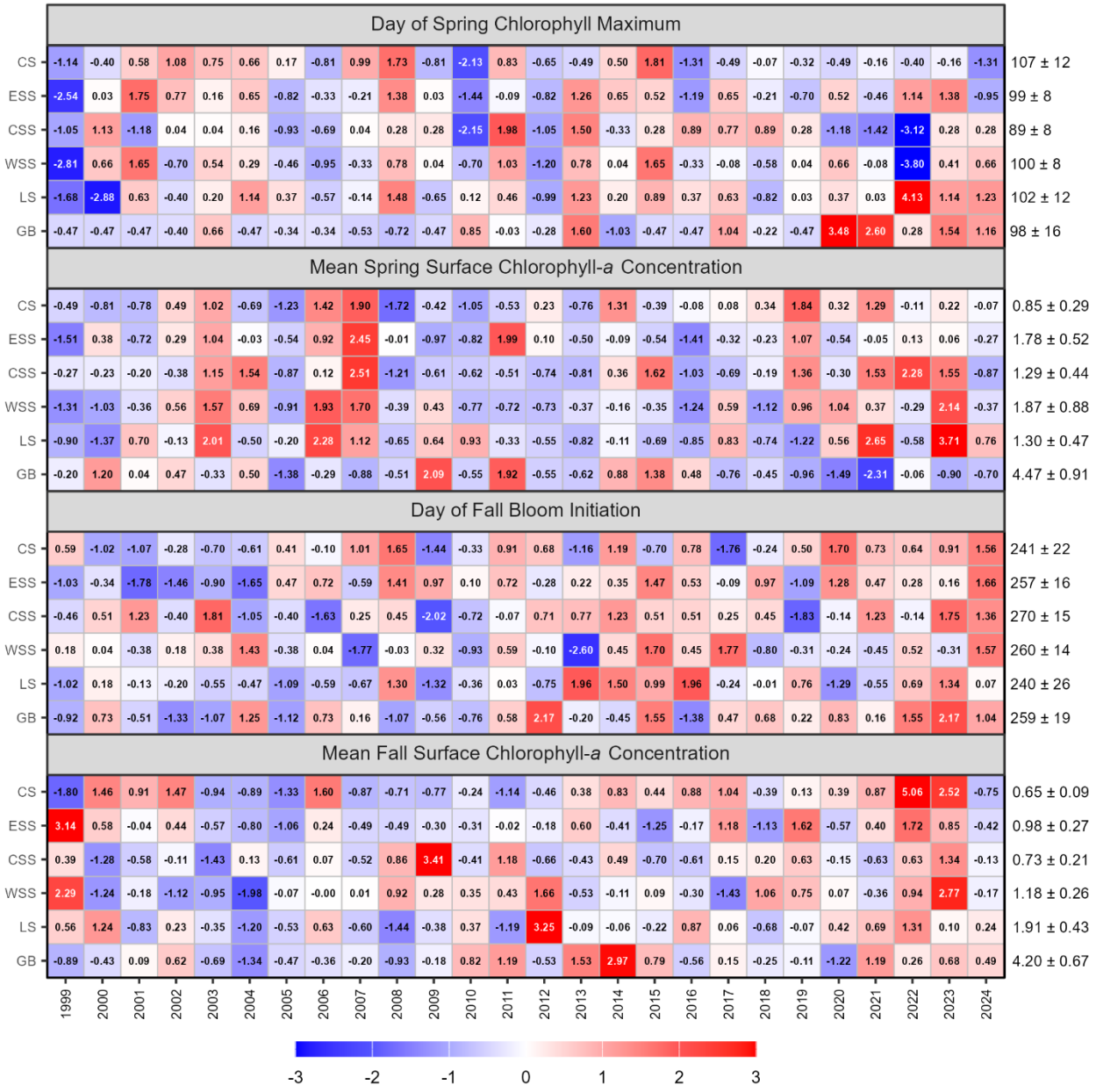

Figure 15. Annual anomaly scorecards for spring and fall phytoplankton bloom metrics. Values in each cell are anomalies from the mean for the reference period 1999–2020, in standard deviation (sd) units (mean and sd listed at right in units of Day-of-Year for spring maximum and fall initiation, $mg_{chl} \cdot m^{-3}$ for spring and fall intensity); red (blue) cells indicate later (earlier) timing, or higher- (lower-) than-normal intensity of the bloom, with shading intensity reflecting the magnitude of the anomaly.

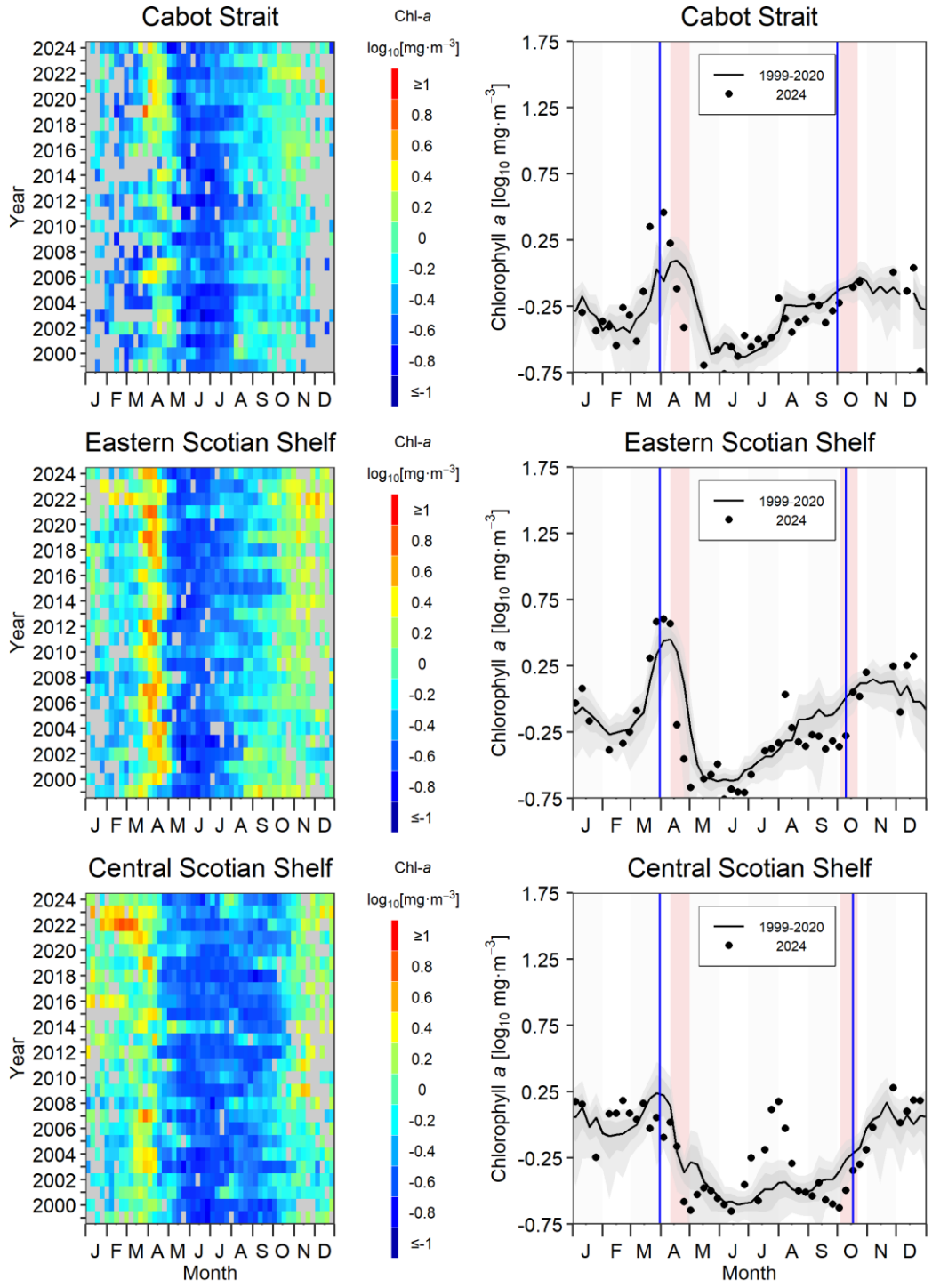

Figure 16a. Surface chlorophyll-a concentrations from remote sensing ocean color data in the Maritimes sub-regions. Left panels: Time series of weekly mean surface chlorophyll-a concentrations; gray pixels indicate missing data. Right panels: Weekly mean surface chlorophyll-a concentrations; the solid circles represent the 2024 data; the solid line represents the weekly climatological means for the reference period 1999-2020; the gray shaded ribbons represent the standard deviation (±0.5 and ±1 sd) of the weekly means; the vertical blue lines indicate the day of year of the spring bloom maximum intensity (left) and the day of year of the fall bloom initiation (right); the pink vertical stripe indicates the timing of the spring and fall surveys.

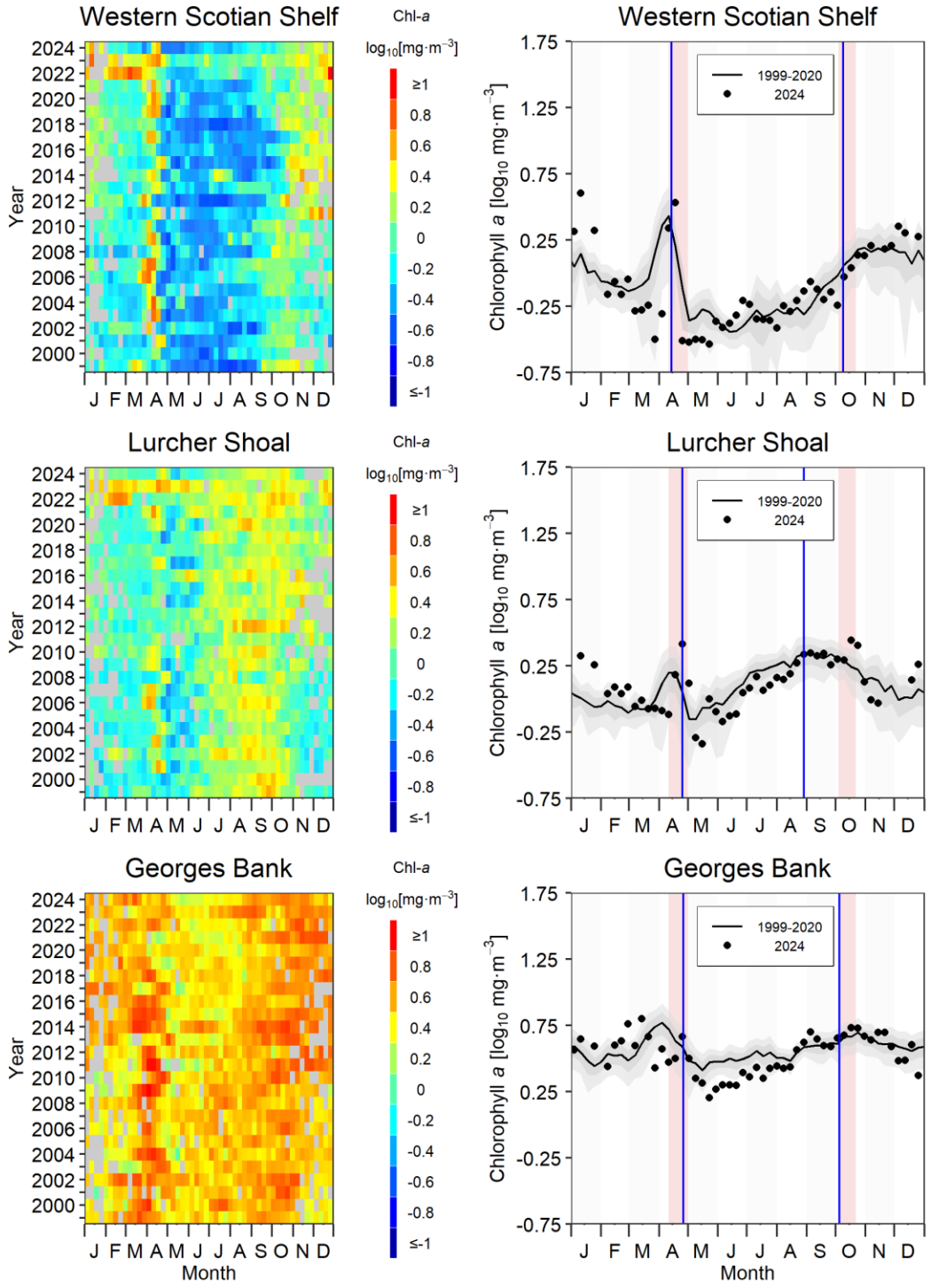

Figure 16b. Surface chlorophyll-a concentrations from remote sensing ocean color data in the Maritimes sub-regions. Left panels: Time series of weekly mean surface chlorophyll-a concentrations; gray pixels indicate missing data. Right panels: Weekly mean surface chlorophyll-a concentrations; the solid circles represent the 2024 data; the solid line represents the weekly climatological means for the reference period 1999-2020; the gray shaded ribbons represent the standard deviation (±0.5 and ±1 sd) of the weekly means; the vertical blue lines indicate the day of year of the spring bloom maximum intensity (left) and the day of year of the fall bloom initiation (right); the pink vertical stripe indicates the timing of the spring and fall surveys.

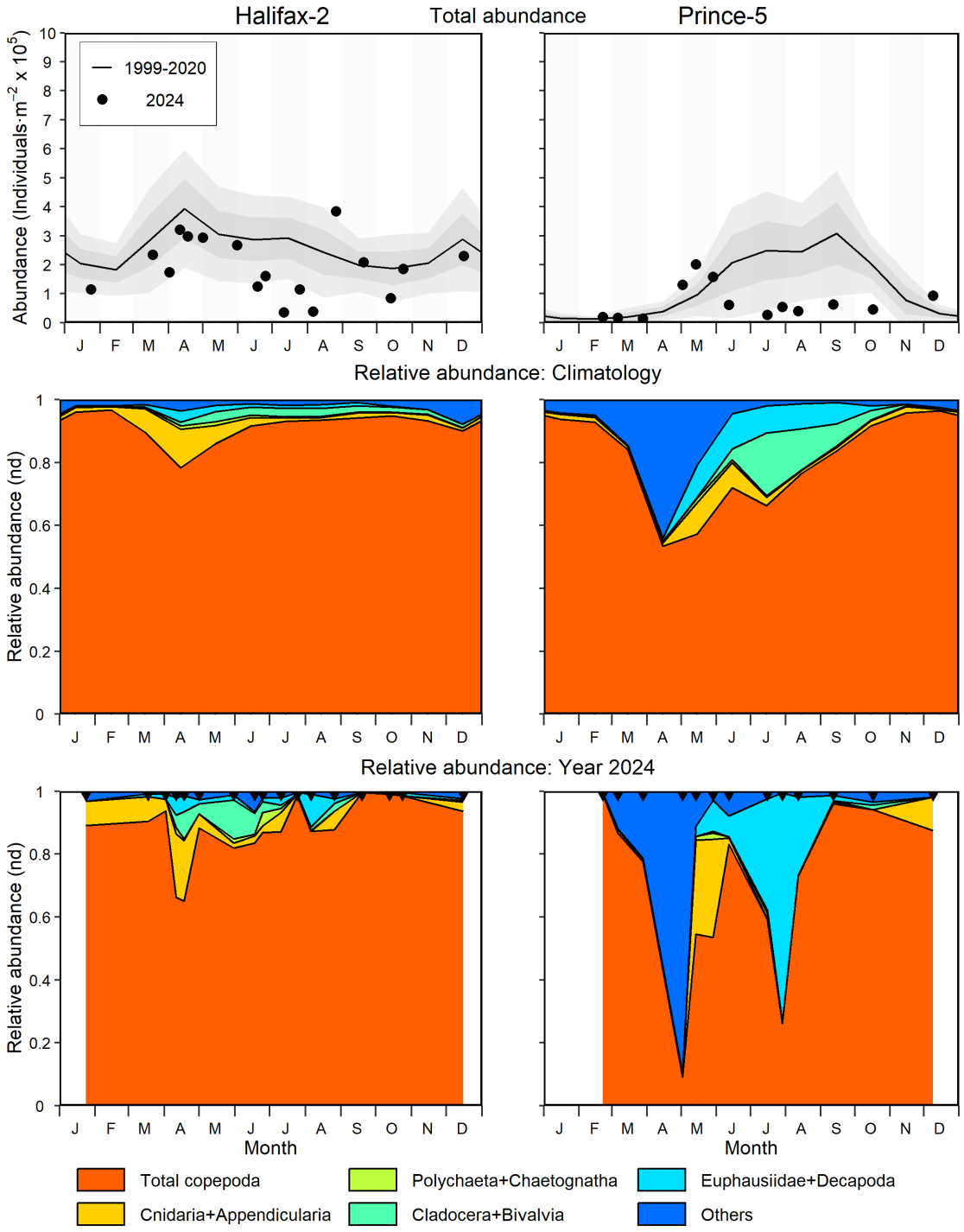

Figure 17. Zooplankton (> 200 µm) abundance and community composition at the Maritimes high-frequency sampling stations. Top panels: Zooplankton abundance; the solid circles represent the 2024 data; the solid line represents the monthly climatological means for the reference period 1999-2020; the gray shaded ribbons represent the standard deviation (±0.5 and ±1 sd) of the monthly means. Middle panels: Climatological mean zooplankton relative abundance for the reference period 1999-2020. Bottom panels: Zooplankton relative abundance in 2024. Black triangles in the bottom panels indicate sampling dates. White areas indicate no data.

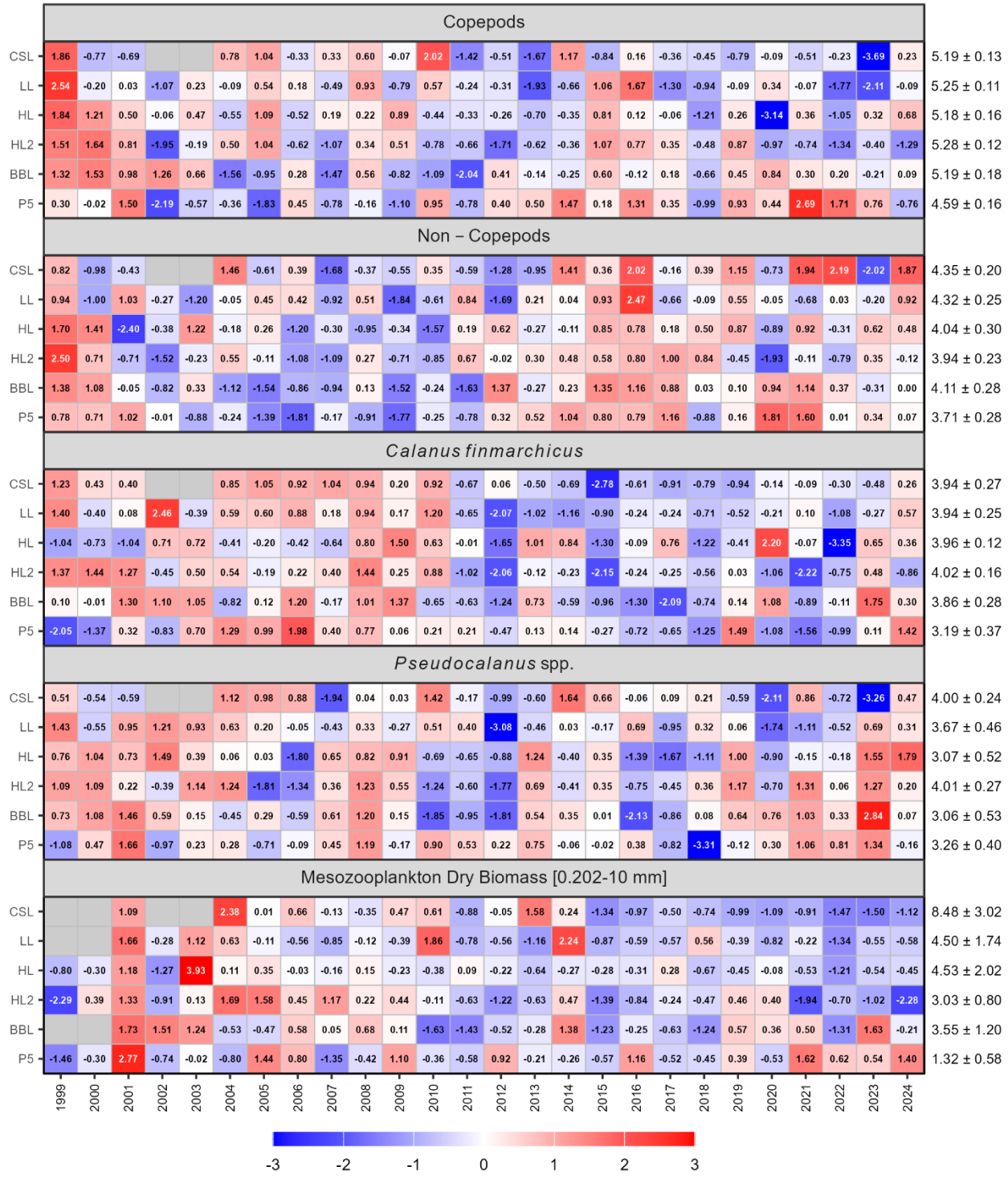

Figure 18. Annual anomaly scorecards for zooplankton abundance and biomass. Values in each cell are anomalies from the mean for the reference period 1999–2020, in standard deviation (sd) units (mean and sd listed at right in units of log_{10}(individuals·m^{-2}+1) for abundance and g·m^{-2} for biomass). Red (blue) cells indicate higher- (lower-) than-normal abundances or biomass, with shading intensity reflecting the magnitude of the anomaly. Gray cells indicate missing data. CSL: Cabot Strait section; LL: Louisbourg section; HL: Halifax section; HL2: Halifax-2; BBL: Browns Bank section; P5: Prince 5.

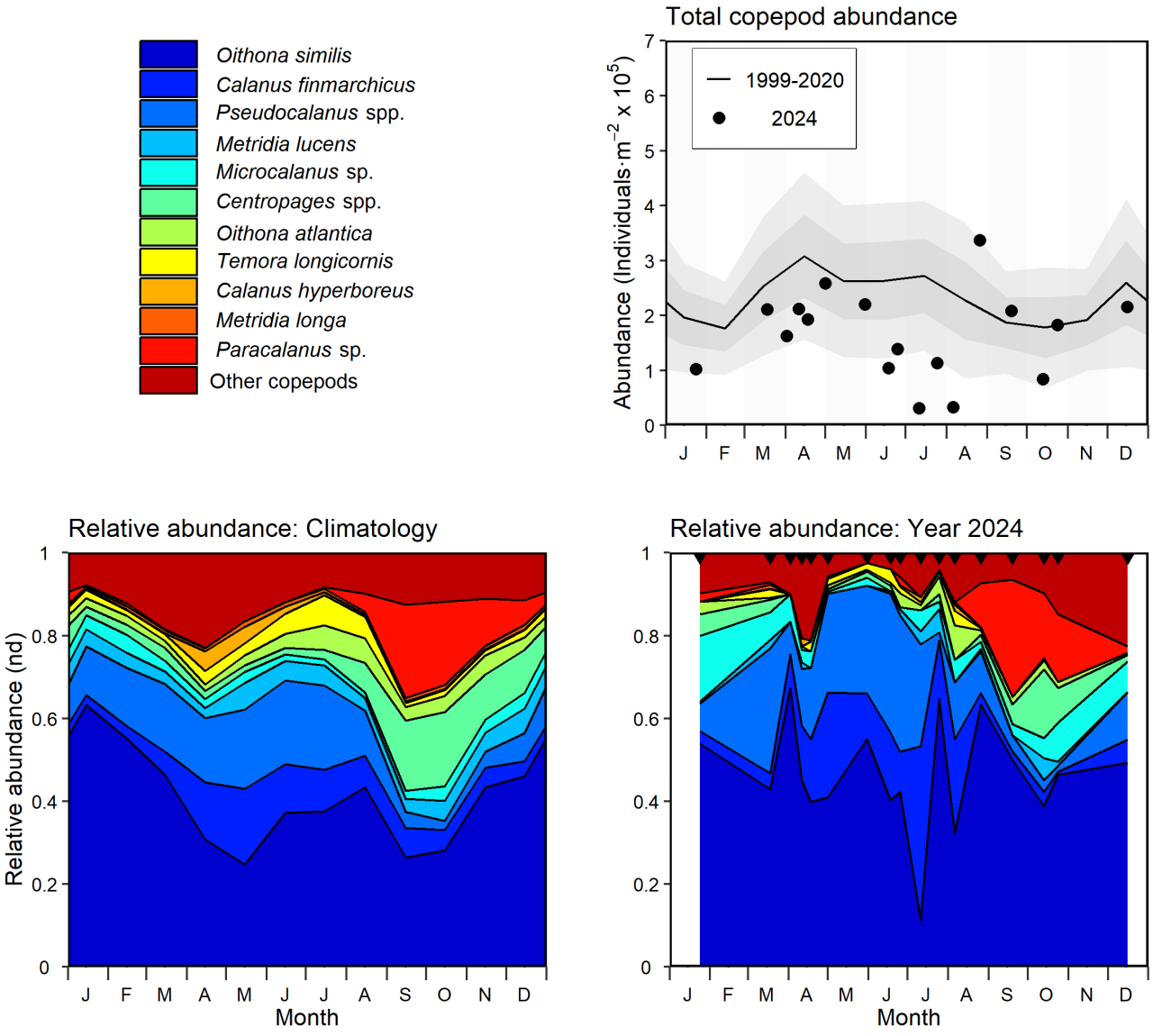

Figure 19a. Copepod abundance and composition at Halifax-2; the top 95% copepod taxa by abundance (ordered from most to least abundant) are shown individually; unidentified copepods (mostly nauplii) are grouped as "others". Top right panel: Copepod abundance; the solid circles represent the 2024 data; the solid line represents the monthly climatological means for the reference period 1999-2020; the gray shaded ribbons represent the standard deviation (±0.5 and ±1 sd) of the monthly means. Bottom left panel: Climatological mean copepod relative abundance for the reference period 1999-2020. Bottom right panel: Copepod relative abundance in 2024. Black triangles in the bottom right panel indicate sampling dates. White areas indicate no data.

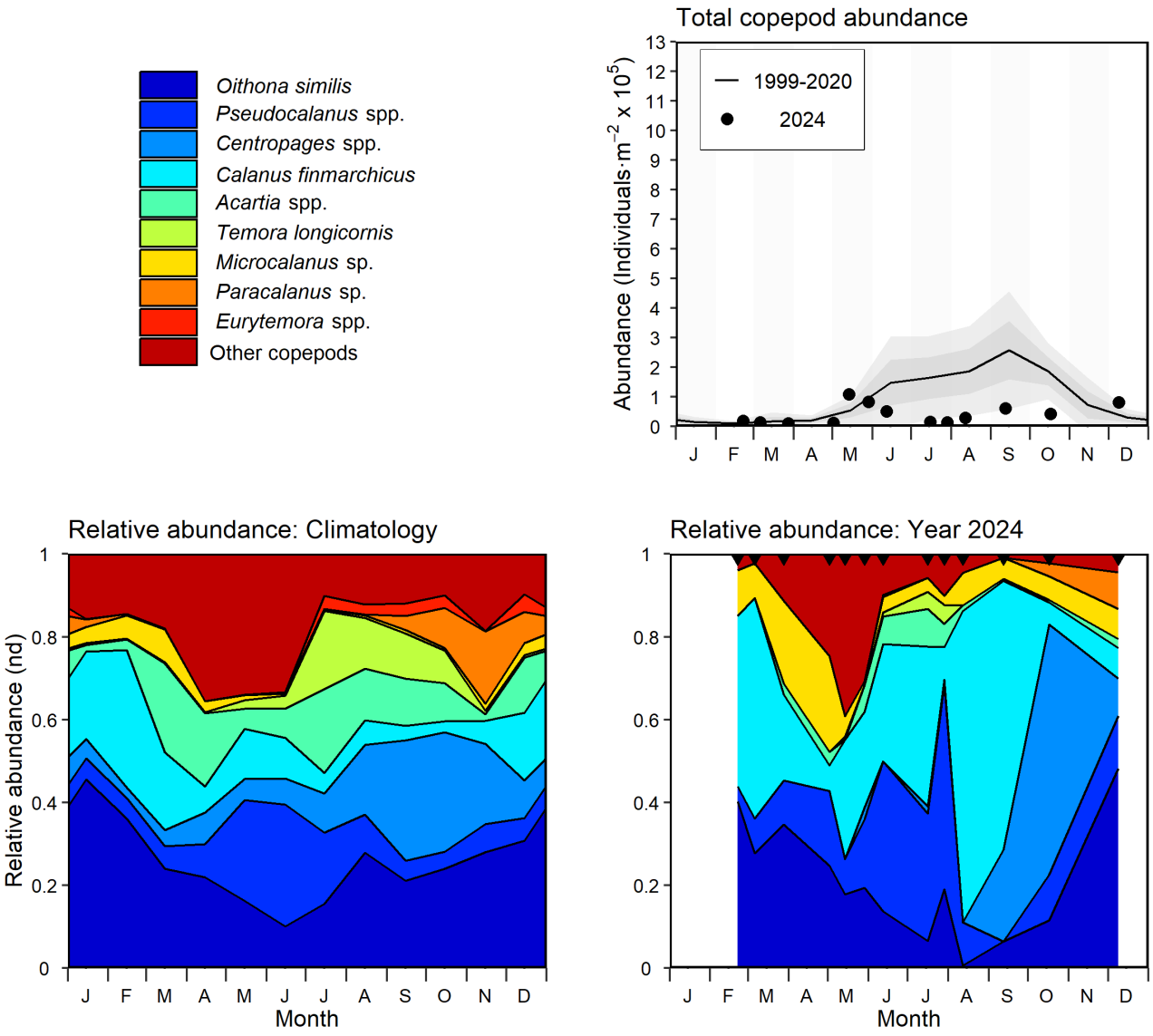

Figure 19b. Copepod abundance and composition at Prince 5; the top 95% copepod taxa by abundance (ordered from most to least abundant) are shown individually; unidentified copepods (mostly nauplii) are grouped as "others". Top right panel: Copepod abundance; the solid circles represent the 2024 data; the solid line represents the monthly climatological means for the reference period 1999-2020; the gray shaded ribbons represent the standard deviation (±0.5 and ±1 sd) of the monthly means. Bottom left panel: Climatological mean copepod relative abundance for the reference period 1999-2020. Bottom right panel: Copepod relative abundance in 2024. Black triangles in the bottom right panel indicate sampling dates. White areas indicate no data.

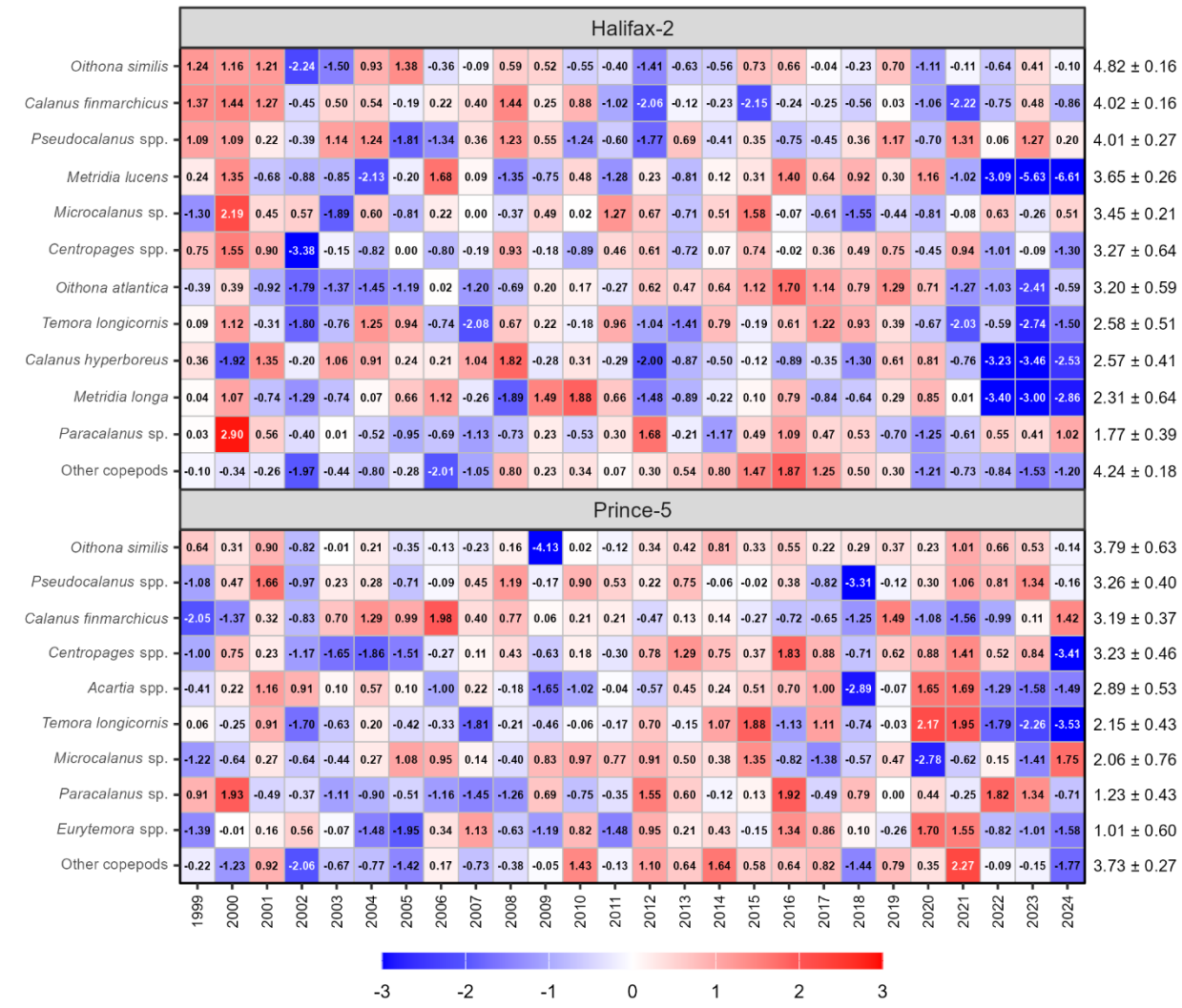

Figure 20. Annual anomaly scorecards for the top 95% of copepod taxa by abundance (ordered from most to least abundant) at the Maritimes high-frequency sampling stations. Values in each cell are anomalies from the mean for the reference period 1999–2020, in standard deviation (sd) units (mean and sd listed at right in units of log_{10}(individuals·m^{-2}+1)). Red (blue) cells indicate higher- (lower-) than-normal abundances, with shading intensity reflecting the magnitude of the anomaly.

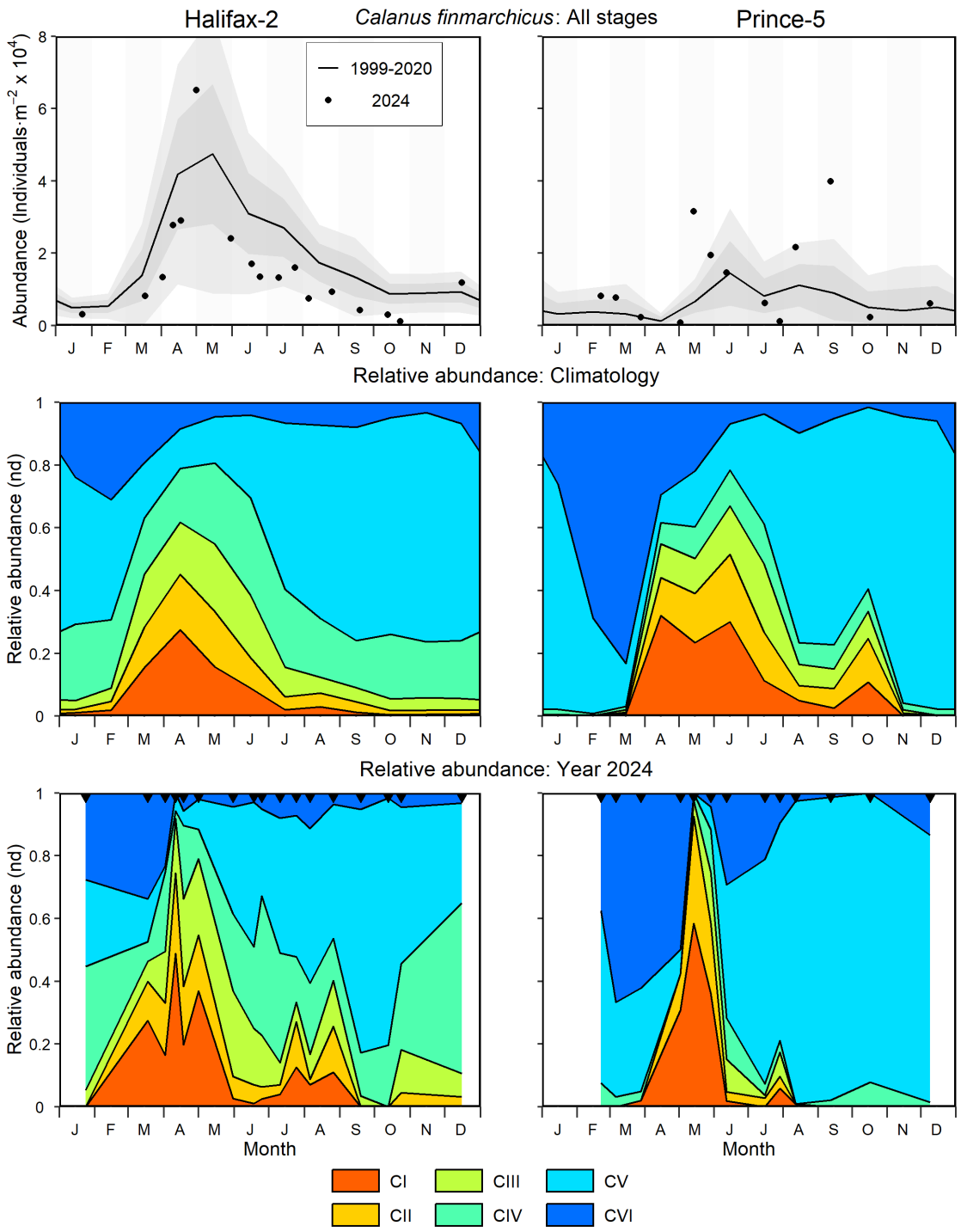

Figure 21. Calanus finmarchicus abundance and developmental stage distribution at the Maritimes high-frequency sampling stations. Top panels: C. finmarchicus abundance; the solid circles represent the 2024 data; the solid line represents the monthly climatological means for the reference period 1999-2020; the gray shaded ribbons represent the standard deviation (±0.5 and ±1 sd) of the monthly means. Middle panels: Climatological mean C. finmarchicus stage relative abundance for the reference period 1999-2020. Bottom panels: C. finmarchicus stage relative abundance in 2024. Black triangles in the bottom panels indicate sampling dates. White areas indicate no data.

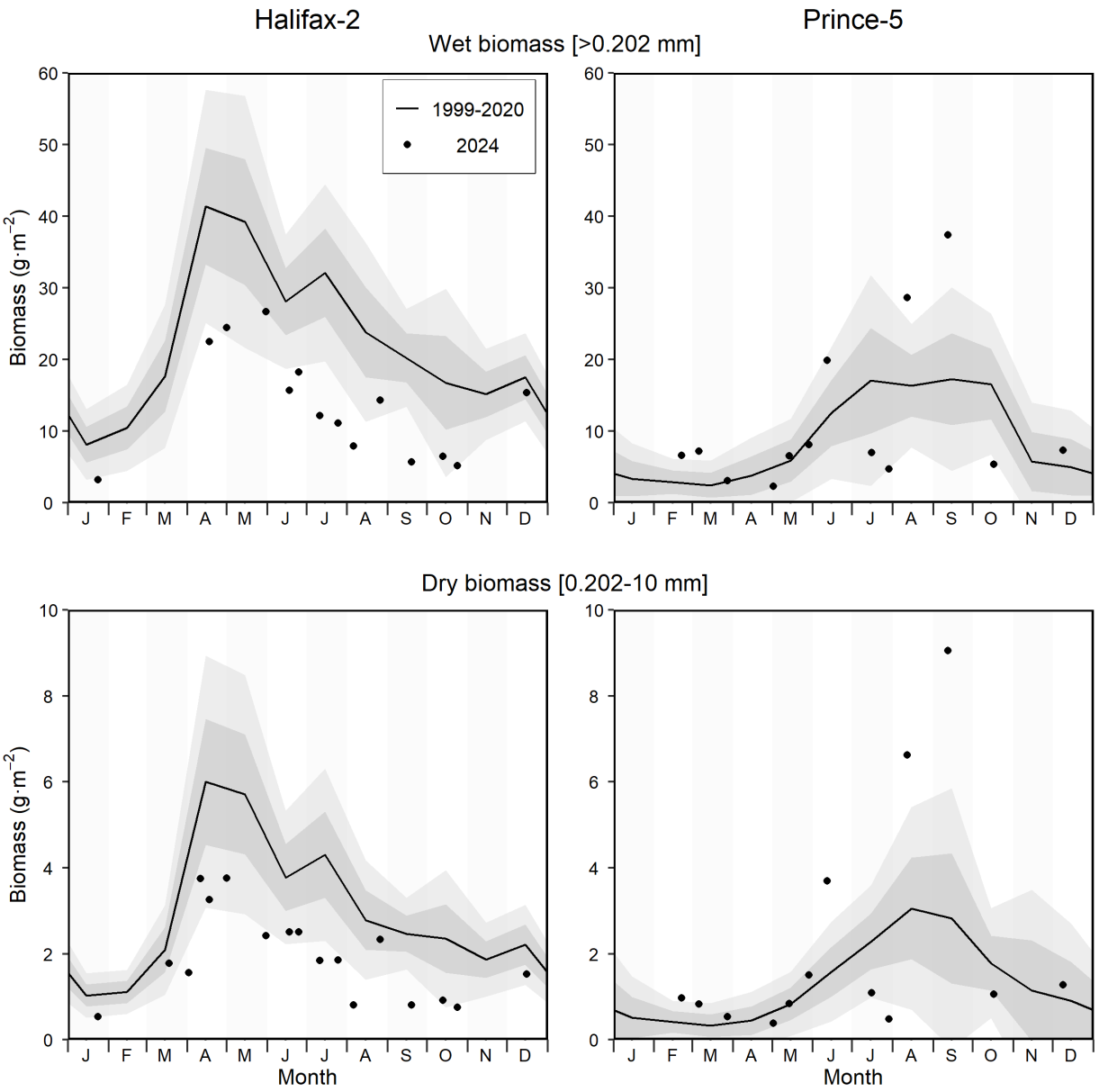

Figure 22. Zooplankton biomass at the Maritimes high-frequency sampling stations. Top panels: Total zooplankton wet biomass. Bottom panels: Mesozooplankton dry biomass. The solid circles represent the 2024 data; the solid line represents the monthly climatological means for the reference period 1999-2020; the gray shaded ribbons represent the standard deviation (±0.5 and ±1 sd) of the monthly means.

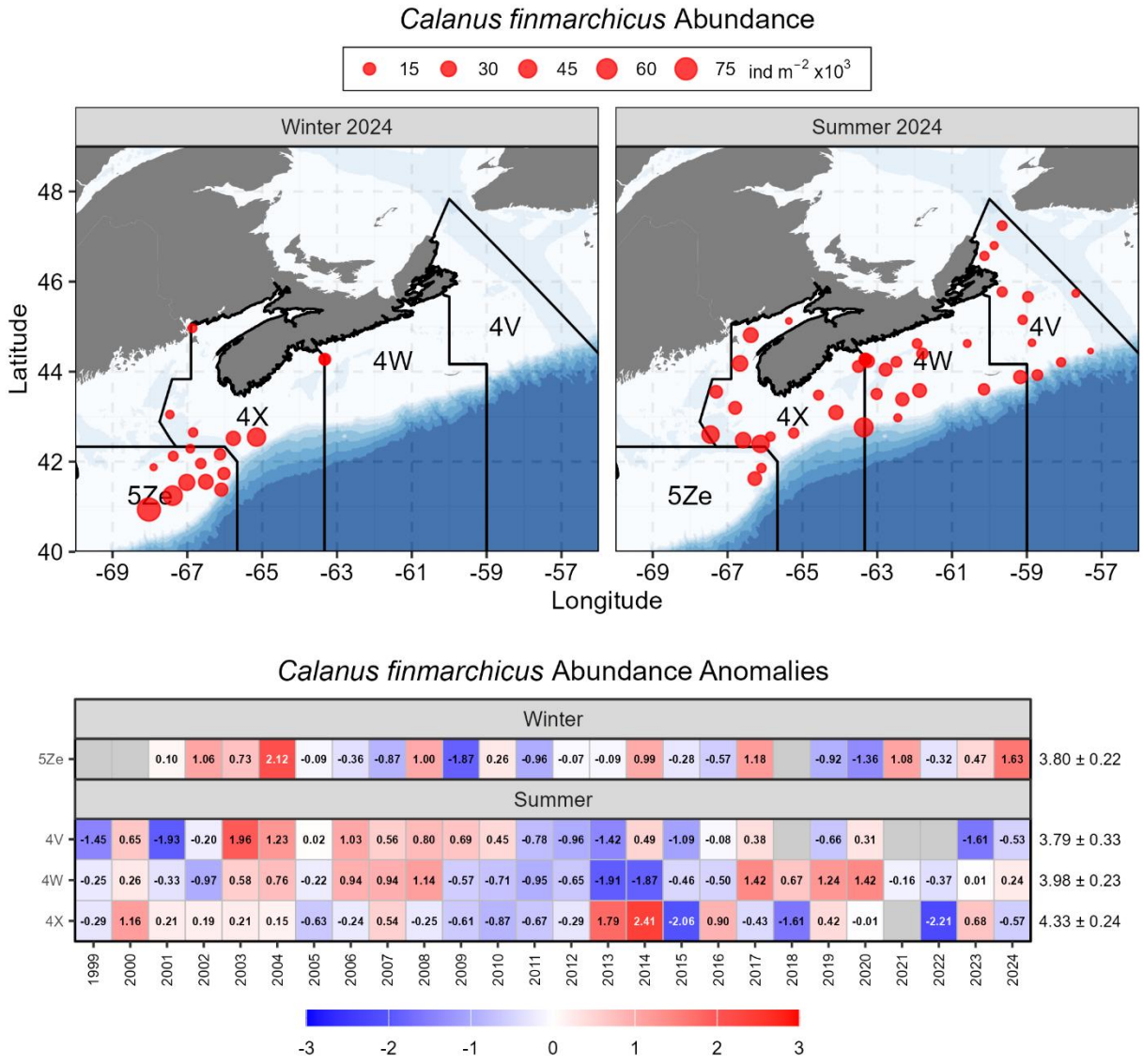

Figure 23. Calanus finmarchicus abundance during the ecosystem trawl surveys. Top panels: Spatial distribution of C. finmarchicus in winter (left) and summer (right) 2024. Bottom panels: Seasonal anomaly scorecards for C. finmarchicus abundance on Georges Bank (5Ze in winter) and the Scotian Shelf and eastern Gulf of Maine (4X, 4W, and 4V in summer); values in each cell are anomalies from the mean for the reference period 1999–2020, in standard deviation (sd) units (mean and sd listed at right in units of log_{10}(individuals·m^{-2}+1)). Red (blue) cells indicate higher- (lower-) than-normal abundances, with shading intensity reflecting the magnitude of the anomaly. Gray cells indicate missing data.

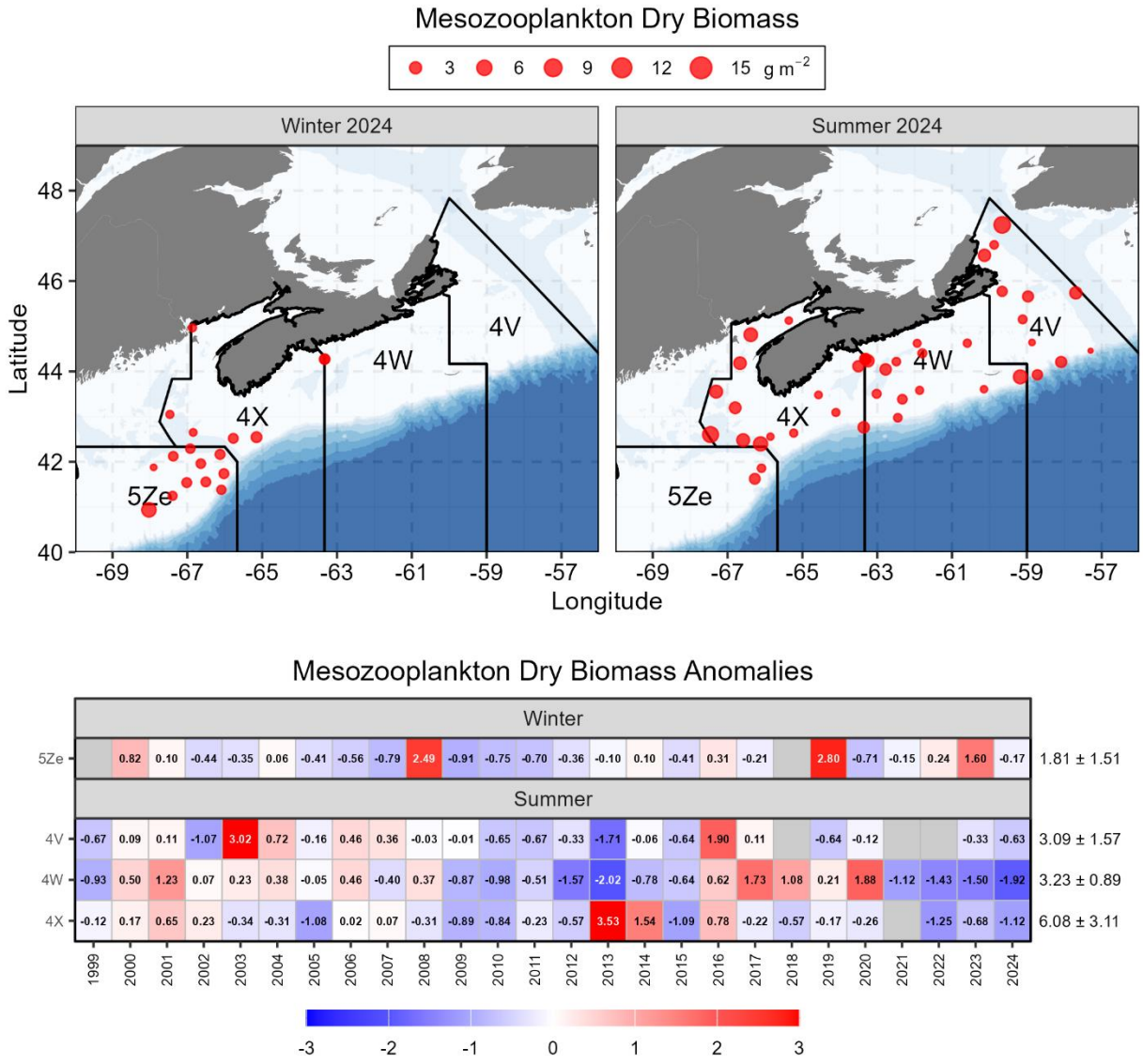

Figure 24. Mesozooplankton dry biomass during the ecosystem trawl surveys. Top panels: Spatial distribution of mesozooplankton dry biomass in winter (left) and summer (right) 2024. Bottom panels: Seasonal anomaly scorecards for mesozooplankton dry biomass on Georges Bank (5Ze in winter) and the Scotian Shelf and eastern Gulf of Maine (4X, 4W, and 4V in summer); values in each cell are anomalies from the mean for the reference period 1999–2020, in standard deviation (sd) units (mean and sd listed at right in units of g·m^{-2}). Red (blue) cells indicate higher- (lower-) than-normal abundances, with shading intensity reflecting the magnitude of the anomaly. Gray cells indicate missing data.

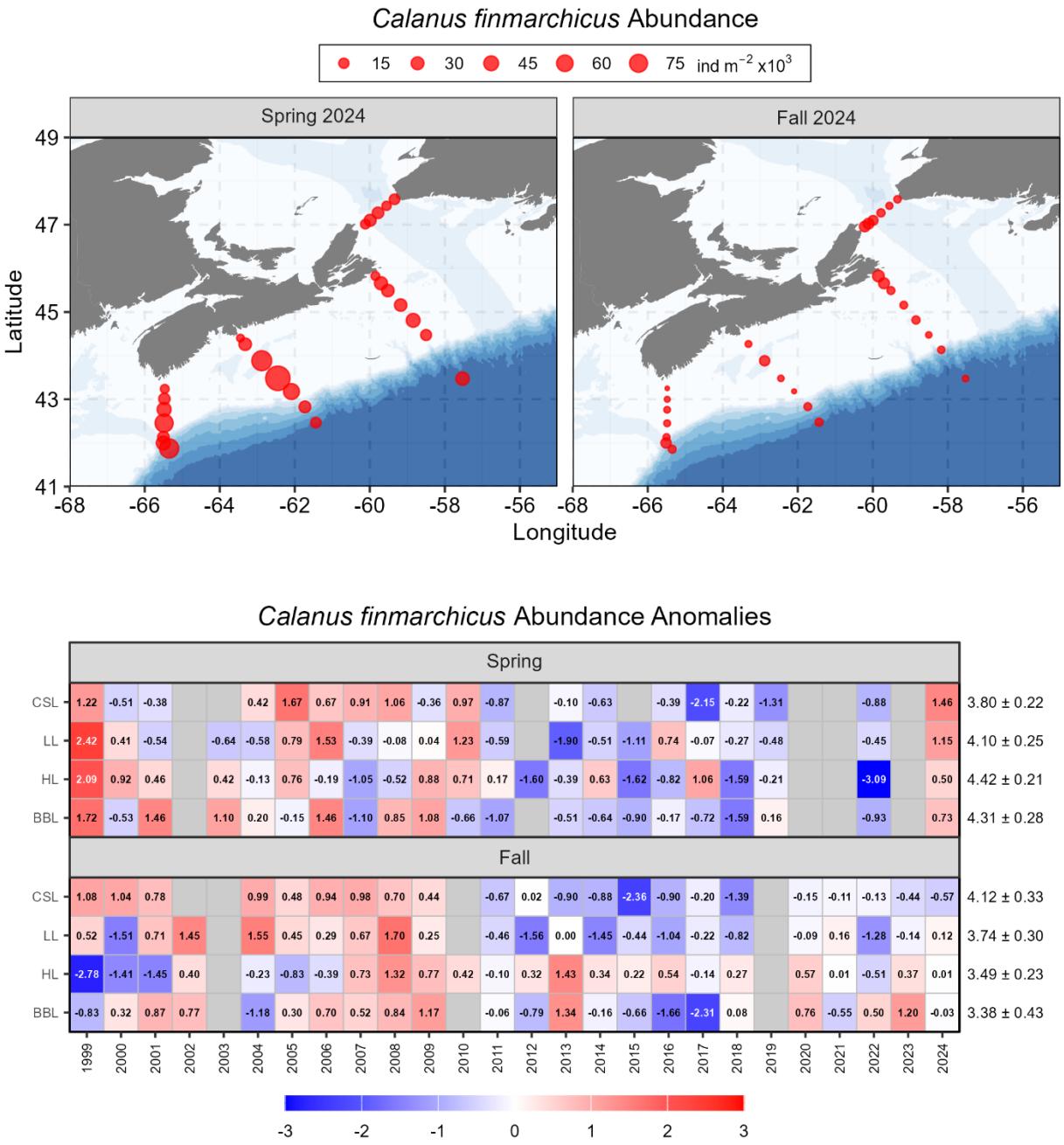

Figure 25. Calanus finmarchicus abundance during the seasonal surveys on the core sections. Top panels: Spatial distribution of C. finmarchicus in spring (left) and fall (right) 2024. Bottom panels: Seasonal anomaly scorecards for C. finmarchicus abundance during spring and fall surveys; values in each cell are anomalies from the mean for the reference period 1999–2020, in standard deviation (sd) units (mean and sd listed at right in units of $\log_{10}$(individuals·m^{-2}+1)). Red (blue) cells indicate higher-(lower-) than-normal abundances, with shading intensity reflecting the magnitude of the anomaly. Gray cells indicate missing data. CSL: Cabot Strait section; LL: Louisbourg section; HL: Halifax section; BBL: Browns Bank section.

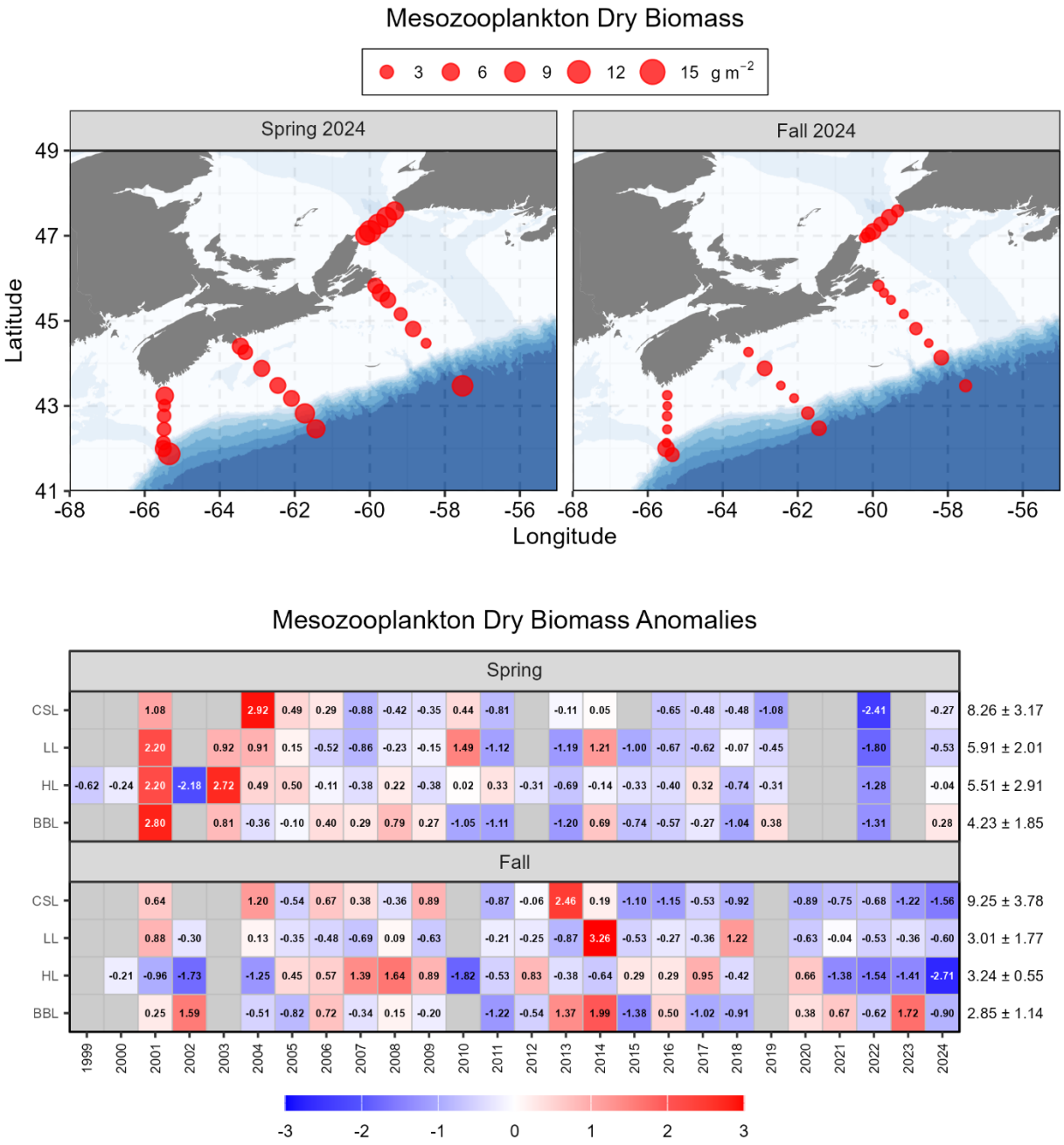

Figure 26. Mesozooplankton dry biomass during the seasonal surveys on the core sections. Top panels: Mesozooplankton dry biomass in spring (left) and fall (right) 2024. Bottom panels: Seasonal anomaly scorecards for mesozooplankton dry biomass during spring and fall surveys; values in each cell are anomalies from the mean for the reference period 1999–2020, in standard deviation (sd) units (mean and sd listed at right in units of g·m^{-2}). Red (blue) cells indicate higher- (lower-) than-normal abundances, with shading intensity reflecting the magnitude of the anomaly. Gray cells indicate missing data. CSL: Cabot Strait section; LL: Louisbourg section; HL: Halifax section; BBL: Browns Bank section.

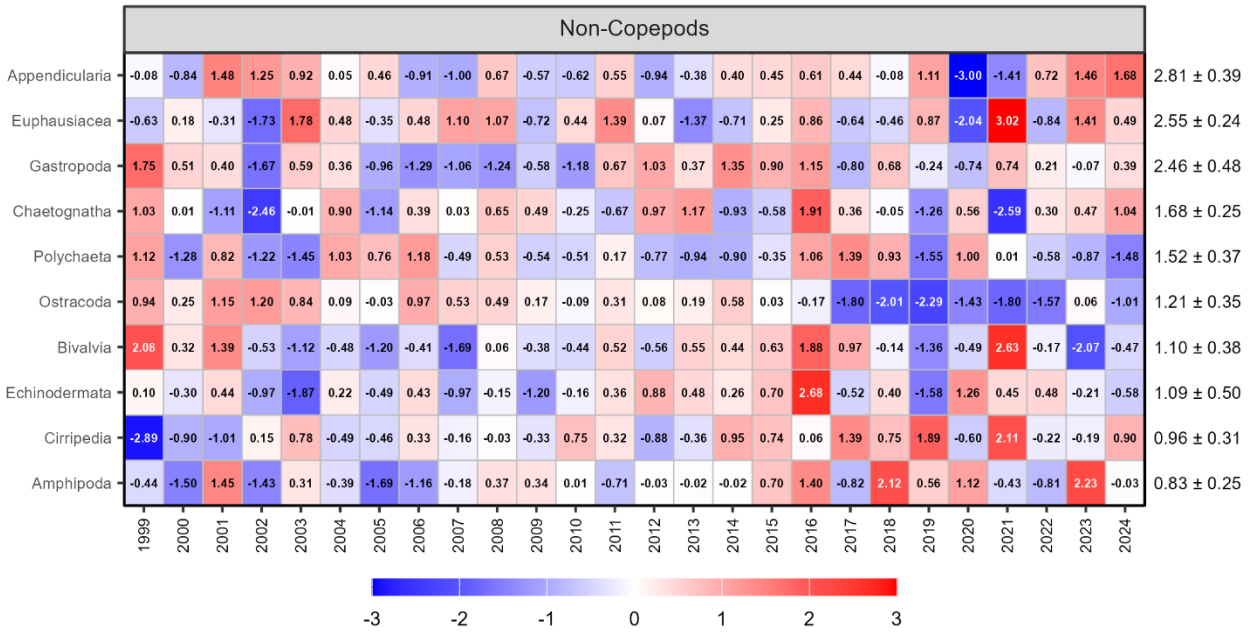

Figure 27. Annual anomaly scorecard for non-copepod groups abundance on the Scotian Shelf sections, ordered from higher to lower abundance. Anomalies are based on annual abundances estimated using a general linear model fitted with data from all stations of the four core sections. Values in each cell are anomalies from the mean for the reference period 1999–2020, in standard deviation (sd) units (mean and sd listed at right in units of log_{10}(individuals·m^{-2}+1)). Red (blue) cells indicate higher- (lower-) than-normal abundances, with shading intensity reflecting the magnitude of the anomaly.

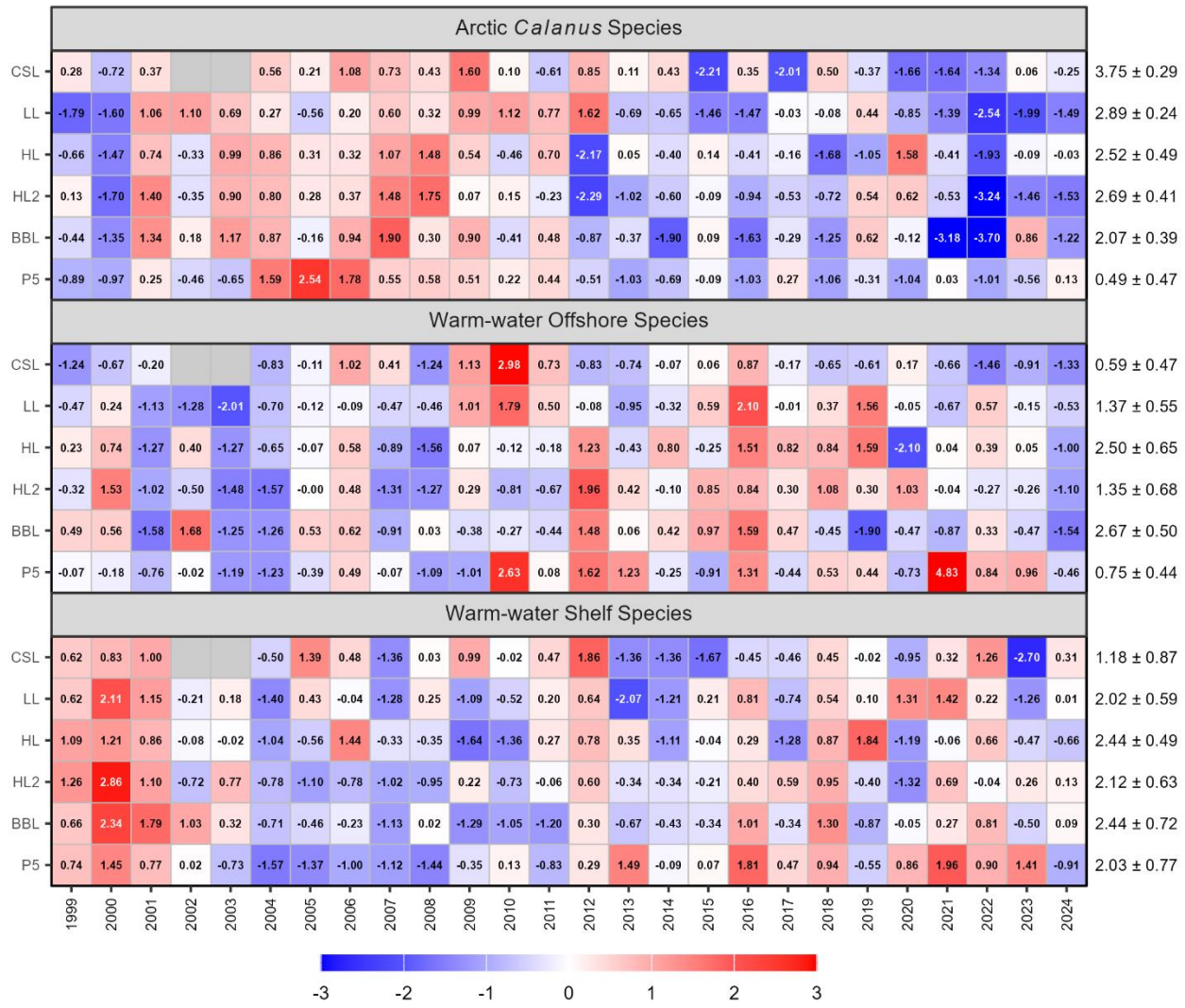

Figure 28. Annual anomaly scorecards for copepod indicator species grouped abundance. Values in each cell are anomalies from the mean for the reference period 1999–2020, in standard deviation (sd) units (mean and sd listed at right in units of log_{10}[individuals·m^{-2}+1]). Red (blue) cells indicate higher- (lower-) than-normal abundances, with shading intensity reflecting the magnitude of the anomaly. Gray cells indicate missing data. CSL: Cabot Strait section; LL: Louisbourg section; HL: Halifax section; HL2: Halifax-2; BBL: Browns Bank section; P5: Prince 5.

APPENDIX A: OPTICAL PROPERTIES AT THE HIGH-FREQUENCY SAMPLING STATIONS

The optical properties of seawater (attenuation coefficient [K_d], euphotic depth [Z_{eu}]) are derived from *in situ* light attenuation measurements using a rosette-mounted PAR radiometer and Secchi disk, according to the following procedures:

1. The downward vertical attenuation coefficient for PAR ($K_{d\text{-}PAR}$) is estimated as the slope of the linear regression of $\ln(E_d(z))$ as a function of depth z (where $E_d(z)$ is the value of downward irradiance at depth z) in the depth interval from minimum depth to around 50 m. The minimum depth is typically around 2 m although the calculation is sometimes forced below that target when near-surface PAR measurements appear unreliable.
2. The value of the light attenuation coefficient $K_{d\text{-}Secchi}$ from Secchi disc observations is found using:

$$K_{d\_secchi}\ (m^{-1}) = 1.44 / Z_{sd}$$

where Z_{sd} is the depth (in m) at which the Secchi disc disappears from view (Holmes 1970).

Estimates of the euphotic depth (Z_{eu}), defined as the depth where PAR is 1% of the surface value, are obtained using the following expression (Churilova et al. 2017):

$$Z_{eu}\ (m) = 4.6 / K_d$$

Estimates of the euphotic depth (Z_{eu}) at the high-frequency sampling stations are summarised in Figure A1.

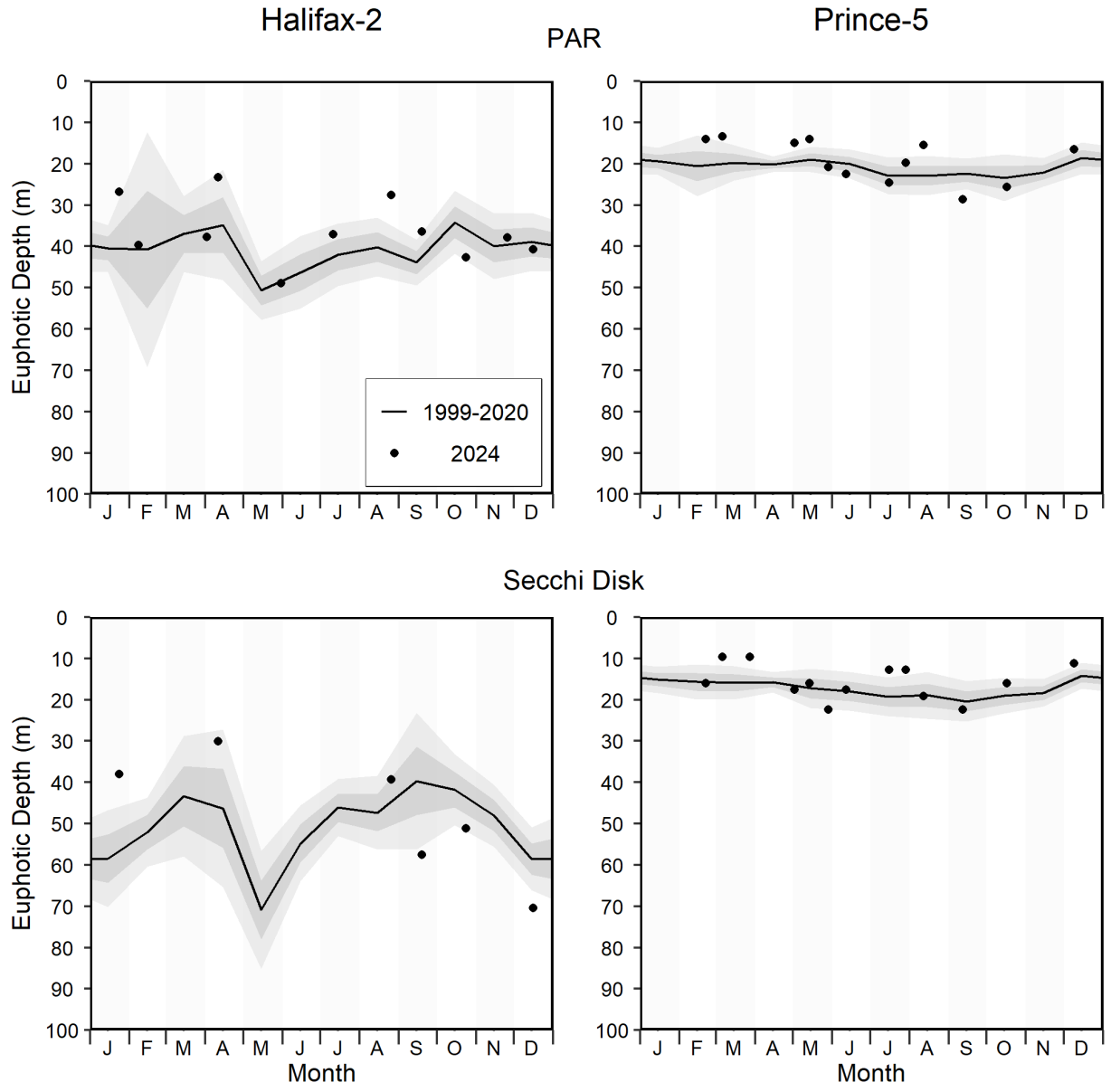

Figure A1. Euphotic depth at the Maritimes high-frequency sampling stations. Top panels: Euphotic depth calculated from PAR irradiance meter. Bottom panels: Euphotic depth calculated from Secchi disc measurements. The solid circles represent the 2024 data; the solid line represents the monthly climatological means for the reference period 1999-2020 (except 2001–2020 for euphotic depth from PAR at Prince 5); the gray shaded ribbons represent the standard deviation (±0.5 and ±1 sd) of the monthly means.

APPENDIX B: SUPPLEMENTARY FIGURES

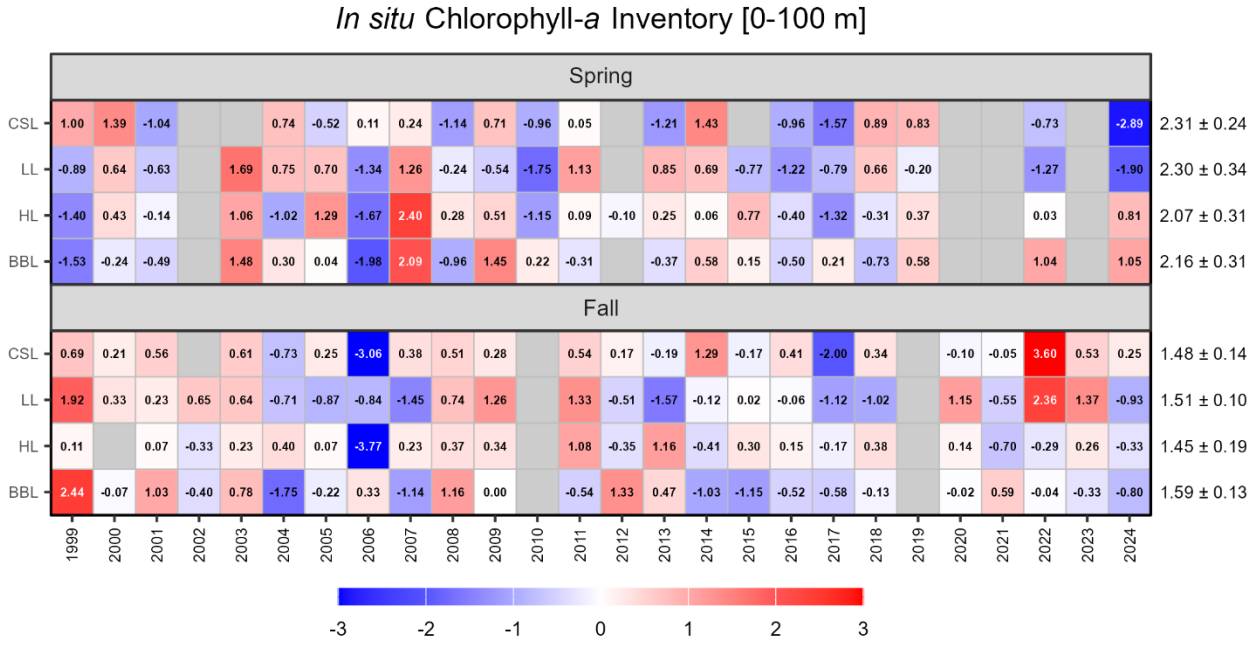

Figure B1. Seasonal anomaly scorecards for in situ chlorophyll-a inventory (0–100 m) on the Cabot Strait [CSL], Louisbourg [LL], Halifax [HL] and Browns Bank [BBL] sections. Values in each cell are anomalies from the mean for the reference period 1999–2020, in standard deviation (sd) units (mean and sd listed at right in units of $\log_{10}(mg \cdot m^{-2})$. Red (blue) cells indicate higher- (lower-) than-normal chlorophyll-a inventories, with shading intensity reflecting the magnitude of the anomaly. Gray cells indicate missing data.

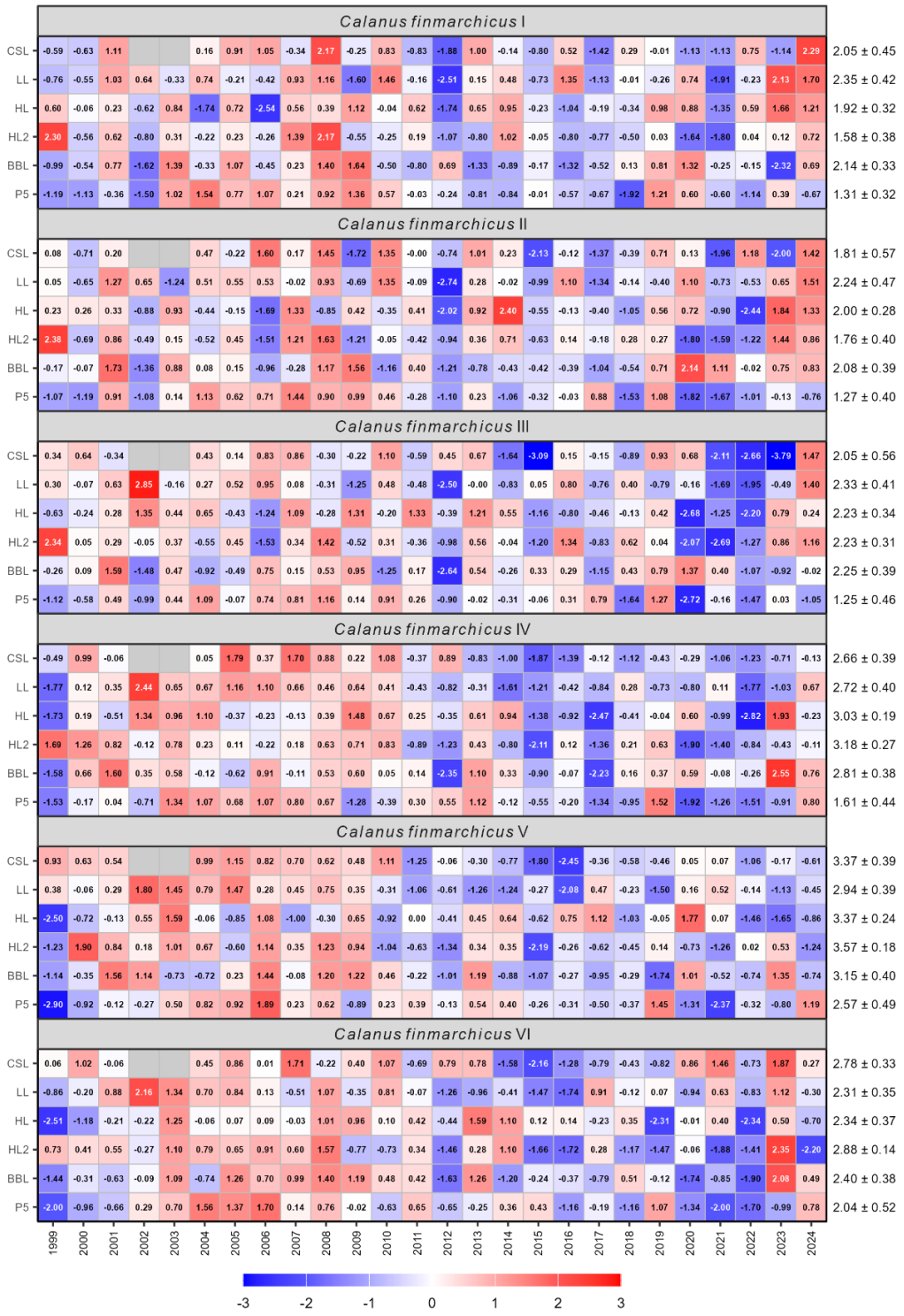

Figure B2. Annual anomaly scorecards for staged Calanus finmarchicus abundance. Values in each cell are anomalies from the mean for the reference period 1999–2020, in standard deviation (sd) units (mean and sd listed at right in units of $\log_{10}$(individuals·m^{-2}+1)). Red (blue) cells indicate higher- (lower-) than-normal abundances, with shading intensity reflecting the magnitude of the anomaly. Gray cells indicate missing data. CSL: Cabot Strait section; LL: Louisbourg section; HL: Halifax section; HL2: Halifax-2; BBL: Browns Bank section; P5: Prince 5.